AD-A135 441 POSSIBLE TIDAL MODULATION OF THE INDIAN MONSOON ONSET (U) AIR FORCE INST OF TECH WRIGHT-PATTERSON AFB OH W H CAMPBELL MAY 83 AFIT/CI/NR-83-60D 1/2

UNCLASSIFIED F/G 4/2 NL

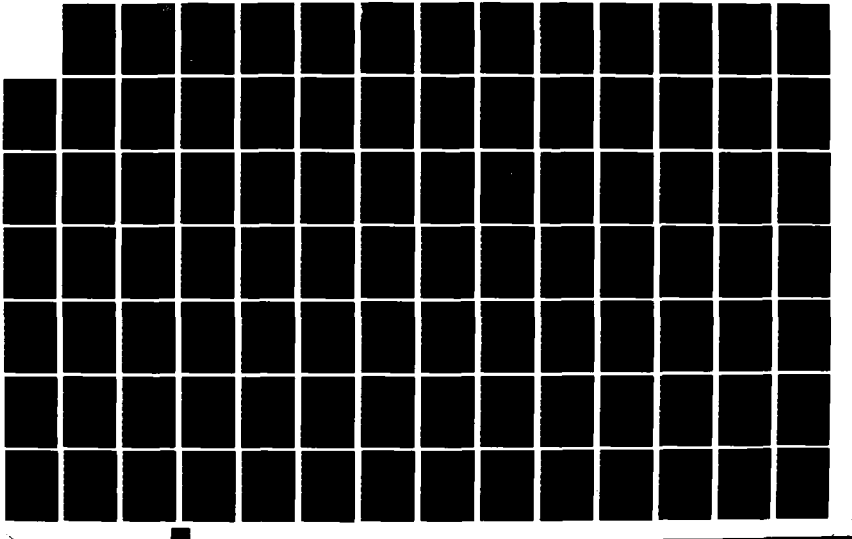

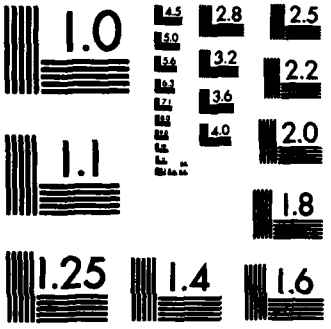

POSSIBLE TIDAL MODULATION OF THE INDIAN MONSOON ONSET

by

WILLIAM HENRY CAMPBELL

A thesis submitted in partial fulfillment of the

requirements for the degree of

DOCTOR OF PHILOSOPHY

(Meteorology)

at the

UNIVERSITY OF WISCONSIN-MADISON

1983

UNCLASS

SECURITY CLASSIFICATION OF THIS PAGE (When Data Entered)

REPORT DOCUMENTATION PAGE

READ INSTRUCTIONS BEFORE COMPLETING FORM

1. REPORT NUMBER: AFIT/CI/NR 83-60D	2. GOVT ACCESSION NO.: AD-A135 641
3. RECIPIENT'S CATALOG NUMBER:	
4. TITLE (and Subtitle): Possible Tidal Modulation of the Indian Monsoon Onset	5. TYPE OF REPORT & PERIOD COVERED: THESIS/DISSERTATION
	6. PERFORMING ORG. REPORT NUMBER:
7. AUTHOR(s): William Henry Campbell	8. CONTRACT OR GRANT NUMBER(s):
9. PERFORMING ORGANIZATION NAME AND ADDRESS: AFIT STUDENT AT: University of Wisconsin - Madison	10. PROGRAM ELEMENT, PROJECT, TASK AREA & WORK UNIT NUMBERS:
11. CONTROLLING OFFICE NAME AND ADDRESS: AFIT/NR WPAFB OH 45433	12. REPORT DATE: 1983
	13. NUMBER OF PAGES: 139
14. MONITORING AGENCY NAME & ADDRESS (if different from Controlling Office):	15. SECURITY CLASS. (of this report): UNCLASS
	15a. DECLASSIFICATION/DOWNGRADING SCHEDULE:

16. DISTRIBUTION STATEMENT (of this Report)

APPROVED FOR PUBLIC RELEASE; DISTRIBUTION UNLIMITED

17. DISTRIBUTION STATEMENT (of the abstract entered in Block 20, if different from Report)

18. SUPPLEMENTARY NOTES

APPROVED FOR PUBLIC RELEASE: IAW AFR 190-17

29 NOV 83

Lynn Wolaver
LYNN E. WOLAVER
Dean for Research and
Professional Development

19. KEY WORDS (Continue on reverse side if necessary and identify by block number)

20. ABSTRACT (Continue on reverse side if necessary and identify by block number)

[redacted]

Accession For	
NTIS GRA&I	X
DTIC TAB	☐
Unannounced	☐
Justification	
By	
Distribution/	
Availability Codes	
Dist	Avail and/or Special
A/1	

DD FORM 1 JAN 73 1473 EDITION OF 1 NOV 65 IS OBSOLETE

UNCLASS

SECURITY CLASSIFICATION OF THIS PAGE (When Data Entered)

POSSIBLE TIDAL MODULATION OF THE INDIAN MONSOON ONSET

A thesis submitted to the Graduate School of the
University of Wisconsin-Madison in partial fulfillment of
the requirements for the degree of Doctor of Philosophy

by

WILLIAM HENRY CAMPBELL

Degree to be awarded: December 19____ May 1983 August 19____

Approved by Thesis Reading Committee:

Major Professor — 12 April 1983 Date of Examination

Dean, Graduate School

TITLE OF THESIS POSSIBLE TIDAL MODULATION OF THE INDIAN MONSOON ONSET

MAJOR PROFESSOR Professor Reid A. Bryson

MAJOR DEPARTMENT Meteorology

MINOR Statistics

NAME William Henry Campbell

PLACE AND DATE OF BIRTH Kansas City, Missouri 14 July 1948

COLLEGES AND UNIVERSITIES: YEARS ATTENDED AND DEGREES

Case Western Reserve University: 1966-1970 B.S. in Engineering

Pennsylvania State University: 1970-1971 B.S. in Meteorology

University of Wisconsin - Madison: 1976-1977 M.S. in Meteorology

MEMBERSHIPS IN LEARNED OR HONORARY SOCIETIES Tau Beta Pi, Sigma Xi, Chi Epsilon Pi

PUBLICATIONS

Bryson, R.A. and W.H. Campbell, 1982: Year-in-advance forecasting of the Indian monsoon rainfall. Environmental Conservation, Vol 9, 51-56.

Campbell, W.H., J.B. Blechman, and R.A. Bryson, 1983: Long-period tidal forcing of Indian monsoon rainfall: An hypothesis. Journal of Climate and Applied Meteorology, Vol 22, 287-296.

continued on next page

DATE 13 May 1983

Houghton, D.D., W.H. Campbell, and N.D. Reynolds, 1981: Isolation of the gravity-inertial motion component in a nonlinear atmospheric model. Monthly Weather Review, Vol 109, 2118-2130.

POSSIBLE TIDAL MODULATION OF THE INDIAN MONSOON ONSET

William Henry Campbell

Under the supervision of Professor Reid A. Bryson

Abstract

The a priori hypothesis that soli-lunar atmospheric tides can induce an element of the variability in mean monthly climatic data is tested using precipitation (1895-1960), station pressure (1895-1960) and 300 mb height data (1950-1977) for India during the monsoon onset month of June. Since the monsoon onset occurs, on average, very late in the month in northern India, this region is very sensitive to small departures from normal in the onset date. These departures can be seen in the year to year fluctuations of June rainfall amounts.

To test the hypothesis involving lunar atmospheric tides, a time series of mean monthly lunar tidal potential for June (1895-1960) was calculated. A periodogram of this time series is dominated by two frequencies, .0537 year^{-1} and .263 year^{-1}, which explain almost 100 percent of the variance. The frequency spectrum of the first eigenvector of June precipitation is dominated by these two frequencies with the frequency .0537 year^{-1} being shifted somewhat lower. This frequency shift was caused by a nonlinearity in the atmospheric response to the forcing. It was found that the amplitude

of the response was not constant in time but dependent upon the temperature of the Northern Hemisphere which determines, to a large extent, the intensity of the monsoon circulation. When the circulation is strong (i.e., when the Northern Hemisphere is warm), the effects of lunar atmospheric tides on climatic variability are minimal and vice versa. Thus, the atmosphere is more susceptible to lunar forcing at certain times than at others making the atmospheric response nonlinear. The ramifications of this nonlinear response are discussed in depth.

CONT'D → The results of this research showed that there is an important periodic component (on the order of one standard deviation during hemispherically cold periods) in the interannual variability of pressure, precipitation, and upper air winds for the Indian monsoon onset month of June at the two dominant lunar frequencies and that the atmospheric response is in phase with the forcing. This strongly suggests that lunar atmospheric tides do produce an element of the observed interannual variability.

Approved: R. E. Thompson

Date: 12 May 1983

Acknowledgements

Without Professor Reid A. Bryson none of this research would have occurred. As my major professor he put me on the track of one of the most fascinating topics imaginable. Through my association with him I have had a unique learning experience because of his wide ranging interdisciplinary knowledge and research. As I pursued my own research, his example was always there to strive for. Professor Bryson gave willingly of his time; and when I felt sure the answer would forever elude me, he gave me the encouragement to continue. His keen insight, advice, and sincere interest in my work were essential elements in the completion of this dissertation. I will never forget his support and I value greatly his friendship.

Special thanks go to my committee. Professor John Kutzbach has provided an example to emulate on how to do good, sound research, and I appreciate his constructive criticism that made this a better thesis. I am grateful to Professor Eberhard Wahl for his review of this thesis and the useful comments that resulted. I thank Professor John Young for his encouragement over the years and for his ability to instill a real excitement into the study of the atmospheric sciences. I also appreciate the advice given by Professor Gregory Reinsel on the statistical aspects of this study.

There have been many others at the university who have helped me during my research - most notably Pat Behling and Melanie Woodworth. Pat provided an accurate data base from which all the rest of this

research evolved. She has also been a great technical consultant, counselor and friend. Melanie took the time to educate me on the use of the word processor and has always been available for help and advice on any number of subjects. My office mates, Brian Goodman and Eric Nash, kept my research days interesting with discussions - scientific and otherwise. Thanks also go to Peter Guetter for assistance in the use of his eigenvector program and for the data handling programs he has written. It has been a rewarding experience to have been associated with all the people of the Center for Climatic Research and the Department of Meteorology.

I thank the United States Air Force for providing me with this educational opportunity through the Air Force Institute of Technology. I am grateful to the Graduate School and to an anonymous donor for the computer funds I expended. The facilities of the Center for Climatic Research, especially the word processor, have also been an invaluable help in completing my dissertation.

I am forever grateful to my parents who have always accepted me as I am and who provided the basic foundation for all of my life's pursuits.

There is no way that I can adequately acknowledge my wife, Susan. She has had to cope alone with our three adorable but demanding children - Scott, Mark, and Todd; and through it all she has helped me to keep my perspective on life, especially when this research effort seemed totally overwhelming. Her love has sustained me, and to her I dedicate this dissertation.

TABLE OF CONTENTS

ABSTRACT ii

ACKNOWLEDGEMENTS iv

TABLE OF CONTENTS vi

LIST OF TABLES viii

LIST OF FIGURES ix

1. INTRODUCTION 1

1.1 Background 1
1.2 Research Perspective 6

2. PERIODIC COMPONENT: HYPOTHESIZED FORCING 10

2.1 Introduction 10

2.2 Basic tidal analysis 14
2.2.1 Calculation of tidal potential 20
2.2.2 Effect of varying Earth-Moon distance 23
2.2.3 Magnitude of lunar tidal potential 27
2.2.4 Affect of geographic location on each term . . . 28
2.2.5 Important frequencies associated with each term 31

2.3 Lunar tidal potential at the nodal frequency 32

2.4 Lunar tidal potential at frequency of .263 year^{-1} . . . 37
2.4.1 Time of maximum declination, ϕ_{max} 37
2.4.2 Hour angle of the Moon, α_0 42

2.5 Component Force (F_x and F_y) derived from lunar potential 44

2.5.1 F_y component 44
2.5.2 F_x component 45

2.6 Summary 48

3. PERIODIC COMPONENT: TEST OF HYPOTHESIS - OBSERVED RESPONSE . 50

3.1 Introduction 50
3.1.1 Atmospheric susceptibility 52
3.1.2 Methodology used to test the hypothesis 63

3.2 Data 67

3.2.1 Station pressure 67
3.2.2 Precipitation 70
3.2.3 300 mb heights 70

3.3 Response to lunar forcing at .0537 year^{-1} 73

3.3.1 Station pressure 73
3.3.2 Precipitaion 85
3.3.3 300 mb U_g component 95
3.3.4 Possible physical relationship between lunar forcing and the observed climatological data 99

3.4 Response to lunar forcing at .263 year^{-1} 104

3.4.1 Introduction 104
3.4.2 Station pressure 105
3.4.3 Precipitation 113
3.4.4 300 mb data 119
3.4.5 Possible physical relationship between lunar forcing and the observed climatological data 123

3.5 Summary 123

4. CONCLUSIONS 130

REFERENCES 135

LIST OF TABLES

Table	Page	
2.1	29	Instantaneous lunar tidal potential.
2.2	33	Important frequencies for June lunar potential at 25°N, 75°E.
2.3	36	Relationship of average potential to δ_{max} and ϕ_{max}.
2.4	47	Average August values of lunar potential (Term 2 + Term 3) at 25°N.
3.1	69	WMO numbers and names of stations in Figure 3.4 (Station Pressure)
3.2	72	WMO numbers and names of stations in Figure 3.5 (Precipitation)
3.3	82	Pressure anomaly difference compared to the TMEDLF response.
3.4	124	Summary of statistics for the kF_{05} and kF_{26} models for the three climatic variables.

LIST OF FIGURES

Figure	Page	
1.1	3	The normal dates of the onset of the monsoon (after Das, 1968).
1.2	8	Schematic of research perspective.
2.1	16	Latitudinal geometry used for the tidal potential equation development. The North Pole is at N; the center of the Earth is at O; the Moon is at M; and the point of interest is at P. The figure is not drawn to scale.
2.2	18	Longitudinal geometry used for the tidal potential equation development. The outer circle represents the Moon's orbit and the inner circle represents the Earth with center at O. P is the point of interest. The figure is not drawn to scale.
2.3	30	Instantaneous lunar potential for the first instant of August 1948 (units are $m^2s^{-2} \times 10^{-1}$).
2.4	35	Effect of the nodal cycle on the latitudinal range of the sublunar point (from Wood, 1976).
2.5	38	Latitudinal distribution of the lunar potential anomaly at the extremes of the nodal cycle (units are m^2s^{-2}).
2.6	43	Scatter diagram of the hour angle of the Moon at the beginning of the month versus the day of maximum declination in days.
2.7	46	Monthly average of the x-component of the lunar force (units are $ms^{-2} \times 10^{-10}$) for August 1947.
2.8	49	Example of the sublunar latitude (in degrees) versus the day of the month showing the sidereal month period (27.3216 days). The nodal cycle is dependent upon the latitudinal range of the Moon during the month while the frequency .263 $year^{-1}$ is dependent upon the latitudinal position of the Moon at the end of the month.

3.1	56	The solid line is the Northern Hemisphere annual mean surface temperature anomalies from the 1946-1960 mean (after Jones et. al., 1982). The dashed line is the best fitting cosine (explaining 58 percent of the variance) used in the susceptibility factor.
3.2	59	Periodograms of the lunar tidal potential (from Term 1) and the associated TMEDLF response for the years 1899 through 1960. The TMEDLF response time series was calculated using the amplitudes and phases for the frequencies .0537 year $^{-1}$ and .263 year^{-1} from the lunar tidal potential time series (Term 1) along with the representative values of the susceptibility threshold as shown in Equation 3.6.
3.3	60	Time series for a response to a forcing with a five year period and a 180 year modulation. The only difference between each time series is the value of the susceptibility threshold. These plots show how sensitive the response is to the value of the susceptibility threshold.
3.4	68	Approximate locations of the 40 stations used in the station pressure analysis. The station names and WMO numbers are given in Table 3.1.
3.5	71	Approximate locations of the 39 stations used in the precipitation analysis. The station names and WMO numbers are given in Table 3.2.
3.6	74	The percent of the station pressure variance explained by the kF_{05} model (units are percent).
3.7	75	The value of the susceptibility threshold from the regression of the station pressure data against the kF_{05} model (units are value x 10^{-2}). The two areas outlined show that the threshold values are different in northeastern India from what they are in western India.
3.8	76	Anomaly maps of station pressure for the years indicated from the kF_{05} model (units are mb x 10^{-1}).
3.9	78	The average position of the monsoon trough (solid line) for the years 1899 through 1977 taken from the gridded Northern Hemisphere sea level pressure data tape which has been updated by Trenberth (1981). The pivotal axis of the nodal cycle anomaly oscillation is shown with a dashed line.

3.10	80	Composite surface pressure anomalies (units are 10^{-1} mb) for eight drought and eight flood years (from Bhalme and Mooley, 1980).
3.11	84	Station pressure anomaly map for 1941 from the regression against the kF_{05} model.
3.12	86	The percent of the precipitation variance explained by the kF_{05} model (units are percent).
3.13	87	Normalized anomaly maps of precipitation for the years indicated from the kF_{05} model (units are standard deviations x 10^{-1}).
3.14	89	A periodogram of the coefficients of the first eigenvector of June cuberooted precipitation (1895-1975). The two dominant peaks are at .0482 $year^{-1}$ and .262 $year^{-1}$.
3.15	92	The solid line is the percent of the stations in northern India with less than half of the normal rainfall in a given year (running ten year averages). The dashed line represents the predicted values from a regression of the data against both the kF_{05} model and the Northern Hemisphere annual mean surface temperature. The dashed curve explains over 51 percent of the variance.
3.16	93	Flood Area Index time series for the indicated flood intensities (after Bhalme and Mooley, 1981). The dashed curves represent the predicted values of a regression of these data against the 22 year double sunspot cycle, while the solid curves represent the predicted values of a regression of these data against the kF_{05} model.
3.17	96	The percent of the geostrophic zonal wind (U_g) variance explained by the kF_{05} model (units are percent). Level is 300 mb.
3.18	98	Anomaly maps of U_g for the year indicated from the kF_{05} model (units are ms^{-1}). Level is 300 mb.
3.19	100	Normalized anomaly map of precipitation for 1978 (units are standard deviation x 10^{-1}).

3.20	106	Normalized amplitudes of the regression of the first eigenvector coefficients (June precipitation) against the cosine with frequency .263 year^{-1} for overlapping 19 year periods plotted against the last year of the period.
3.21	107	The percent of the station pressure variance explained by the kF_{26} model (units are percent).
3.22	109	The value of the susceptibility threshold from the regression of the station pressure data against the kF_{26} model (units are value x 10^{-2}).
3.23	110	Anomaly maps of station pressure for the years indicated from the kF_{26} model (units are 10^{-1} mb).
3.24	112	Anomaly map of station pressure for 1950 from the kF_{26} model (units are 10^{-1} mb).
3.25	114	The percent of the precipitation variance explained by the kF_{26} model (units are percent).
3.26	115	The value of the susceptibility threshold from the regression of the precipitation data against the kF_{26} model (units are value x 10^{-2}).
3.27	117	Normalized anomaly maps of precipitation for the years indicated from the kF_{26} model (units are standard deviations x 10^{-1}).
3.28	121	The percent of the geostrophic zonal wind (U_g) variance explained by the kF_{26} model (units are percent).
3.29	122	Anomaly map of U_g for 1971 from the kF_{26} model (units are ms^{-1}).

CHAPTER 1

Introduction

1.1 Background.

The planetary monsoon circulation is a dominant element of the large-scale atmospheric response to the annual solar cycle. As the Northern Hemisphere warms in the spring, the expanse of the westerlies contracts, the subtropical highs move northward and the onset of the monsoon begins. Since this planetary phenomenon, which includes the southwest summer monsoon in India, results from thermal inhomogeneities at the earth's surface created by the distribution of the continental land mass and oceans, the large-scale features of the monsoon circulation are similar from one year to the next. However, significant interannual variability of rainfall exists in the monsoon region. For example, very heavy rains fell in India during the 1917 monsoon whereas the 1918 monsoon season produced one of the worst droughts of the last century. A reconstructed history of monsoon precipitation (Bryson and Swain, 1981) shows that the monsoon has not been a constant and reliable phenomenon, and this variability will almost certainly continue in the future. With the economy of India being so fragile that one drought is a sufficient factor alone to disrupt the country, it is imperative that we develop the capability to forecast the year to year fluctuations in precipitation if anyone is to plan rationally for the future of the region.

June is the month of the monsoon onset over most of the Indian subcontinent. The onset can be viewed as a front (Das, 1968) which, on the average, enters the southeastern tip of India around 1 June and reaches the Pakistani-Indian border by 1 July (Fig. 1.1). Prior to monsoon onset, India is basically dry and hot except for scattered pre-monsoon showers. When the monsoon front arrives there is a tremendous burst of precipitation. However, once the monsoon front is past, the cloud tops are generally not very high and drizzle to light rain is the predominant form of precipitation with intervals of heavier rainfall and deeper convection associated with monsoon depressions from the Bay of Bengal.

There is considerable variability in the date of onset from year to year. For example, along the west coast south of $20^{o}N$ the standard deviation of the onset is about seven days (Rao, 1976). It is the variability in onset date which greatly affects the June precipitation pattern in northern India, where the advance of the monsoon front begins to slow down. In this region small displacements of the monsoon front with its associated large rainfall gradient will markedly affect the amount of rainfall received in June. If the monsoon front is late, a significant percentage of the opportunity for rain in the calendar month of June is lost, because the pre-monsoon days are drier than the normal post-monsoon "burst" days. Thus, small anomalies in the monsoon front's normal position can be seen in the year to year fluctuations of June rainfall amounts at stations in northern India. For

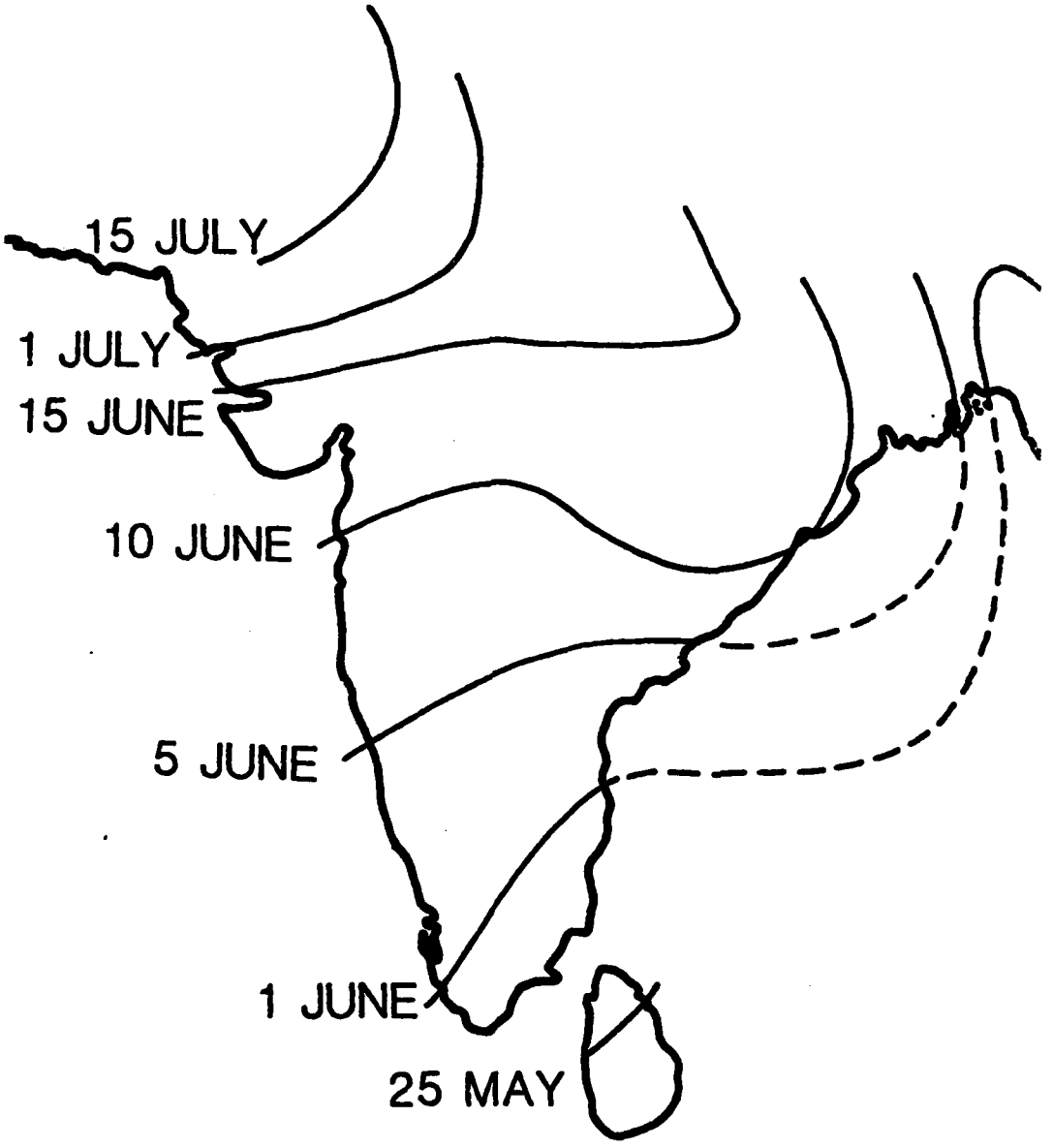

Figure 1.1. The normal dates of the onset of the monsoon (after Das, 1968).

example, if the normal date of arrival of the monsoon is 25 June, a two day delay in arrival time represents a 40 percent reduction in the duration of June monsoon rains. By contrast, at stations in southern India, where the monsoon normally arrives in May or early June, a two day delay in arrival of the rains would have a small percentage effect on June rainfall. Furthermore, in northern India the monsoon front moves slowly, on the order of 25-50 km per day in the mean, so that quite small spatial departures from the normal position represent significant advances or delays in arrival time.

Once the monsoon is established over India, rainfall is the result of a very complex pattern. There are two related systems. One brings rains to the west coast with the strong southwesterly onshore flow, and the other brings rains to the Gangetic Plain where most of the rain in July and August is associated with monsoon lows and depressions which develop in the northern Bay of Bengal and travel westward across northern India. On top of these large scale features are then superimposed substantial effects due to topography along the western Ghats and the Himalayan foothills which tend to obscure the influence of the large-scale circulation features. Added to this already complex pattern is the movement of the monsoon trough. As Raghavan (1973) points out, the track of a monsoon low/depression and the position of the monsoon trough are related - with a more southerly position being favorable for rain over most of the country and a more northerly position against the Himalayas being associated with breaks in the monsoon.

The Indian summer monsoon has been the subject of extensive study for many years. For example, Krishnamurti has studied the elements of the monsoon circulation in detail (e.g., Krishnamurti, 1971; Krishnamurti et al., 1973; Krishnamurti and Bhalme, 1976). Others have performed observational studies on the interannual variability of Indian summer monsoon rainfall. Hahn and Shukla (1976) showed an apparent association with Eurasian snow cover - the more the snow the less the rain. Shukla and Misra (1977) and Weare (1979), among others, have studied the effects of sea surface temperatures on the amount of Indian rainfall with differing results. Still others have used numerical models to try and understand the monsoon. For example, Hahn and Manabe (1975), using a general circulation model showed the importance of the Himalayan mountains in helping to extend the monsoon climate farther north onto the Asian continent. Shukla (1975) modelled the effect of Arabian sea surface temperatures on the monsoon. Other numerical studies have included a simulation of the Indian summer monsoon by Godbole (1973) and a model of the seasonal structure of a simple monsoon system by Webster and Chou (1980). Matsuno (1966) and Gill (1980) have studied the atmospheric response to both symmetric and antisymmetric heating about the equator where Gill's antisymmetric heating produced some of the basic features of the Indian monsoon circulation.

The relationship of the Southern Oscillation to droughts and floods in India has been the subject of investigation ever since Sir

Gilbert Walker (1924) found a tendency for increased precipitation in India when the pressure increases in the Pacific and lowers in the Indonesian region. Most recently Bhalme et. al. (1983) studied the relationship between an Indian drought/flood area index and a Southern Oscillation index based on April pressures and found significant correlations between the two indices. Using a coherence spectrum analysis, they concluded that the Southern Oscillation is one possible mechanism for introducing a 3-6 year oscillation in the drought area index. The research presented in the following chapters will add another mechanism to the possible causes of the observed interannual variability in the monsoon circulation.

1.2 Research perspective.

Climate can be viewed as the state of the earth-atmosphere-ocean system resulting from a set of boundary conditions imposed on this system. This climatic state then establishes an array of weather patterns; and if the climatic state changes, a different array of weather patterns results. Thus, in order to determine a climatic state with its attendent synoptic patterns one must be able to specify the boundary conditions, both internal and external, that are imposed on the atmosphere. These are the ultimate causes of climate and include such conditions as the energy output of the sun, the earth's orbital characteristics (e.g., time of year of perihelion), pole and gravitational tidal forcing, anthropogenic heat and particulate output, and volcanic activity. These ultimate

boundary conditions result in what one might call proximal causes of climate like the amount of solar radiation reaching the earth's surface which is dependent on several of the ultimate causes given above. If the ultimate causes vary, then the climate must vary also. Thus, in order to understand climatic variability and be able to predict a future climatic state we must be able to specify the appropriate boundary conditions and understand how they vary. Over the last 100 years some of the boundary conditions can be assumed constant (e.g., earth's orbital parameters) while others cannot (e.g., volcanic activity, pole and gravitational tidal forcing). Figure 1.2 shows a schematic which puts this research effort into perspective.

Interannual variability of a parameter like rainfall amount can be separated into at least two parts - a periodic and a secular component. The secular, or trend, component might be associated with the thermodynamic state of the atmosphere and also could be a periodic component but one with a period near the length of the data record or longer. A third possible component might be a stochastic one (i.e., the part of climatic variability that is currently unknown or that is truly random).

It is important to emphasize that there are many causes of climatic variability and change. The scope of this research effort has been narrowed to an analysis of <u>one</u> of the forcing mechanisms that might produce a periodic component in the interannual variability found in the monsoon onset month of June. The research

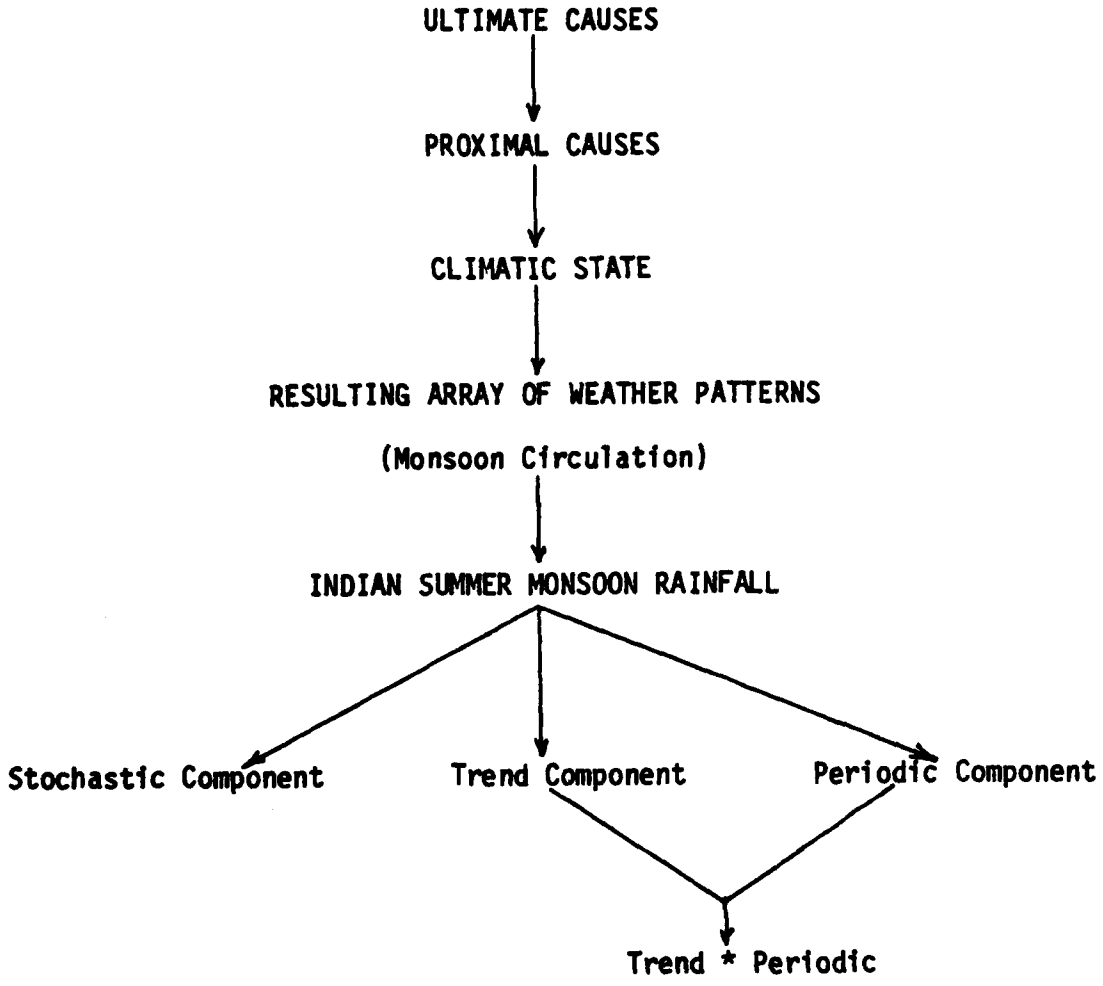

Figure 1.2 Schematic of research perspective

was conducted with the a priori hypothesis that soli-lunar atmospheric tides can induce an element of the periodic variability in mean monthly climatic data. Lunar tidal forcing of climate is not a new idea; for example, Bryson (1948) found that the latitudinal position of the eastern Pacific High was highly correlated with the equatorward component of the bifortnightly lunar tidal force. Thirty-five years later there is still much research needed in this area.

Chapter 2 will examine the hypothesized lunar forcing by developing a lunar tidal potential time series averaged over the month of June for the years 1895 through 1960. The periodic components of this time series will be determined, and the Moon's orbital characteristics that produce this part of the lunar potential interannual variability will be discussed.

Chapter 3 will then test the hypothesis through a diagnostic study which examines the response of surface pressure, precipitation, and 300 mb data at the two dominant lunar forcing frequencies. Campbell et. al. (1983) found that these two frequencies were most important in explaining the interannual variability of precipitation in northern India. A unique way of defining how the atmosphere responds to the hypothesized forcing will be described in the development of a nonlinear model combining the trend and periodic components of variability.

Chapter 4 will present the major conclusions of this research.

CHAPTER 2

Periodic Component: Hypothesized Forcing

2.1 Introduction

Many studies of Indian summer monsoon rainfall have found a periodic component in the data. Koteswaram and Alvi (1969) and Bhargava and Bansal (1969) found quasi-biennial variations (QBVs) in both monsoon and annual rainfall at some stations on the west coast of southern India. Jagannathan and Parthasarathy (1973) found a QBV in the annual precipitation of other stations throughout India. Parthasarathy and Mooley (1978) in their study of a single homogeneous time series of Indian summer monsoon rainfall, derived from an areal weighting of over 3000 rain gauges, found a significant cycle (at the 5 percent level) in the QBV range. Bhalme (1972) found the frequency of southwest monsoon cyclonic disturbances (1891-1970) had a significant QBV of 3.3 to 3.5 years. Bhalme and Mooley (1980) found a QBV frequency in the occurrence of droughts in India and an interval of about 20 years between large-scale floods. Jagannathan and Parthasarathy (1973) found periodicities of approximately 11 years which they related to the solar cycle. Interestingly enough, Parthasarathy and Mooley (1978) found no significant relationship between the sunspot cycle and monsoon rainfall in India. However, Bhalme and Mooley (1981) found a significant signal in their Flood Area Index (FAI) at 22 years

which they attributed to the double (Hale) sunspot cycle. They used a Fast Fourier Transform analysis on 88 years of data which automatically puts band 4 at a 22 year periodicity; whereas, a periodogram, which looks at the spectral behavior between the bands, shows that the spectral peak was actually around .048 $year^{-1}$ (i.e., a 20.8 year period).

One must ask what ultimate cause can produce periodicities in measured atmospheric variables like wind, pressure and precipitation; for until we can answer this question, accurate climatic forecasts of one to five years in advance will not be possible. Bryson and Goodman (1980) have shown that the variations in the amount of solar radiation reaching the ground have a possible, non-sunspot periodic component. Feedback loops within the earth-atmosphere-ocean system may induce a periodicity in rainfall amounts. However, it seems hard to envision a closed feedback system that would oscillate for many years, unless it is forced, because of the high correlations that would be required between the meteorological variables. Another possible candidate is the periodic, mechanical forcing produced by both the long period soli-lunar tides and the "pole tide" associated with the Chandler wobble. Studies by Bryson and Starr (1977), Maksimov (1958) and Maksimov et al. (1967) have provided insight into the effects of the pole tide on the atmosphere.

Soli-lunar tidal forcing is of particular interest since its periodicities are so highly predictable. There have been many

studies which have related lunar periods to particular meteorological phenomena (e.g., the synodic period[1] to rainfall). Brier and Bradley (1964) examined 16,057 maximum monthly 24-hour precipitation occurrences in the U.S. from 1900-1949. By relating the date of occurrence to the respective point in the synodic cycle, they derived a frequency distribution that showed a significant tendency for heavy precipitation to occur three times more frequently in the middle of the first and third weeks of the synodic month compared to the second and fourth weeks. Adderly and Bowen (1962) found similar results in the Southern Hemisphere for New Zealand. Visvanathan (1966b) examined the distribution of heavy rainfall in India with respect to the synodic period and found a definite lunar component in the frequency of occurrence - again with two maxima and minima during the period. He also found a shift in phase and decrease in amplitude of the precipitation frequency of occurrence curves with an increase in latitude. Bradley (1964) studied the transition of 269 North Atlantic tropical depressions into hurricanes and found the timing to be dependent on both the half-synodic and the anomalistic (perigee to perigee) periods which are the most important cycles for determining the magnitude of the instantaneous soli-lunar gravitational force. Visvanathan (1966a) found that the frequency of formation of monsoon depressions in the Bay of Bengal and Arabian Sea from 1877 to 1960 as a function of the

[1]One half of the lunar synodic period is 14.7365 days and aliases at the frequency .26 yr^{-1} in a spectrum of data that is sampled once per year.

synodic month had a strong 14.765 day wave component.

Brier (1968) has also presented the possibility that quasi-biennial variations may be forced by the soli-lunar gravitational force, for in an analysis of the zonal index he found a significant spectral peak at 3.25 years and was then able to relate the characteristics of the zonal index time series to those of the soli-lunar gravitational tidal force.

Thus, there is empirical evidence for soli-lunar tidal forcing on the atmosphere. However, few, if any, of these ideas have found their way into practical use, mainly because the arguments are usually statistical and linear and because the forces involved are generally felt to contribute trivially to the total atmospheric response. This research is based on the hypothesis that soli-lunar tidal forcing does, in fact, produce an element of climatic variability and will address a case where lunar tidal forcing apparently contributes in a significant manner to that part of the variance which lies in the interannual range.

The diurnal and semi-diurnal tides in the ocean and atmosphere are well known manifestations of the lunar tides. However, as shown by Bryson (1948) and discussed by Brier (1968) the longer period lunar tides may be more important in the atmosphere in that they may cause shifts in the geographic locations of steady or regular features, such as subtropical anticyclones. Such shifts would result in large departures from normal in the areas where the gradients are the largest. Recently Currie (1981) has provided

evidence of the 18.6 year lunar nodal cycle in North American temperature and drought data.

In this chapter I will present the information needed to understand the source of the two most important interannual lunar tidal periodicities. The next chapter will then test the lunar tidal forcing hypothesis by analyzing the response of station pressure, precipitation, and the 300 mb u-component of the geostrophic wind at the hypothesized forcing frequencies to see what relationship exists, if any, between lunar tidal forcing and the atmosphere.

2.2 Basic tidal analysis.

Only the lunar component will be considered here. The Sun's effect on tidal forcing will be discussed when considering the variations in Earth-Moon distance in section 2.2.2.

Note: In the discussion that follows it will be necessary, at times, to use the equatorial coordinate system. In this coordinate system right ascension and declination bear the same relationship to the celestial equator and poles as longitude and latitude, respectively, bear to the terrestial equator and poles. Right ascension gives the number of degrees measured eastward along the celestial equator from the vernal equinox which is the point where the celestial equator and the ecliptic planes intersect. Declination gives the number of degrees north or south of the celestial equator.

Following the development given by Chapman and Lindzen (1970), the tidal potential due to the Moon at a point P (see Fig 2.1) on the Earth is the difference between the attraction of the Moon at point P and the attraction for the Earth as a whole. The local tidal potential is:

$$U_p = GM/L = GM/(D^2 - 2aD\cos\lambda + a^2)^{1/2}, \qquad 2.1$$

where G is the universal gravitation constant, M is the mass of the Moon, and a is the radius of the Earth and where L, the distance from point P to the Moon, has been rewritten using the Law of Cosines. The tidal potential associated with the Earth is:

$$U_{Earth} = (GM/D^2)a\cos\lambda.$$

Then we have:

$$U_{tidal} = U_{Earth} - U_p = \frac{aGM\cos\lambda}{D^2} - \frac{GM}{(D^2 - 2aD\cos\lambda + a^2)^{1/2}} \qquad 2.3$$

The first term of an expansion in powers of a/D yields:

$$U_{tidal} = -3/2\ \frac{GMa^2}{D^3}(\cos^2\lambda - 1/3) \qquad 2.4$$

which is an approximate form of the tide generating potential.

The potential is then basically a function of the angle between the Moon and the point P. This angle is constantly changing and is dependent upon three basic processes:

1. The rotation of the Earth about its axis. It takes 23 hr 53 min 4 sec for the Earth to rotate once with respect to the stars. This is a sidereal day which is .9973 of a solar day (24 hrs).

2. The revolution of the Moon in its orbit about the Earth from ascending node to ascending node. This is the nodical month and

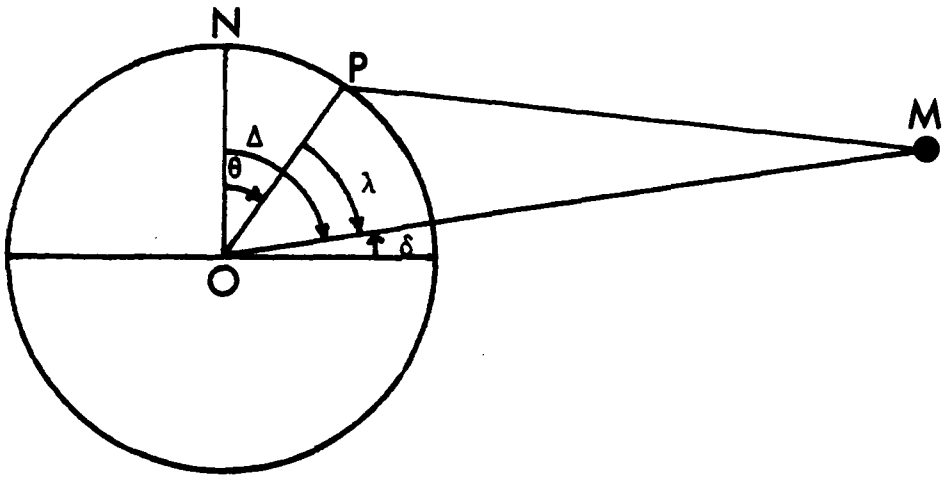

Δ = NOM	D = OM
θ = NOP	L = PM
λ = POM	a = OP

Figure 2.1. Latitudinal geometry used for the tidal potential equation development. The North Pole is at N; the center of the Earth is at O; the Moon is at M; and the point of interest is at P. The figure is not drawn to scale.

takes 27.2122 days. The nodes of the Moon's orbit occur at the intersection of the Moon's orbital plane and the ecliptic plane.

3. The retrogression of the line of nodes which takes 18.6133 years (6798.3658 days). Since the line of nodes is retrogressing at the same time the Moon is revolving about the Earth, when the Moon is back to its ascending node again it is still not back to the same place in its orbit with respect to the stars. This period, called the sidereal month, takes slightly longer than the nodical month and is 27.3216 days long.

Let Δ and θ be the colatitude of the sublunar point and the location of interest, respectively, as shown in Figure 2.1. Then if we let ϕ be the east longitude of point P and α be the hour angle of the Moon to the west of the Greenwich meridian (see Fig. 2.2), the $\cos\lambda$ can be written as:

$$\cos\lambda=\cos\Delta\cos\theta+\sin\Delta\sin\theta\cos(\alpha+\phi). \qquad 2.5$$

The angles θ and ϕ are related to point P's latitude and longitude, respectively. The angle, Δ, can be represented as follows:

$$\Delta = \pi/2-(23.45^\circ+5.15^\circ\cos No)\cos Sm, \qquad 2.6$$

where 23.45° is the latitude of intersection of the ecliptic plane with the earth,

5.15° is the angle at which the Moon's orbital plane is inclined to the ecliptic plane,

No is $2\pi f_{No}t$ where f_{No} is the nodal frequency of .0537 $year^{-1}$,

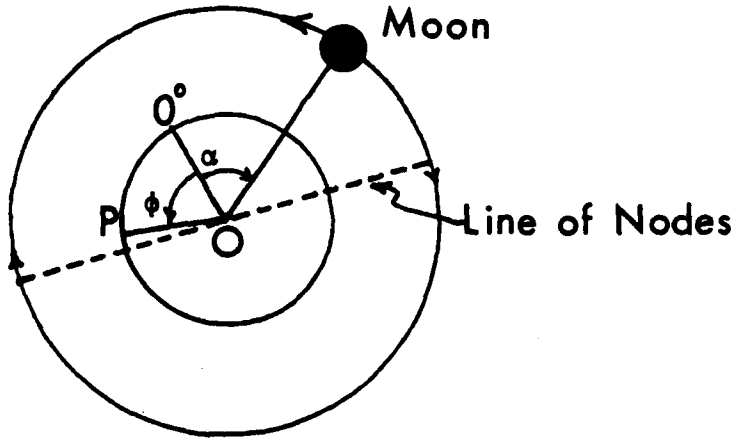

Figure 2.2. Longitudinal geometry used for the tidal potential equation development. The outer circle represents the Moon's orbit and the inner circle represents the Earth with center at O. P is the point of interest. The figure is not drawn to scale.

Sm is $2\pi f_{Sm}t$ where f_{Sm} is the sidereal month frequency 13.3683 $year^{-1}$(i.e., 365.2422/27.3216).

Next let's consider the hour angle, α. If the Moon were stationary, then the only thing affecting α would be the rotation of the earth and α would go through 360° in one sidereal day. In this case $\alpha=2\pi t/.9973$ with t measured in solar days. However, the Moon revolves around the Earth as shown in Figure 2.2. It takes the Moon 27.2122 days to travel west to east around the Earth from ascending node to ascending node, so if one were to measure α at the end of each Earth rotation it would be smaller in terms of degrees west of the Greenwich meridian. At this point,

$$\alpha=(2\pi/.9973 - 2\pi/27.2122)t. \qquad 2.7.1$$

There is still one other factor to consider and that is the retrogression of the line of nodes from east to west as depicted in Figure 2.2. This retrogression increases α so we have,

$$\alpha=(2\pi/.9973 - 2\pi/27.2122 + 2\pi/6798.4)t. \qquad 2.7.2$$

Alpha can also be represented as:

$$\alpha=(2\pi/.9973 - 2\pi/27.255241 - 2\pi/\text{apsides})t, \qquad 2.8$$

where instead of the nodical month and the nodal period the anomalistic month and the period of the revolution of the line of apsides are used. The line of apsides joins the points of perigee and apogee and makes one revolution in 8.849 years.

Now in order to be able to calculate the potential at a given location the expression $(\cos^2\lambda - 1/3)$ must be evaluated. It is the sum of the following three terms:

Term 1: $(3/2)(\cos^2\Delta - 1/3)(\cos^2\theta - 1/3)$ 2.9

Term 2: $(1/2)\sin 2\Delta \sin 2\theta \cos(\alpha+\phi)$ 2.10

Term 3: $(1/2)\sin^2\Delta \sin^2\theta \cos 2(\alpha+\phi)$ 2.11

2.2.1 Calculation of tidal potential.

Terms 1, 2, and 3 have been evaluated to get a physical idea of what influences the value of the lunar potential. Certain simplifying assumptions have been made in the calculations:

1. The distance between Moon and Earth is constant (i.e., D in Eqn. 2.4 is constant). See section 2.2.2 for a discussion of the varying Earth-Moon distance.

2. In Eqn 2.6 the value of $(23.45^\circ + 5.15^\circ \cos No)$ was assumed constant for a given month and year. The maximum declination of the Moon goes through an 18.6 year cycle, thus the value is fairly constant for a 30 day period. This value was taken to be the maximum northward declination for the month and year with the phasing on the cosSm term of Eqn. 2.6 being the time of this maximum northward declination. Both the declination and the time were found in the American Ephemeris and Nautical Almanac (1855-1982).

In order to calculate the hour angle, α, the following equations taken from the American Ephemeris and Nautical Almanac (1980) were used:

$L = 270^\circ.434358 + 13^\circ.1763965268 - 0.001133T^2 + 0.0000019T^3$ 2.12

$L' = 279^\circ.69668 + 0.9856473354d + 0.000303T^2$ 2.13

$P = 334^\circ.329653 + 0.1114040803d - 0.010325T^2 - 0.000012T^3$ 2.14

$$P' = 281^{\circ}.22083 + 0.0000470684d + 0.000453T^2 + 0.000003T^3 \quad 2.15$$

$$N = 259^{\circ}.183275 - 0.0529539222d + 0.002078T^2 + 0.000002T^3 \quad 2.16$$

$$e = 0.054900489 \quad 2.17$$

$$i = 5^{\circ}.145396 \quad 2.18$$

where

L is the mean longitude of the Moon, measured in the ecliptic from the vernal equinox to the ascending node and then along the orbit to the Moon.

P is the longitude of perigee of the Moon's orbit.

N is the longitude of the Moon's ascending node.

i is the inclination of the Moon's orbit to the ecliptic.

e is the average eccentricity of the Moon's orbit.

L', P' are similar to L and P except they pertain to the Sun.

In these equations T is measured in Julian centuries from 1900 January 0.5 Ephemeris Time and d is the number of ephemeris days from this date. (An ephemeris day is 86400 ephemeris seconds where an ephemeris second is 1/31556925.9747 of the tropical year.)

These formulas must then be corrected for certain well known perturbations of the Moon's orbit. Voigt (1974, p. 59) discusses evection, variation and the annual equation. Goldstine (1973) made use of the following equations to take these perturbations into account.

$$A_1 = 4467'' \sin(L - 2L' + P) \quad 2.19$$

$$A_2 = 2145'' \sin 2(L - L') \quad 2.20$$

$$A_3 = 658'' \sin(L' - P' + 180^{\circ}) \quad 2.21$$

$$A_4 = 198''\sin(L - 3L' + P + P') \qquad 2.22$$

$$A_5 = 155''\sin(2L - 3L' + P') \qquad 2.23$$

L can then be replaced by the corrected mean longitude:

$$LM = L + A_1 + A_2 + A_3 + A_4 + A_5. \qquad 2.24$$

In order to find the true longitude, γ, of the Moon in its orbit the equation of center, as discussed by Voigt (op.cit., p.59) and Goldstine (op. cit.) is used. When retaining terms through e^4, the equation becomes:

$$\gamma = L + (180/\pi)\,[(2e - e^3/4)\sin(L-P) + (5e^2/4 - 11e^4/24)\sin2(L-P) + (13e^2/12)\sin3(L-P) (103e^4/96)\sin4(L-P)]. \qquad 2.25$$

Thus, we now have the true longitude of the Moon's orbit. This angle is measured from the vernal equinox to the ascending node in the plane of the ecliptic and then along the orbit to the Moon's true position. The Moon's position must then be projected onto the plane of the ecliptic using the approximate formula known as the reduction to the ecliptic found in Brower and Clemence (1961, p. 47):

$$SL = L + (180/\pi)\,[p^2\sin2(\gamma - N) - (p^4/2)\sin4(\gamma - N) + (p^6/3)\sin6(\gamma - N)] \qquad 2.26$$

where $p=\tan(i/2)$

All of the above equations were used to find the change in the angle, α, during the course of the month. This change will be denoted as $\Delta\alpha_t$. Thus, by knowing the hour angle at the first instant of each month (α_0), the sidereal day, and $\Delta\alpha_t$, the hour angle at any time during the month can be calculated by:

$$\alpha = \alpha_0 + (360^\circ/.9973)t - \Delta\alpha_t. \qquad 2.27$$

The declination of the Moon, which is the number of degrees north or south of the celestial equator, was calculated using the time of maximum northward declination during the month and the value of the declination at that time. Thus, to find the colatitude of the declination, Δ, at any given time during the month the following equation was used:

$$\Delta = 90. - \delta = 90. - \delta_{max}\cos[(2\pi/Sm)(t-\phi_{max})] \qquad 2.28$$

where

ϕ_{max} is the time of maximum declination in days.

δ is the declination of the Moon,

δ_{max} is the maximum northward declination at time ϕ_{max},

Sm is the sidereal month, 27.3216 days, and

t is the time of the month in days.

With the values for α and Δ we are then able to calculate the average potential for a given month.

The values for α_0, ϕ_{max}, and δ_{max} were obtained from the American Ephemeris and Nautical Almanac (1855-1982).

It is important to emphasize that we are calculating the monthly average potential because the climatic data we will be analyzing are all monthly averages. This makes the external forcing data set comparable to the observed data.

2.2.2 Effect of varying Earth-Moon distance on the forcing.

In the preceding analysis the distance between Moon and Earth was

assumed to be constant, producing a constant amplitude. In fact, because of the eccentricity of the Moon's elliptical orbit (e=.0549) around the Earth (with the Earth at one focus), the Moon has a closest approach to the Earth during the month called perigee and about two weeks later it reaches its furthest distance called apogee. The time from perigee to perigee is known as the anomalistic month of 27.55455 days. In addition, the orbital axis joining perigee and apogee, the line of apsides, rotates in a counterclockwise direction completing one revolution in 8.849 years. Because of the rotation of the line of apsides, the point in the lunar orbit where perigee occurs is constantly changing.

Looking at the tidal potential (Eqn. 2.4 and 2.9 - 2.11), one can see that a variation in distance will cause the amplitude of the periodic cosine terms to change significantly in instantaneous value since the amplitude is a function of the cube of the distance.

When the Moon is at perigee, it is closest to the Earth in its orbit and, thus, the tide raising forces are the strongest. This effect can be enhanced further if perigee occurs at the time of Moon-Earth-Sun alignment known as syzygy (i.e., full or new moon) for then the gravitational attractions of the Moon and Sun act to reinforce each other. When this close alignment of perigee and syzygy occurs (i.e., the line of apsides and line of syzygies are nearly coincident) a perturbation called lunar evection increases the eccentricity of the lunar orbit which in turn decreases the Earth-Moon distance at perigee with a subsequent increase in the gravitational

attraction. As a result, the tidal potential at the sublunar point will be even more negative than usual. However, since the eccentricity of the Moon's orbit is increased, it not only makes perigee closer but it also makes the point of apogee farther from the Earth producing an opposite effect on the monthly average lunar potential.

Given a perigee-syzygy event there are basically three factors which can further enhance this effect: 1.) the phase of the Moon (i.e., full or new), 2.) the declinational planes of the Moon and Sun, and 3.) whether the Earth is at perihelion. The phase of the Moon is important because the gravitational attraction of the Sun on the Moon is not the same at full and new moon. At full moon the gravitational attraction of both the Earth and Sun on the Moon are in the same direction and causes the Moon to move to a position closer to the Earth than if just the Earth were present. At new moon the gravitational attraction of the Earth and the Sun on the Moon are directed in opposite directions plus the Moon is now closer to the Sun than at full moon. As a result the lunar evection perturbation is not as great and the distance at perigee is not decreased as much as it is with full moon at perigee.

The only requirement for syzygy to occur is that the Moon and Sun be in the same celestial longitude. However, if they also are in the same declinational plane the combined gravitational attraction of the Earth and Sun on the Moon is noticeably increased at full moon, increasing the eccentricity of the orbit and bringing the Moon even

closer to the Earth.

The importance of perihelion is that the above influences are all enhanced when the Sun is closest to the Earth and thus to the Moon. In fact, Wood (1976) has tabulated all of the extreme perigee-syzygy events over the 400 year period from 1600 through 1999 and found that they all occurred near perihelion (Oct 31 through Mar 8), at full moon when the Sun and Moon were nearly in the same declinational plane. Voigt (1974) has stated that the minimum Earth-Moon distance occurs under the following conditions:

a. Full Moon

b. Perigee

c. Moon between the nodes

d. Earth at perihelion

At perihelion the Sun is at about 281° in right ascension so the full moon would be at 101° which puts it near its maximum positive declination and since the Sun is at about its maximum negative declination, having just passed through the winter solstice, the two bodies are nearly coplanar.

Having examined the main factors influencing the Earth-Moon distance, it remains to be seen what effect this has on the forcing. If we now define this distance, D, as the average distance plus some sinusoidal variation (e.g., the anomalistic month) then:

$$\begin{aligned} D^3 &= (\bar{D} + D'\cos A)^3 \\ &= \bar{D}^3 + 3\bar{D}^2 D'\cos A + 3D'^2\bar{D}\cos^2 A + D'^3\cos^3 A \\ &= \bar{D}^3[1+3(D'/\bar{D})\cos A + 3(D'^2/\bar{D}^2)\cos^2 A \\ &\quad + (D'^3/\bar{D}^3)\cos^3 A] \end{aligned} \qquad 2.29$$

Letting h=D'/D and x=cosA we have

$$D^{-3}=\bar{D}^{-3}[1 + 3hx + 3h^2x^2 + h^3x^3]^{-1}. \qquad 2.30$$

Using a Taylor Series expansion of D about 0 yields:

$$D^{-3}=\bar{D}^{-3}[1 - 3hx + 6h^2x^2 + ...]^{+1} \qquad 2.31$$

By retaining only the second order terms equation 2.4 becomes:

$$U_{tidal}=-(3/2)(Gma^2/\bar{D}^3)[1 - (3D'/\bar{D})\cos A + (6D'^2/\bar{D}^2)\cos^2 A][\cos^2\lambda - 1/3]. \qquad 2.32$$

We will see that the nodal frequency dominates the forcing. Looking then at the varying part of equation 2.32 we have:

$$U'_{tidal} = [1-(3D'/\bar{D})\cos A + (6D'^2/\bar{D}^2)\cos^2 A]\cos No. \qquad 2.33$$

The maximum <u>instantaneous</u> distance variation possible is 27,990 km. Thus D'/D is .0728 and this value squared is .0053 making the main contribution to U'_{tidal} the unmodulated nodal cycle. When dealing with monthly averages, the D' value is much less making the effect of distance variation seemingly minimal on the monthly average of the forcing. Thus, even though D was a constant in the calculations, this did not have any great impact on the monthly average potential values.

2.2.3 Magnitude of lunar tidal potential.

At a given location on the Earth, Term 1 (Eqn. 2.9) is only dependent on the declination of the Moon, while Terms 2 and 3 are also dependent upon the longitude of the sublunar point. The Moon passes over the same longitude once every 24 hr 50.47 min. Thus, over that period the part of the potential determined by Terms 2 and 3 nearly averages out to zero. It does not average out exactly to zero,

however, since the latitude of the sublunar point changes slightly over that time. This can be seen by looking at Table 2.1 which shows the instantaneous values of the three terms at various configurations of the Moon's declination and hour angle. The global pattern corresponding closely to Table 2.1.1 is seen in Figure 2.3 which is the instantaneous potential for August 0.0 1948. The sublunar point is at 24.85°N, 239.67°W. The slight difference between these numbers and those in Table 2.1.1 exists because the table assumes a constant Earth-Moon distance whereas the figure uses Doodson (1921) harmonics which have the effect of the variable Earth-Moon distance included.

Instantaneously, Terms 2 and 3 can be an order of magnitude larger than Term 1 as seen in Table 2.1. However, the magnitude of Terms 2 and 3 are two orders of magnitude less than Term 1 when a monthly average is considered. For example, the values for June 1904 were: Term 1, -0.34174 m^2s^{-2}; Term 2, -0.00165 m^2s^{-2}; and Term 3, 0.00049 m^2s^{-2}.

One interesting point to note about Term 1 is that at 35.26°N and at 35.26°S the term goes to zero. Poleward of this latitude the factor, $(\cos^2\theta - 1/3)$ of Eqn. 2.9, is positive and equatorward it is negative. Terms 2 and 3 are zero at the poles while Term 2 is also zero at the equator.

2.2.4 Affect of geographic location on each term.

2.2.4.1 Term 1.

A look at Equation 2.9 for Term 1 shows that it has no longitude

TABLE 2.1

Instantaneous Lunar Tidal Potential

Table 2.1.1 Moon at 25°N with Earth location at 25°N, 75°E

$\delta = 25°N$ $(\alpha+\phi)$	0°	90°	180°	270°
Term 1	-0.1888	-0.1888	-0.1888	-0.1888
Term 2	-1.5430	0.0	1.5430	0.0
Term 3	-1.7740	1.7740	-1.7740	1.7740
Total	-3.5058	1.5852	-0.4198	1.5852

Table 2.1.2 Moon at 0°N with Earth location at 25°N, 75°E

$\delta = 0°N$ $(\alpha+\phi)$	0°	90°	180°	270°
Term 1	-0.4068	-0.4068	-0.4068	-0.4068
Term 2	0.0	0.0	0.0	0.0
Term 3	-2.1597	2.1597	-2.1597	2.1597
Total	-2.5665	1.7529	-2.5665	1.7529

Table 2.1.3 Moon at 25°S with Earth location at 25°N, 75°E

$\delta = 25°S$ $(\alpha+\phi)$	0°	90°	180°	270°
Term 1	-0.1888	-0.1888	-0.1888	-0.1888
Term 2	1.5430	0.0	-1.5430	0.0
Term 3	-1.7740	1.7440	-1.7440	1.7740
Total	-0.4198	1.5852	-3.5058	1.5852

Term 1, Term 2, and Term 3 were calculated from equations 2.9, 2.10, 2.11, respectively.

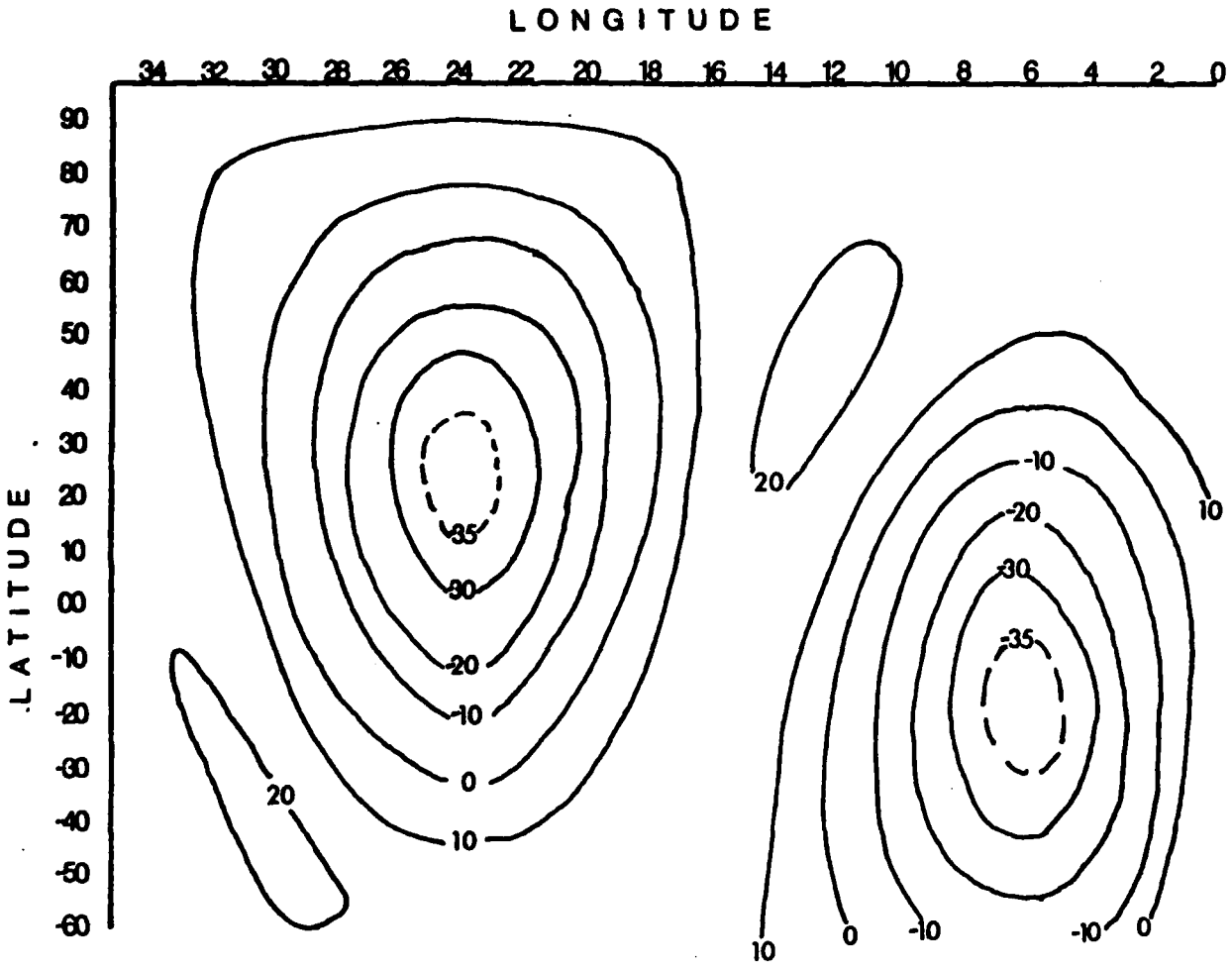

Figure 2.3. Instantaneous lunar potential for the first instant of August 1948 (units are $m^2 s^{-2} \times 10^{-1}$).

dependence and that it varies latitudinally by the factor, $(\cos^2\theta - 1/3)$, where θ is the colatitude of the location. Thus all points between 35.26°S and 35.26°N are in phase with each other and 180° out of phase with all points poleward of these latitudes.

2.2.4.2 Term 2 and Term 3.

Both of these terms have a latitudinal and longitudinal dependence. Looking at the factor $\cos(\alpha+\phi)$ and considering the hour angle α as the sum of the initial hour angle at the beginning of the month, α_0, plus the change, α_t, up to time t we have $\cos(\alpha_t+\alpha_0+\phi)$. Thus, the phase for this term is $\alpha_0+\phi$. In other words, the timing of maximum and minimum values at a location is dependent on both the initial hour angle, α_0, and the longitude, ϕ, of the point.

2.2.5 Important frequencies associated with each term.

The calculations described above were performed for a location at 25°N, 75°E for the years 1899 through 1960 for June. Five monthly average time series were generated:

Total lunar potential U ($=U_1 + U_2 + U_3$)

Term 1 potential, U_1

Term 2 potential, U_2

Term 3 potential, U_3

Term 2 + Term 3 potential, U_{23}.

To see which frequencies were predominant a periodogram of each time

series was constructed. The results are summarized in Table 2.2.

Note: The periodogram was calculated using tenth band intervals, therefore, with a 62 year time period a resolution of .0016 $year^{-1}$ was attainable. Thus, for the frequency .0532 $year^{-1}$, the next lower frequency would be .0516 $year^{-1}$ and the next higher frequency would be .0548 $year^{-1}$.

This table shows that the two frequencies .0532 $year^{-1}$ and .2645 $year^{-1}$ explained almost 100 percent of the variance for U. For U_1 the two frequencies were .0532 $year^{-1}$ and .2629 $year^{-1}$. Most of the variance for U_2 and U_3 is explained by the frequency between .2629 $year^{-1}$ and .2645 $year^{-1}$. Thus, all three terms exhibit a frequency around .263 $year^{-1}$; however, looking at the amplitudes of this frequency for the three terms, we see that U_1's amplitude is over three times that of U_{23}.

The origin of the two frequencies .0537 $year^{-1}$ and .263 $year^{-1}$ will be examined in the next two sections.

2.3 Lunar tidal potential at the nodal frequency (.053725 $year^{-1}$)

As Table 2.2 shows, the nodal cycle is the predominant frequency in the monthly mean lunar potential time series and explains over 95 percent of the interannual variance for the month of June.

The nodal cycle of 18.6 year period is the time it takes the pole of the Moon's orbit to rotate about that of the ecliptic. The Moon's orbital plane is inclined to the ecliptic at an average angle of 5°9'. Figure 2.4 taken from Wood (1976) shows how the nodal cycle

TABLE 2.2

Important Frequencies for June Lunar Potential at 25°N, 75°E

Term	Freq	Percent Var/ Amplitude	Phase	Freq	Percent Var/ Amplitude	Phase
U	.0532	96.9/4.0E-02	96.9	.2645	2.7/6.6E-03	166.9
U_1	.0532	95.5/4.0E-02	96.3	.2629	4.0/8.1E-03	-156.5
U_2	--	--	--	.2629	89.6/2.7E-03	84.1
U_3	--	--	--	.2645	76.9/8.0E-04	-46.7
U_{23}	--	--	--	.2645	85.1/2.5E-03	49.3

varies the latitudinal range over which the Moon traverses during one sidereal month. His diagram assumes an inclination of 5° for simplicity.

When the ascending node is at the vernal equinox (i.e., the subsolar point on the celestial sphere at the time of the vernal equinox), the Moon achieves its maximum declination of 28.6° north and south; whereas 9.3 years later when the ascending node is at 180° from the vernal equinox, the maximum lunar declination is 18.3° north and south.

As Table 2.1 and Figure 2.3 show, the instantaneous potential at the sublunar point is negative. If during the course of the sidereal month, the Moon is constrained to the $\pm$ 18.3° latitudinal range then the average potential for the month will be lower in this region than if it had a larger range, for the large area of negative potential seen in Figure 2.3 is also constrained. Table 2.3 shows this effect. In the table are the calculated values of the average June lunar potential for the years 1903-1922 at 25°N, 75°E along with the maximum declination for that particular June. As one can see the further north the sublunar point can be the less negative the average potential. The lack of an exact correspondence between the average potential and the maximum declination is because of an effect related to the date during the month on which the Moon reaches its maximum declination. This will be discussed in section 2.4.

Since the nodal cycle arises from Term 1, this cycle has no longitude dependence. Thus, in years when the ascending node is near

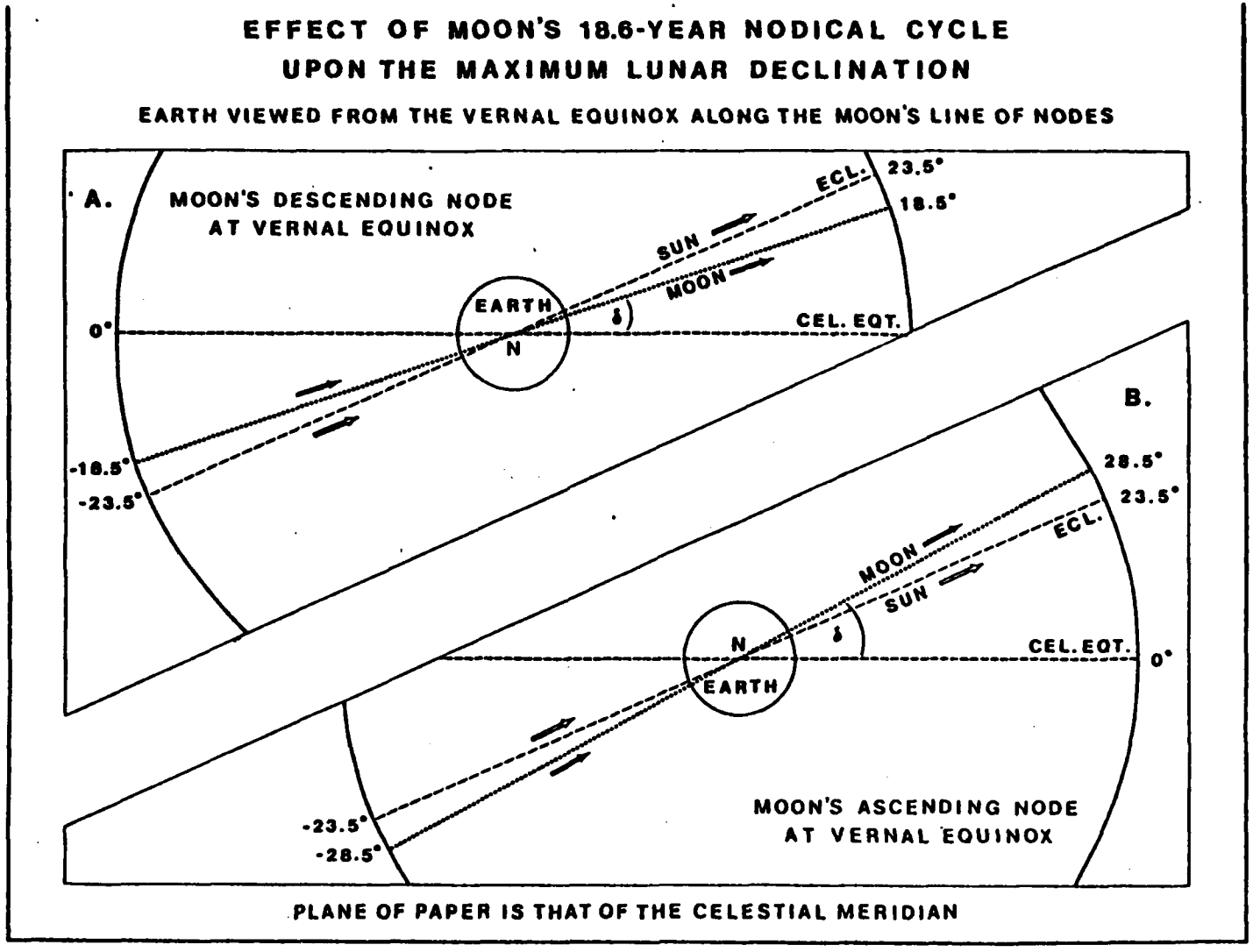

Figure 2.4. Effect of the nodal cycle on the latitudinal range of the sublunar point (from Wood, 1976).

TABLE 2.3

Relationship of Average Potential to δ_{max} and ϕ_{max}

YEAR	JUNE AVERAGE POTENTIAL	δ_{max} MAX DECLINATION	ϕ_{max} TIME OF MAX DECLINATION
1903	-.3478 m^2s^{-2}	18.58°N	day 23.38
1904	-.3429	18.48	13.04
1905	-.3375	19.08	3.67
1906	-.3355	20.32	21.33
1907	-.3217	21.86	11.46
1908	-.3025	23.53	0.33
1909	-.2897	25.16	17.58
1910	-.2893	26.58	7.63
1911	-.2743	27.61	25.21
1912	-.2591	28.26	14.38
1913	-.2616	28.48	4.54
1914	-.2770	28.19	21.79
1915	-.2766	27.46	11.54
1916	-.2780	26.37	0.25
1917	-.2907	24.95	17.33
1918	-.3165	23.30	7.46
1919	-.3253	21.62	25.21
1920	-.3296	20.12	14.75
1921	-.3407	18.96	5.33
1922	-.3487	18.46	23.38

the vernal equinox the latitudinal distribution of the lunar potential anomaly due to the nodal cycle is as seen in Fig. 2.5.1 and just the opposite when the ascending node is at the autumnal equinox as in Figure 2.5.2.

2.4 Lunar tidal potential at frequency of .263 year^{-1}.

Once the nodal cycle has been considered, the only other frequency that explains more than one percent of the variance is a frequency around .263 year^{-1}. There are two parameters of the Moon's orbit for a given month that determine the lunar tidal potential anomaly at this frequency. They are the time of maximum declination and the hour angle at the first instant of the month.

2.4.1 Time of maximum declination, ϕ_{max}.

2.4.1.1 Influence on Term 1.

Table 2.3 shows the day (ϕ_{max}) when the Moon is at its maximum declination for the month of June in the years indicated. This timing is the single most important factor in determining the magnitude of the lunar potential monthly average for Term 1 if the nodal cycle influence is held constant. As already discussed, Term 1 is the largest of the three terms by a factor of 100 when monthly averages are calculated and the amplitude of this frequency is over three times that of the other two terms combined. Therefore, by considering just this term we can see the effect that the time of maximum declination has on the tidal potential.

FIGURE 2.5.1 - NODE AT 0 DEGREES RIGHT ASCENSION

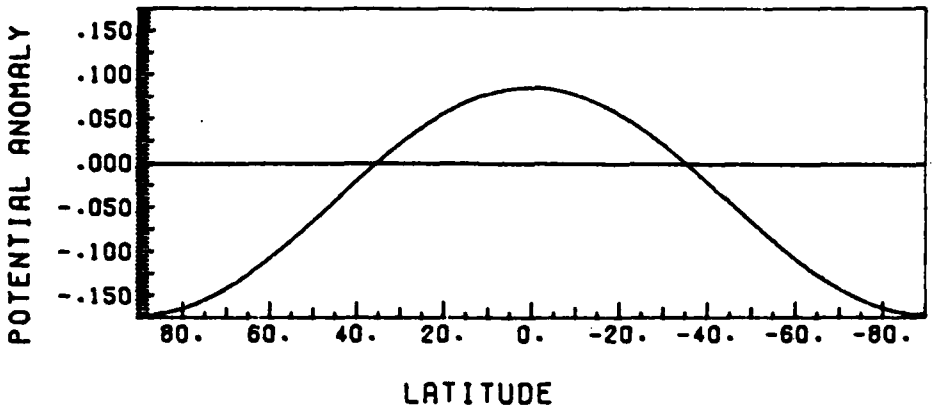

FIGURE 2.5.2 - NODE AT 180 DEGREES RIGHT ASCENSION

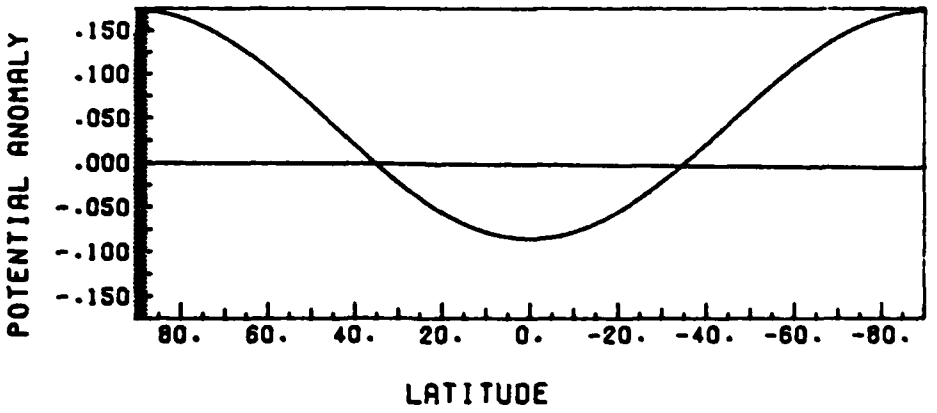

Figure 2.5. Latitudinal distribution of the lunar potential anomaly at the extremes of the nodal cycle (units are m^2s^{-2}).

Term 1 is dependent on the declination of the Moon (Δ in Fig 2.1 and Eqn. 2.9) only and not on the hour angle. Since Δ is a function of the cosine of the sidereal month (see Eqn. 2.28), the average value of Δ, for a given δ_{max}, after 27.3216 days is the same no matter what value ϕ_{max} has. Thus, it is the remaining days of the month that determine if the potential will be above or below the first 27.3216 day average. If the Moon begins the month near maximum north declination, it will end the month in that position also. This configuration produces the maximum potential (smallest negative). Likewise if the Moon starts the month at maximum south declination, the same result is achieved since the tidal potential at the sublunar point is nearly matched on the opposite side of the earth (e.g. see Figure 2.3). The minimum monthly average potential occurs when the average latitude of the Moon for the remaining days of the month is over the equator. The reason for this can be seen qualitatively from Figure 2.3. In this figure the sublunar latitude is about 25°N. To calculate an approximate lunar potential average for a location at latitude 25°N for the day depicted in this figure, all one need do is average the instantaneous values across all longitudes. This average is a smaller negative number than one would obtain if the Moon were over the equator. In this case both large areas of negative potential in Figure 2.3 would be displaced toward the equator producing a more negative daily average at 25°N.

Since the number of days involved in the residual beyond the sidereal month varies depending on the length of the month, the time

of maximum declination that produces the maximum/minimum potential varies slightly from month to month. For a month with 30 days the following values for the time of maximum declination, ϕ_{max}, pertain for a location between 35.26°N and 35.26°S:

maximum average monthly potential with ϕ_{max} either at 1.34 or 15.00 days, and

minimum average monthly potential with ϕ_{max} either at 8.17 or 21.83 days. Thus, the largest of the three terms contributing to the total potential is very dependent on the timing of maximum declination during a given month.

2.4.1.2 Origin of the .263 year^{-1} frequency.

A periodogram of the time series (1899-1960) of ϕ_{max} for the month of June yields the two largest peaks at .2629 year^{-1} (15.2 percent of the variance) and at .3677 year^{-1} (61.4 percent). Nonlinear regression more accurately defines these peaks at .26308 year^{-1} and .36834 year^{-1}.

The equation relating the declination and right ascension of the Moon is:

$$\sin\delta = 0.406\sin\alpha + 0.008\sin3\alpha + 0.090\sin(\alpha-N) + 0.006\sin(3\alpha-N), \quad 2.34$$

where δ is the declination,

α is the right ascension,

N is the longitude of the ascending node.

This shows that, by considering the first and by far the largest term

on the right hand side, the Moon attains its maximum northward declination at a right ascension of 90° and its maximum southward declination at a right ascension of 270°. Thus, the point of its maximum northward declination is always at the same point in the orbit with respect to the stars. This period, from 90° back to 90° again, is the sidereal month whose value is determined by considering the nodical month (Nm) and nodal cycle (No) as follows:

$$\text{Sidereal lunar month} = (1/Nm - 1/No)^{-1} \qquad 2.35$$

$$= (1/27.21222 - 1/6798.36575)^{-1} = 27.321582 \text{ days}$$

In one tropical year (365.2422 days) the Moon is thus at its maximum northward declination 13.3683 times. By sampling this cycle only once every year we see the alias at .3683 year^{-1} as was found in the periodogram and nonlinear regression of the ϕ_{max} time series.

In actuality the important frequency is the first harmonic of .3683 year^{-1} since the spectral analysis does not take into account that the same average potential results when the Moon is at its maximum southward declination as discussed in the previous section. There we saw that a maximum northward declination time of about 1.34 days yields the same average monthly potential as a maximum declination time of 15.0 days. We are now looking at a period of 13.6608 (27.321582/2) days which goes through 26.736534 cycles during a tropical year. This frequency aliases at .2635 year^{-1} when sampling is done once a year. This then is the frequency to expect to find in a time series of potential and can be found by calculating the first harmonic of the peak near .368 year^{-1}. In the case of June

(1899-1960) the peak is at .36834 $year^{-1}$ giving a first harmonic at .7367 $year^{-1}$ which aliases at .2633 $year^{-1}$.

For August the two largest peaks in the periodogram of ϕ_{max} are at .2662 $year^{-1}$ (14.1 percent) and at .3677 $year^{-1}$ (57.9 percent). Refinement by nonlinear regression yields .2655 $year^{-1}$ and .3674 $year^{-1}$. The first harmonic of the largest peak aliases at .2652 $year^{-1}$. Thus, there is a difference in the frequency to expect for June and August.

The relative latitudinal distribution of the anomalies at this frequency will be the same as in Figure 2.5 because both frequencies come from Term 1 which has a $(\cos^2\theta - 1/3)$ latitude dependence. The only difference is that the .263 $year^{-1}$ anomalies have a smaller magnitude.

2.4.2 Hour angle of the Moon at the beginning of the month, α_0.

Figure 2.6 shows a scatter diagram of hour angle, α_0, versus ϕ_{max} for the months of June and August. The data were taken from the American Ephemeris and Nautical Almanac. In both months it is clear that associated with each ϕ_{max} there is an α_0; however, the associated α_0 is different from one month to another. Between June and August the difference is 60 to 70 degrees. This difference plays an important role in Terms 2 and 3 which are dependent on the hour angle of the Moon.

As we have seen in Table 2.2 the frequency around .26 $year^{-1}$ appears in all three terms. We have now also seen that ϕ_{max}, which

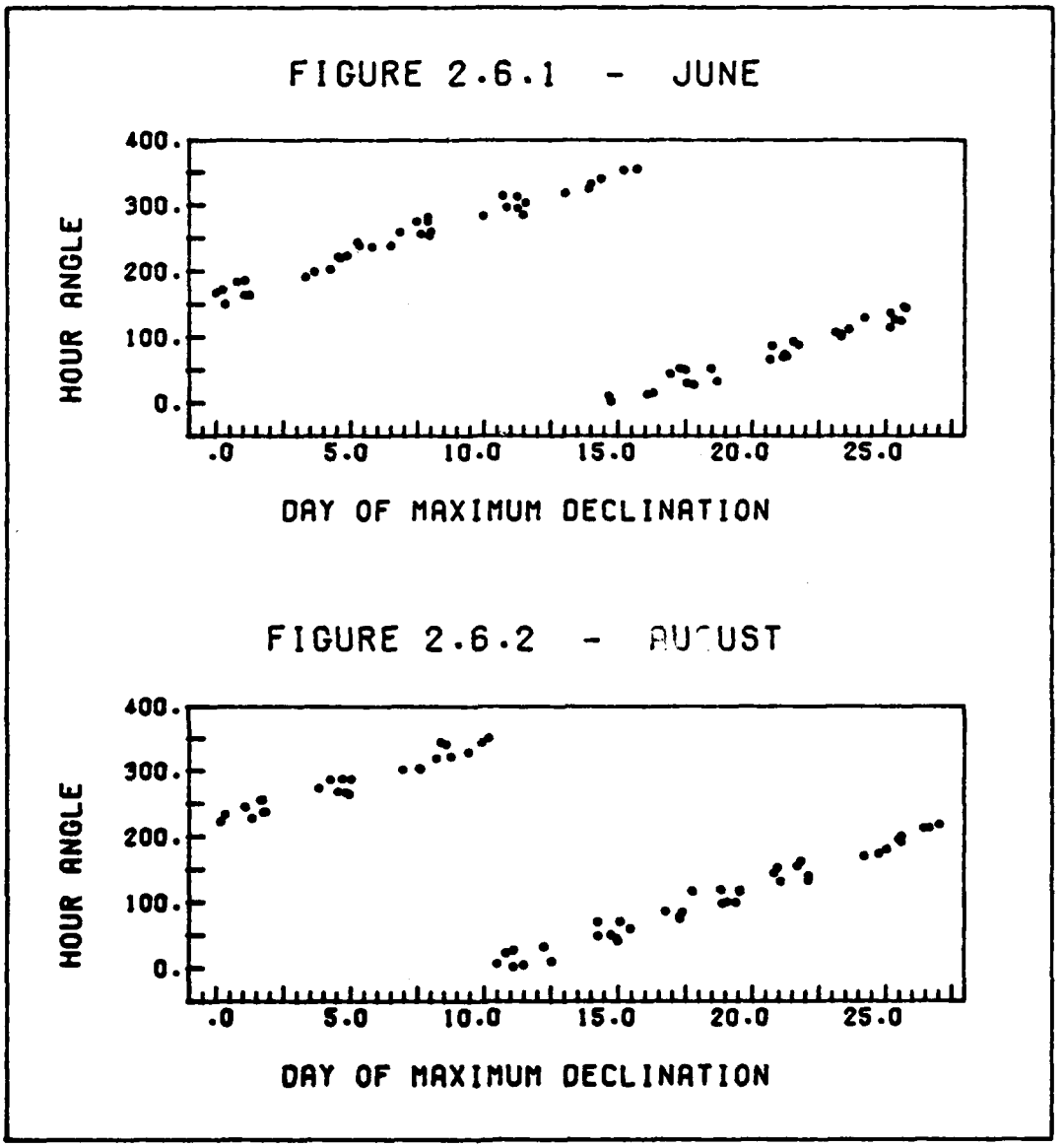

Figure 2.6. Scatter diagram of the hour angle of the Moon at the beginning of the month versus the day of maximum declination.

determines the .26 year^{-1} phase in Term 1, is associated with α_0 which in turn affects when Terms 2 and 3 will be a maximum at a given longitude. Thus, if α_0 produces a maximum value at the frequency .26 year^{-1} in Terms 2 and/or 3 at the same time that ϕ_{max} produces a maximum at that frequency, then the total potential will have a stronger signal at .26 year^{-1}.

2.5 Component Force (F_x and F_y) derived from lunar potential.

Taking the negative gradient of the lunar potential field results in the associated horizontal tidal force:

$F = -dU/dS$ where S is along the gradient.

The tidal force anywhere on the Earth can be resolved into a component vertical to the Earth's surface and another horizontal to it. The horizontal, or tractive, force is the one that produces the tides. We shall briefly consider both the X and Y components of the horizontal force.

2.5.1 F_y component.

Term 1 is the major contributor to this component of the force. As noted earlier there is a nodal point in the potential at 35.26° north and south. This establishes the variability of the potential as a standing wave. As seen before this variability is dominated by two frequencies, .053725 year^{-1} and .263 year^{-1}. Figure 2.5 showed the latitudinal distribution of the potential at the extremes of the nodal cycle. Now, since the force is the negative gradient of the

potential we see the configuration of Figure 2.5.1 gives a positive Y-component (i.e., a northward directed force) and the opposite configuration would give a negative Y-component (i.e, a southward directed force).

The steepest part of the potential gradient is between 35°N and 55°N and thus the largest positive and negative Y-components of the lunar tidal force exist in this region.

2.5.2 F_x component.

The F_x component of the lunar tidal force is totally dependent on Terms 2 and 3. There is absolutely no contribution from Term 1.

As discussed earlier the timing of the maximum/minimum value of potential at a given longitude and latitude is dependent upon α_0 (for Terms 2 and 3). At a given longitude where a relative maximum in the east/west direction occurs, the X-component would be positive to the east of this longitude and negative to the west. The opposite would be true for a longitude where a relative minimum occurs.

Figure 2.7 shows the average F_x component of the lunar force for August 1947. The potential is a relative minimum approximately along 230°W and 50°W, thus, there is a net acceleration towards these longitudes in the X direction.

Table 2.4 shows a time series (1940-1960) of average monthly (August) values of lunar potential for Term 2 plus Term 3 at 25°N for three longitudes, 30°E, 75°E, and 120°E. Note that in certain years (e.g., 1947 and 1949) the northern India location (25°N, 75°E) is a

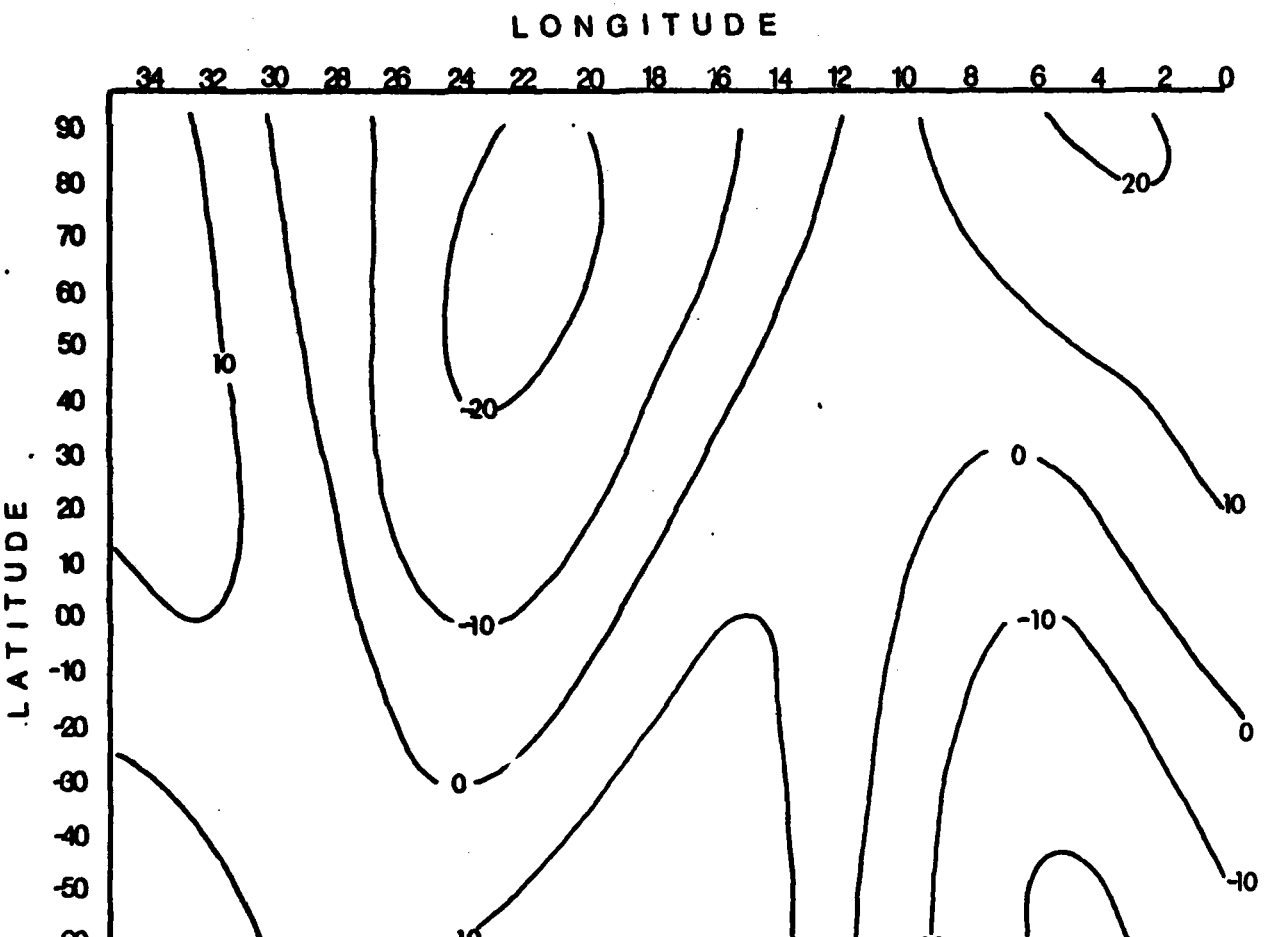

Figure 2.7. Monthly average of the x-component of the lunar force for August 1947 (units are $ms^{-2} \times 10^{-10}$).

TABLE 2.4

Average August Values of Lunar Potential (Term 2 + Term 3) at 25°N for the Longitudes and Years Indicated
Units are $m^2s^{-2} \times 10^{-4}$

Year	30°E	75°E	120°E
1940	-49.6	-40.3	26.6
1941	-8.3	44.6	48.0
1942	41.2	25.9	-42.9
1943	-16.2	-68.1	-49.9
1944	-46.7	-15.8	42.6
1945	9.3	54.0	39.8
1946	50.3	5.0	-75.9
1947	-34.7	-68.9	-27.4
1948	-30.2	15.0	53.3
1949	30.6	61.4	21.5
1950	45.7	-22.9	-100.0
1951	-55.6	-76.0	-18.2
1952	-40.2	24.1	55.0
1953	22.1	59.9	19.7
1954	32.7	-36.4	-96.7
1955	-57.5	-59.8	1.2
1956	-22.6	38.3	49.9
1957	34.5	50.6	-11.4
1958	13.6	-49.9	-76.8
1959	-40.9	-28.6	22.6
1960	-5.1	50.6	39.8

relative minimum or maximum producing an acceleration either toward or away from the region.

2.6 Summary.

The nodal frequency (.053725 year^{-1}) dominates the spectrum of average monthly lunar potential. A frequency around .263 year^{-1} is the only other one that explains more than one percent of the variance. Both of these frequencies are directly related to some aspect of taking the monthly average of the fortnightly tide. Fig. 2.8 shows the approximate latitude of the sublunar point versus the day of the month with ϕ_{max} equal to 0.0 or 27.32 and δ_{max} equal to 28.6°N. The nodal cycle is dependent on the range of latitude while the other lunar tidal potential frequency, .263 year^{-1}, is dependent upon what the sublunar latitude is at the beginning of the month. The time of maximum northward declination (ϕ_{max}) for the month was the parameter used to prescribe this latitude in Equation 2.28.

Based on the analysis in this chapter one would expect that if lunar tides in the atmosphere have an impact on climatic interannual variability, the two frequencies found to be the most important in the interannual variability of the lunar potential would exist in the time series of climatic variables. The working hypothesis then is that atmospheric lunar tides <u>do</u> produce a significant signal in climatic variability. It now remains to test this hypothesis. The next chapter will be devoted to this effort.

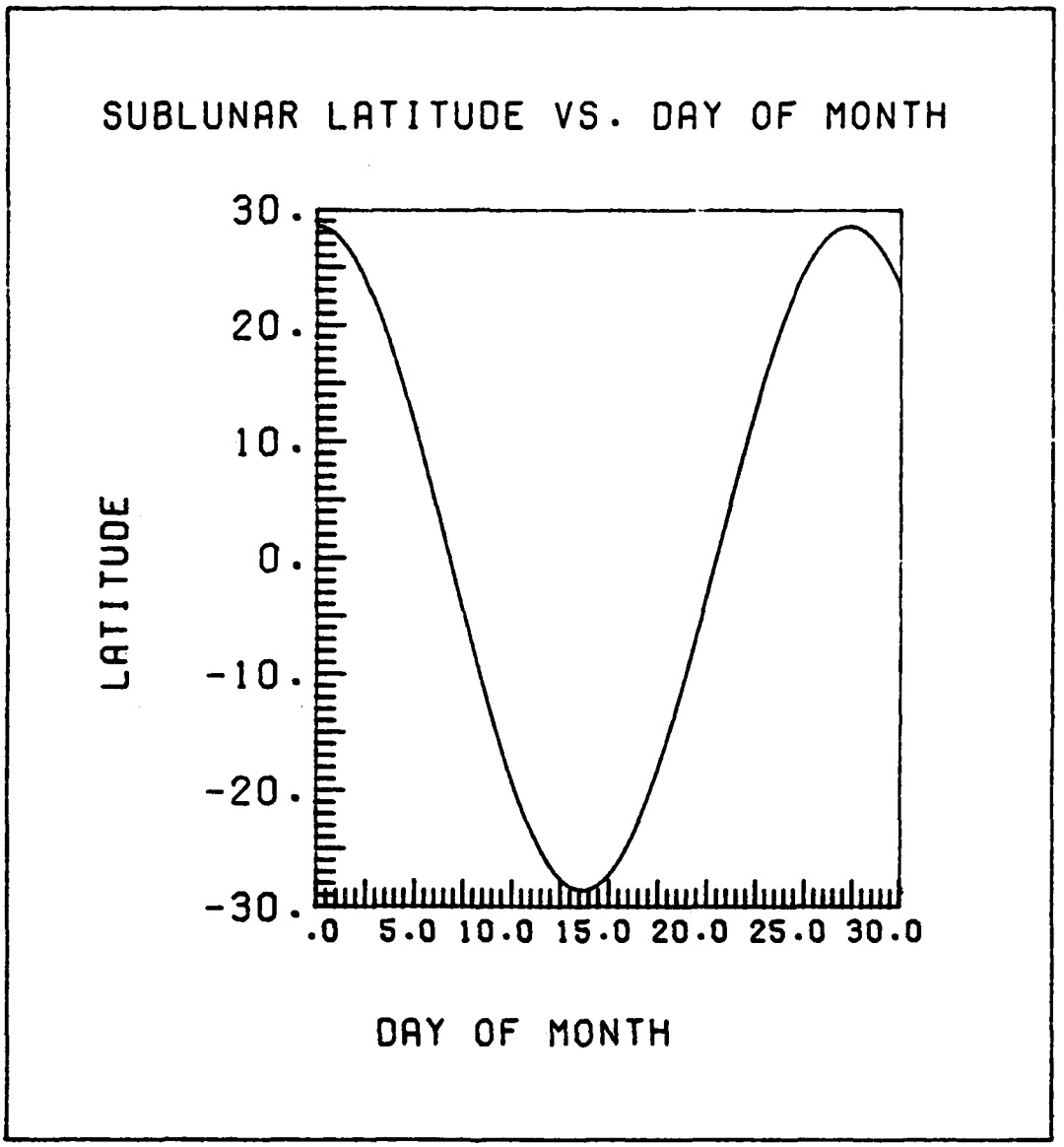

Figure 2.8. Example of the sublunar latitude versus the day of the month showing the sidereal period (27.3216 days). The nodal cycle is dependent upon the latitudinal range of the Moon during the month while the frequency .263 year^{-1} is dependent upon the latitudinal position of the Moon at the end of the month.

CHAPTER 3

Periodic Component: Test of Hypothesis - Observed Response

3.1 Introduction

No single theory of climatic variability can explain all of the observed interannual variance because the climate is controlled by many factors. The last chapter presented one forcing mechanism, lunar tides, that was hypothesized to account for some fraction of the climatic interannual variability. We saw that two frequencies dominate the spectrum of average monthly lunar tidal potential. The frequency that explained the most variance (.0537 $year^{-1}$) was associated with the nodal cycle. The only other spectral peak of any consequence was at a frequency around .263 $year^{-1}$ in June. This frequency was associated with the time of the month that the maximum north or south declination occurred which essentially determined what residual part of the sidereal month (27.3216 days) did not average out to zero during the 30 days of June.

In this chapter the hypothesis that lunar tidal forces have an impact on interannual variability will be tested. To test the hypothesis we must examine a region that is sensitive to this forcing. As Pearson (1982) showed, a highly significant periodic signal (possibly related to the Chandler tide) in the December temperatures in the upper Midwest was observable because this area lies close to the boundary between cold Arctic air and milder Pacific air at this time of year. Thus, a small shift from the

normal position of the Arctic front can have a large influence on the mean December temperatures. This periodicity in temperature results from the interaction of the forcing (the proximal cause being pressure anomalies in northern Canada) and the synoptic singularity which makes the upper Midwest particularly sensitive to the periodic signature of the forcing. In India, June is marked by another climatic singularity, the onset of the monsoon. As discussed in Chapter 1, June precipitation in northern India is particularly sensitive to the timing of the onset just as December temperatures in the upper Midwest are sensitive to the timing of the transition from a late fall to winter flow pattern.

Lunar tidal forcing is always acting on the atmosphere; however, it is likely that its effect would be most readily observable in a region that is especially sensitive to a synoptic singularity like the monsoon front where small departures from the front's normal position can have a large impact on the percent of normal rainfall received. Therefore, if lunar forcing does have an effect on the climate, then in this sensitive region one or both of the two lunar frequencies described in Chapter 2 might be expected to exist in the spectrum of interannual variability.

The lunar forcing hypothesis will be tested by examining how average monthly June station pressure, cube rooted precipitation, and 300 mb height data respond at these two hypothesized frequencies. First the responses of these three climatic variables at the hypothesized frequencies will be calculated to see if the

signal is strong enough to produce a consistent, synoptic climatology between them. If so, then it remains to be seen if these three variables are dynamically related to and in phase with the hypothesized forcing.

It should be emphasized that this research is dealing with interannual variability. In northern India the interannual variability of June precipitation is about 38 percent of the intra-annual variance of monthly precipitation and, thus, equals only one to two percent of the daily variance (if one considers that the variance of monthly precipitation amounts is about 1/30 that of the daily variance using the sampling distribution of means). Therefore, even if lunar tides account for a very small fraction of the total variance, this forcing mechanism becomes a candidate causal factor to consider when trying to understand interannual variability.

3.1.1 Atmospheric Susceptibility.

Under the hypothesis of an external forcing acting on the atmosphere, what is the nature of the response? The relationship between forcing and response can be written simply as :

$$R = kF_L(t) \qquad 3.1$$

where R is the atmospheric response to the forcing,

k is the susceptibility of the atmosphere to the forcing, and

F_L is the lunar forcing which is a function of time.

In the discussion that follows the nomenclature, F_{05} and F_{26}, will be used to represent the lunar forcing at the frequencies .0537 $year^{-1}$ and .263 $year^{-1}$, respectively.

In the case of December temperatures, described by Pearson, Equation 3.1 could be written as

$$R_{temp} = A\cos(2\pi ft + \phi) \qquad 3.2$$

where R_{temp} is the response of temperature to the forcing,
A is the amplitude of the response, and
$\cos(2\pi ft + \phi)$ is the periodic forcing.

The amplitude, A, of the response is the factor k of Equation 3.1 and indicates how susceptible the temperature is to the forcing.

Let us now examine what kind of susceptibility factor, k, might relate Indian monsoon climatic variables to the hypothesized lunar forcing. The factor, k, in the December temperature variability was taken as a constant and made the relationship between forcing and response linear. However, considering the nonlinearity of the atmosphere, this factor certainly does not have to be linear. Let us assume that the atmosphere is more susceptible to lunar forcing at certain times than at others. If this is so, then the susceptibility factor is also a function of time and the problem is no longer linear, for then we have:

$$R = k(t)F_L(t). \qquad 3.3$$

It is reasonable to think of k as being related to the strength of the monsoon circulation, for when the monsoon circulation is particularly strong, one would expect the effects of lunar forcing

to be minimal because northern India would no longer be sensitive to small fluctuations in the timing of monsoon onset since with a strong circulation the monsoon would arrive well before the end of the month.

Hemispheric temperature is one factor which has an important effect on the intensity of the monsoon circulation. Bryson and Swain (1981) compared a reconstructed history of monsoon rainfall in Rajasthan, India to what was happening to the temperature in the high latitudes and found that the period of very heavy monsoon rains (after 10,800 BP up to 3,700 BP) corresponded to a period when the region of cold Arctic climate (defined as the area to the north of the tundra/boreal forest boundary) had retreated 280 km to the north of its present day position. During the monsoon drought period in Rajasthan from 3,700 BP to 2,000 BP the tundra region expanded to the south of its present position. Other fluctuations in the monsoon rainfall since 2,000 BP can similarly be related to the Arctic temperatures. Studies (e.g., Van Loon and Williams, 1976; Brinkmann, 1979; and Groveman and Landsberg, 1979) have shown that the temperature trend that occurs in the Arctic and Subarctic region determines to a very large extent the overall trend in Northern Hemispheric temperature. Thus, a definite relationship should exist between Northern Hemisphere temperature changes and the intensity of the monsoon circulation. Providing further support to this idea with an emphasis on seasonality is a study (Kutzbach and Otto-Bliesner, 1982) which showed, by using a low resolution general

circulation model, that 9000 years ago when there was estimated to be 7 percent more solar radiation received during the Northern Hemisphere summer, the monsoon circulation was more intense. Thus, hemispherically warm periods produce strong monsoons; whereas, cold periods have more winter-like circulation patterns with weak monsoon circulations. Therefore, if we assume that the susceptibility factor is dependent on the strength of the monsoon circulation, then making it a function of Northern Hemisphere temperature seems like an appropriate step.

One source of data to determine a susceptibility factor based on Northern Hemispheric temperature comes from Jones et. al. (1982). They have published a 100 year time series of mean monthly and annual Northern Hemispheric temperatures. While there are difficulties with any such data set, the long term characteristics of Northern Hemispheric temperature may be determined. Fig 3.1 shows the mean annual Northern Hemsiphere surface temperature anomalies from Jones et. al. (op. cit.). A definite warming trend into the 1940's and then cooling into the 1970's is observed. As a first approximation to this temperature data, the best fitting cosine curve was found to be:

$$T_{JWK} = 0.37\cos[2\pi(.0057923)t - 2.464]. \qquad 3.4$$

This curve has a period of about 172.6 years with a maximum value occurring in 1948.7, and it explains 58 percent of the variance of the mean annual Northern Hemsiphere surface temperature time series. Looking at the time series of average temperature for the

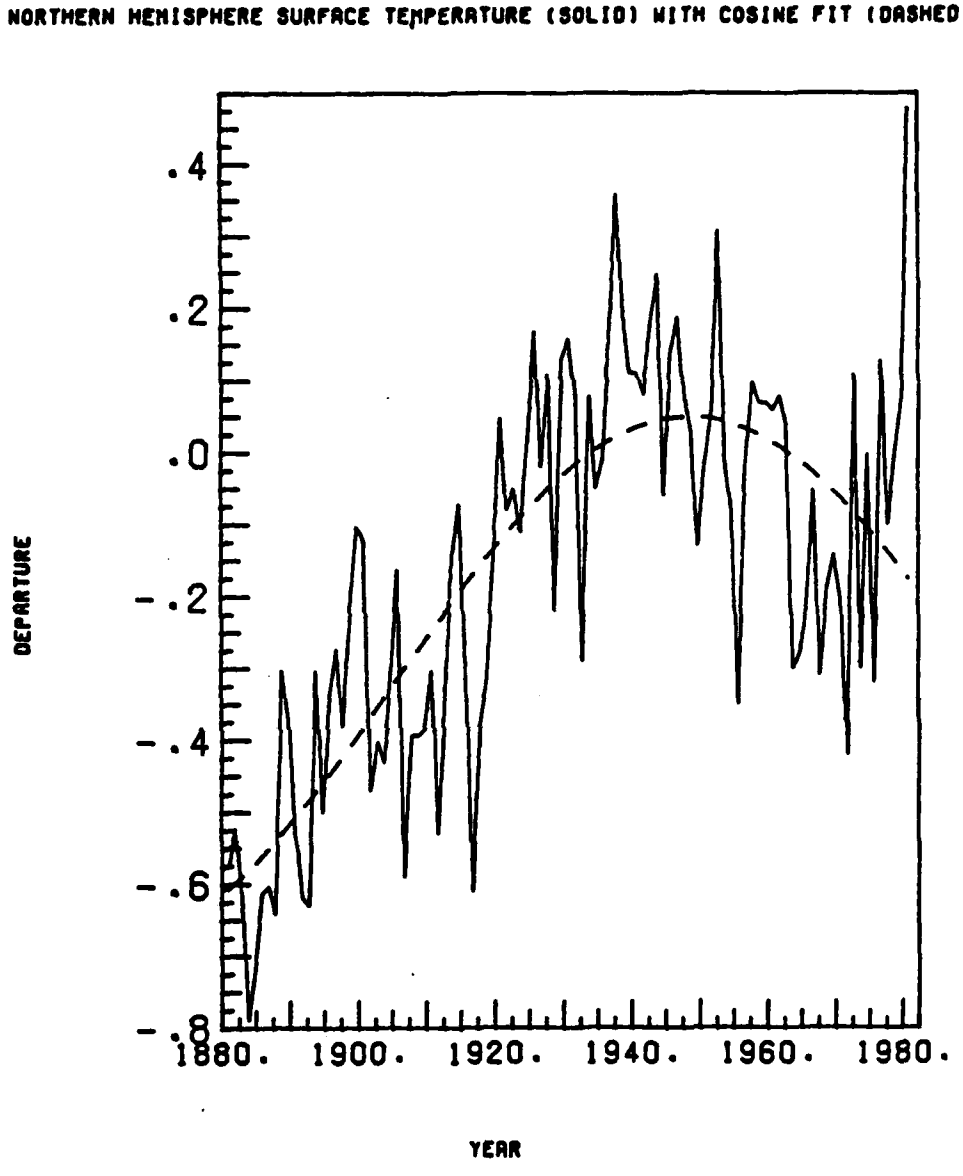

Figure 3.1. The solid line is the Northern Hemisphere annual mean surface temperature anomalies from the 1946-1960 mean (after Jones et. al., 1982). The dashed line is the best fitting cosine (explaining 58 percent of the variance) used in the susceptibility factor.

months April through July (i.e., around the time of the monsoon onset) the best fitting cosine is very similar to the one for the annual data.

A simple a priori hypothesis on how to incorporate this information into a susceptibility factor is to assume that when the hemisphere is warmest the tidal forcing has no effect on the monsoon circulation. This produces the following model for the theoretical response,

$$R = A[Q(t) - B]F_L \qquad 3.5$$

where B is set equal to 1.0, Q(t) is the cosine approximation to the Northern Hemisphere surface temperature in Equation 3.4, and F_L is the lunar forcing cosine. Thus, the factor in brackets ranges from a zero (warmest temperatures) to minus two (coldest temperatures). The parameter A allows for the sign and magnitude of the response. It is important to emphasize that this form of the susceptibility factor is only a first attempt to define this aspect of the variability. It may be, for example, that Q(t) and/or the entire susceptibility factor should be raised to some power. Further research will be required to gain greater insight into the characteristics of this nonlinear factor.

Now the nature of the theoretical response will be examined. As Equation 3.5 indicates, there are three main components to this response:

1. The lunar forcing cosine, F_L. The frequencies used (.0537 $year^{-1}$ and .263 $year^{-1}$) and the phase of each forcing

frequency were determined from the periodogram calculated in Chapter 2 and shown in Figure 3.2.1;

2. The cosine approximation, Q(t), to the Northern Hemisphere surface temperature which was discussed above; and

3. The term B which will be called the susceptibility threshold. The value of B will be empirically determined from the data.

As noted above, if B is one then at the warmest times the response to the forcing is zero. If B is less than one then for a certain period of time the response actually reverses sign. If B is greater than one then the response is always susceptible to the forcing but at varying degrees and it always has the same sign. As B increases the hemispheric temperature effect becomes less and less important. Thus, if B is large enough, this effect is essentially put to zero and only the forcing itself is important. Figure 3.3 shows the effect that the susceptibility threshold has. For the purposes of demonstration, a forcing frequency of 0.20 $year^{-1}$ and a modulating period of 180 years were used. In all four cases in Figure 3.3 year 20 has a relative minimum in the cycle. However, depending on the value of B, year 90 is either in phase, zero, or 180 degrees out of phase with year 20. Thus, the empirically determined value of the susceptibility threshold, B, determines how the temperature cosine (Q(t) in Eqn. 3.5) actually modulates the lunar forcing. We will see that the value of the susceptibility threshold has a regional character.

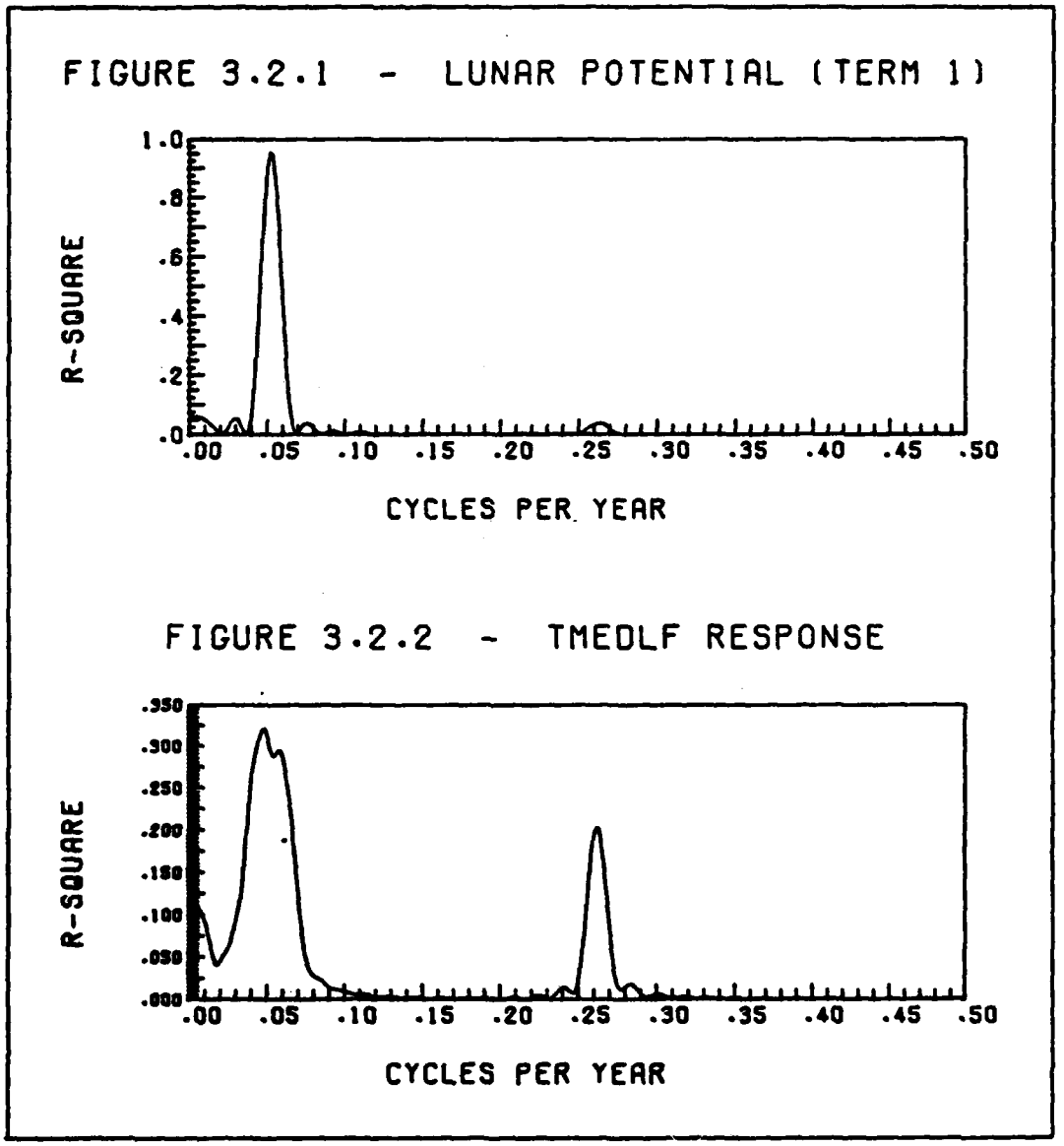

Figure 3.2. Periodograms of the lunar tidal potential (from Term 1) and the associated TMEDLF response for the years 1899 through 1960. The TMEDLF response time series was calculated using the amplitudes and phases for the frequencies .0537 year^{-1} and .263 year^{-1} from the lunar tidal potential time series (Term 1) along with the representative values of the susceptibility threshold as shown in Equation 3.6.

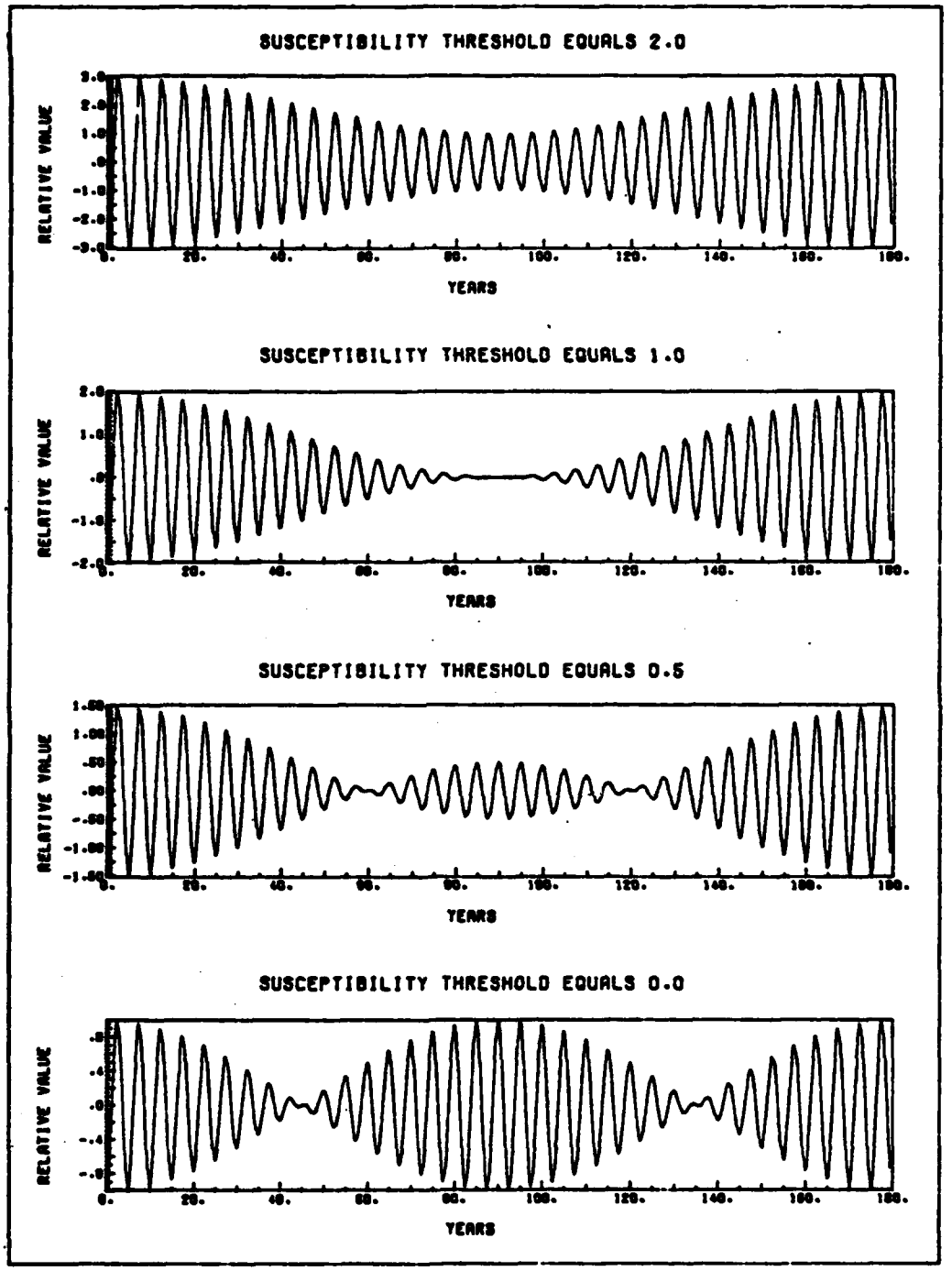

Figure 3.3 Time series for a response to a forcing with a five year period and a 180 year modulation. The only difference between each time series is the value of the susceptibility threshold. These plots show how sensitive the response is to the value of the susceptibility threshold in Eqn 3.5.

Since in this model of the response the amplitude of the lunar forcing is being modulated by a cosine derived from temperature data and since the characteristics of this modulation are governed by the empirically determined susceptibility threshold B, the expression "temperature modulation, empirically determined, of the lunar forcing" (TMEDLF) is appropriate. Therefore, throughout the rest of this thesis the theoretical response will be referred to as the TMEDLF response. It is the expected response based on the above theoretical discussion of lunar forcing and atmospheric susceptibility to this forcing. The TMEDLF response will be compared to the actual response observed in the pressure, precipitation, and 300 mb data to see if this observed response is, in fact, similar to the one predicted (i.e., the TMEDLF response).

A periodogram of the forcing time series developed in Chapter 2 (Fig. 3.2.1) shows the large peak at .0537 $year^{-1}$ and the much smaller one at .263 $year^{-1}$. We saw in Table 2.2 that these two frequencies alone explained almost 100 percent of the lunar potential variance. Therefore, to determine the nature of the TMEDLF response to this forcing, we can multiply each periodic component by the appropriate susceptibility factor as follows:

$$R = A_1[Q(t) - B_1]\cos(2\pi f_1 t + \phi_1) + A_2[Q(t) - B_2]\cos(2\pi f_2 t + \phi_2) + C \qquad 3.6$$

where $Q(t)$ is the cosine approximation to the Northern Hemispheric surface temperature,

f_1 is the frequency, .0537 year^{-1}, in the lunar tidal potential,

A_1, ϕ_1 are the amplitude and phase of f_1,

B_1 is the susceptibility threshold for the response at the f_1 frequency,

f_2 is the frequency, .263 year^{-1}, in the lunar tidal potential,

A_2, ϕ_2, B_2 are to f_2 as A_1, ϕ_1, B_1 are to f_1, and

C is the mean potential value.

There is no reason to assume that the susceptibility factor is the same for both frequencies and, in fact, we will see that the empirically determined value for term B is higher for the response at .263 year^{-1} than it is for the response at .0537 year^{-1}. If we set B_1 equal to 0.93 and B_2 equal to 1.8, which are values found in the regressions of the climatic variables (see Section 3.5), then the periodogram of Fig. 3.2.2 results with the peaks at .0484 year^{-1} and .263 year^{-1} explaining 32.2 and 20.6 percent of the TMEDLF response variance, respectively. There are several important points to note:

a. The peak at the nodal cycle no longer exists but has shifted to the lower frequency of .0484 year^{-1} and its amplitude has decreased with an indication of band splitting. This is the result of the amplitude modulation.

b. When a representative value for B is used for both lunar frequencies, even though in the lunar potential time series the amplitude of .263 $year^{-1}$ is considerably less than the amplitude of the nodal (see Fig. 3.2.1), the spectral characteristics of the TMEDLF response no longer reflect this difference but instead the amplitudes of the two frequencies are fairly close.

c. The peak at .263 $year^{-1}$ is not shifted. It exists in both the forcing and the TMEDLF response.

3.1.2 Methodology used to test the hypothesis.

In order to determine the behavior of the station pressure, precipitation and upper air data using the concept of atmospheric susceptibility to external forcing, the MACC nonlinear regression program NREG was used. The regression equation was:

$$\hat{P} = A[\cos(2\pi f_1 t + \phi_1) - B]\cos(2\pi f_2 t + \phi_2) + C \qquad 3.7$$

where $\hat{P}$ is the predicted value of the climatic element (e.g., station pressure) from the regression,

A provides a magnitude and sign for the response,

f_1, ϕ_1 are the fixed frequency and phase of the best fitting cosine to the Northern Hemisphere temperature time series,

B is the susceptibility threshold (see below for discussion),

f_2 is the forcing frequency (.053725 $year^{-1}$ or .263 $year^{-1}$),

ϕ_2 is the phase of the forcing and is allowed to float, and

C is the mean.

The NREG routine returns the values for the four parameters (A,B,C, and ϕ_2) plus the predicted values for the years of the regression. The susceptibility threshold B is not fixed in the regression so that we may see how sensitive the particular climatic variable is to the effects of hemispheric warming and cooling. The phase of the forcing, ϕ_2, is allowed to float to test whether or not the pressure, precipitation and upper air data are, in fact, in phase with the hypothesized lunar forcing.

To obtain the percent explained variance, the square of the correlation coefficient (R^2) between the observed and the predicted values was calculated. In the analysis that follows the maps of R^2 will be presented along with maps of the predicted values for certain years. In some cases the map of the susceptibility threshold will also be shown. The factor A will not be shown since its magnitude does not necessarily indicate the magnitude of the response to the forcing since it must also be multiplied by the term, B. Thus, A means different things at different stations and is not easily comparable. The phase maps of ϕ_2 will also not be shown since the term A can have a negative sign, so at the stations where this occurs the phase is 180° from what it should be to compare it to the other stations. Instead of adding 180° to the phase in those cases and then plotting the data,

the phasing information will be derived from looking at the actual anomaly maps for the important years in the cycle.

In order to test the significance of the regression, an F ratio test can be applied for a 3 parameter model as follows:

$$F = \frac{R^2/3}{(1-R^2)/N-4} \qquad 3.8$$

where R is the correlation between the predicted values from the NREG regression and the actual observed values, and N is the number of data points. Testing the significance at the 95 percent level establishes the F-ratio for the given degrees of freedom. The R^2 value can then be written as:

$$R^2 = D/(1 + D) \qquad 3.9$$

where $D = 3F/(N-4)$. Thus, any R^2 value greater than 11.8 percent is significant at the 95 percent level for 66 years of data. For 27 years of data R^2 must be greater than 26.5 percent.

In the discussion that follows the phrases, "susceptibility factor", "susceptibility parameter", and "susceptibility threshold" will be used. The first pertains to the entire factor, $A[\cos(2\pi f_1 t + \phi_1) - B]$, the second to the cosine term of this factor and the latter to the term, B. The phrase "TMEDLF response" will mean the forcing frequency multiplied by the susceptibility factor. Also, the nomenclature kF_{05} and kF_{26} will refer to the nonlinear model of Equation 3.7 depending on whether f_2 in this equation is .0537 $year^{-1}$ or .263 $year^{-1}$, respectively.

It will be necessary to correlate the responses observed in

pressure, precipitation and the upper air data with the tidal forcing to see if they are, in fact, in phase. The correlation between two time series generated by cosines with identical frequencies but different phases is merely the cosine of the phase difference. However, our situation is slightly more complicated since the forcing cosine is multiplied by the susceptibility factor. Therefore, a time series of the TMEDLF response (i.e., the susceptibility factor multiplied by the lunar forcing) must be calculated and correlated with the $\hat{P}$ time series of predicted values from the nonlinear regression from Equation 3.7. The susceptibility threshold used in the TMEDLF response (Eqn. 3.5) will be the empirically determined value for the station under consideration. At times the TMEDLF response will be correlated with the average anomaly for a group of stations. When this occurs the susceptibility threshold used in the TMEDLF response will be the average value of the susceptibility threshold for the stations being considered. If a station has a susceptibility threshold that is greater than 5.0, however, then that term will not be included in the threshold average, but the station's anomaly will still be used. The reason for this is that a threshold value that high indicates the station's response is not dependent upon the temperature modulation of the forcing. The phasing information for the forcing was obtained from the lunar tidal potential time series for 25°N, 75°E (a location in northern India). However, as we saw in Chapter 2, there is only a latitudinal dependence for the two

frequencies being considered so the longitude of the location is not important. The F_{05} cycle has a maximum in June 1913, for the Moon's ascending node was at the vernal equinox at that time. The phase for the F_{26} cycle, taken from the periodogram of Term 1, has a maximum in 1900.65. For the sake of consistency in these correlation calculations, the sign of the TMEDLF response coefficient, A, in Eqn. 3.5 was taken to be that from the regression of the 300 mb data at 25°N, 75°E, for as we shall see the upper air anomalies over northern India are an important factor in the synoptic climatology of the monsoon onset.

3.2 Data

3.2.1 Station Pressure.

I have used WMO station pressure data at 40 stations in India and Pakistan for this study. Figure 3.4 shows the locations and Table 3.1 provides the WMO numbers and names of these stations. Station pressure was used rather than sea level pressure for two main reasons:

1. The data record length for most stations was longer for station pressure than for sea level pressure.

2. Station pressure is the actual observation and has not been subjected to the reduction to sea level formula. Since we are looking at periodicities in the data it seemed best to use unaltered data. The resulting anomalies are departures from the station mean and, therefore, even if the means are quite different due to station

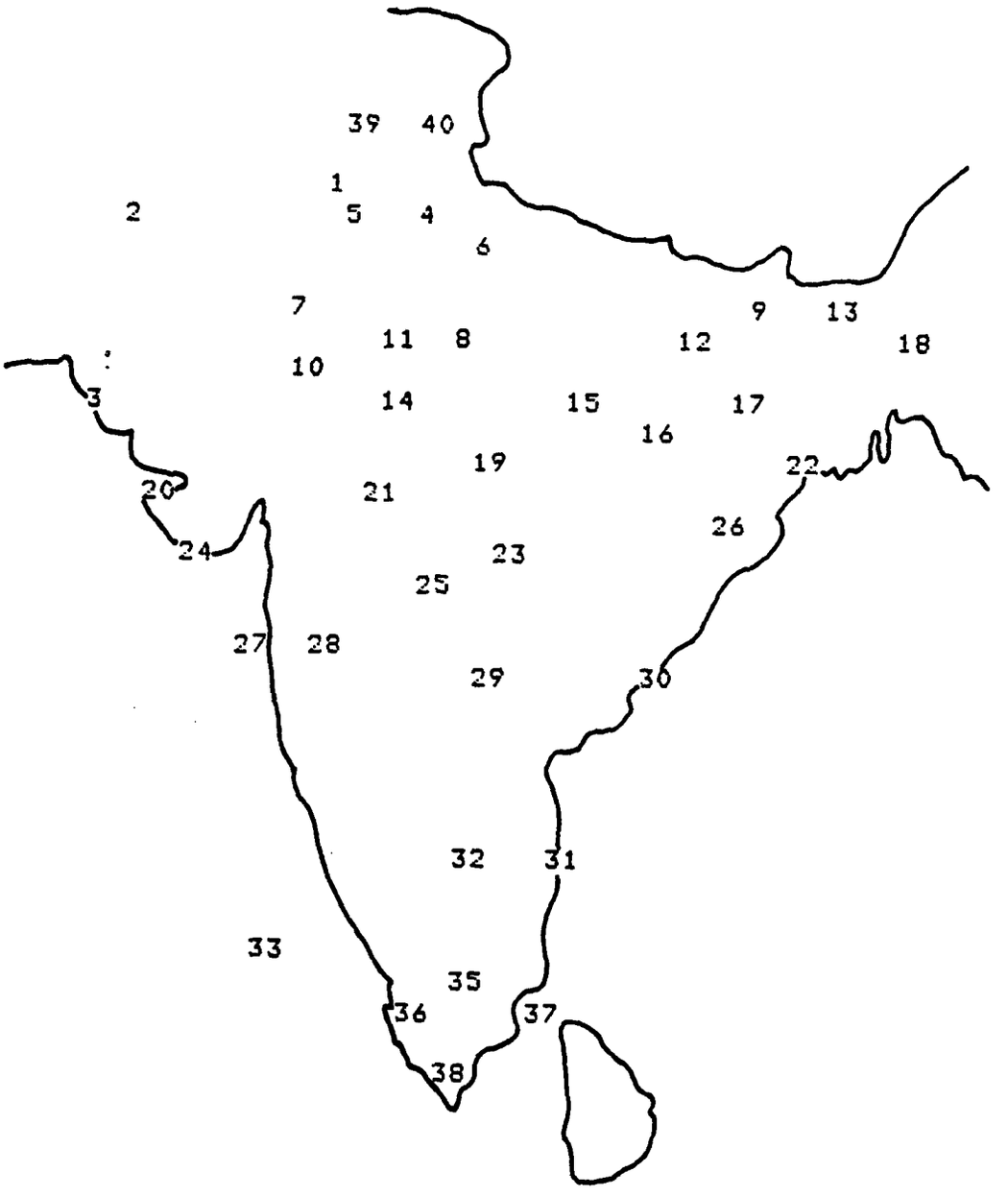

Figure 3.4. Approximate locations of the 40 stations used in the station pressure analysis. The station names and WMO numbers are given in Table 3.1.

TABLE 3.1

WMO Numbers and Names of Stations in Figure 3.4 (Station Pressure)

Figure 3.4 number	Name	WMO Number
1	Lahore City	416400
2	Quetta	416610
3	Karachi	417820
4	Simla	420830
5	Ludhiana	420990
6	Mukteswar	421470
7	Bikaner	421650
8	Agra	422610
9	Darjeeling	422950
10	Jodhpur	423390
11	Jaipur	423480
12	Darbhanga	423910
13	Dhubri	424040
14	Kota	424510
15	Allahabad	424750
16	Daltonganj	425870
17	Dumka	425990
18	Silchar	426190
19	Sagar	426710
20	Dwarka	427310
21	Indore	427540
22	Calcutta	428070
23	Nagpur	428670
24	Veraval	429090
25	Akola	429330
26	Cuttack	429700
27	Bombay	430570
28	Poona	430630
29	Begampet	431280
30	Vishakapatnam	431490
31	Madras	432790
32	Bangalore	432950
33	Amini	433110
34	Port Blair	433330
35	Kodiakanal	433390
36	Fort Cochin	433510
37	Pambam	433630
38	Trivandrum	433710
39	Srinagar	435400
40	Leh Kashmir	435440

elevation differences, the anomalies are comparable.

There is a great deal of missing data after 1960 in most of the records. Therefore, the time period that will be used covers 1895-1960.

3.2.2 Precipitation

As with station pressure the data comes from the WMO and the locations of the 39 stations used are shown in Figure 3.5. Table 3.2 provides the WMO numbers and names of these stations.

The data record for these stations goes through 1982; however, to be comparable to the pressure data set, the years 1895 - 1960 will be used in the regressions.

The frequency distribution of rainfall amounts for a given month can be highly skewed especially in the drier regions of India. If the data are not normally distributed, standard significance tests do not apply. To reduce the skewness, the precipitation data were subjected to a cuberoot transform. This makes the frequency distribution at a given station more nearly normal.

3.2.3 300 mb Heights.

300 mb heights are available on tape every five degrees of latitude (90°N to 20°N) and longitude for the years 1950 through 1977. The data for the year 1958 are missing so there are only 27 years of data.

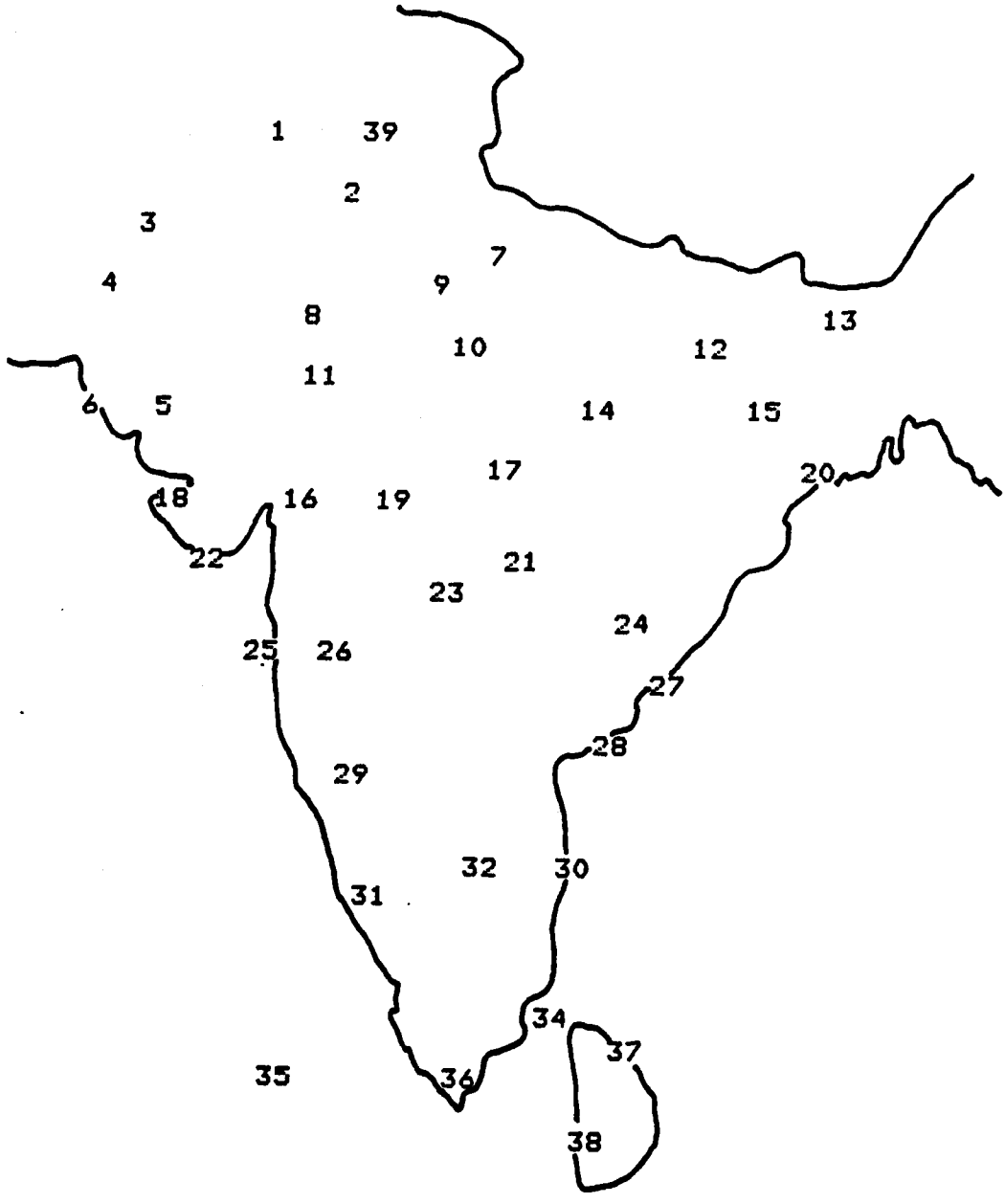

Figure 3.5. Approximate locations of the 39 stations used in the precipitation analysis. The station names and WMO numbers are given in Table 3.2.

TABLE 3.2

WMO Numbers and Names of Stations in Figure 3.5 (Precipitation)

Figure 3.4 number	Name	WMO Number
1	Peshawar	415300
2	Lahore City	416400
3	Quetta	416610
4	Kalat	416960
5	Hyderabad	417650
6	Karachi	417820
7	Mukteswar	421470
8	Bikaner	421650
9	New Delhi	421820
10	Agra	422610
11	Jodhpur	423390
12	Darbhanga	423910
13	Dhubri	424040
14	Allahabad	424750
15	Dumka	425990
16	Ahmadabad	426470
17	Sagar	426710
18	Dwarka	427310
19	Indore	427540
20	Calcutta	428070
21	Nagpur	428670
22	Veraval	429090
23	Akola	429330
24	Jagdalpur	430410
25	Bombay	430570
26	Poona	430630
27	Vishakapatnam	431490
28	Masulipatam	431850
29	Belgaum	431970
30	Madras	432790
31	Mangalore	432830
32	Bangalore	432950
33	Port Blair	433330
34	Pamban	433630
35	Minicoy	433690
36	Trivandrum	433710
37	Trincomalee	434180
38	Colombo	434660
39	Srinagar	435400

3.3 Response to lunar forcing at .0537 year^{-1}.

3.3.1 Station Pressure.

In this section I will present an analysis of the June monsoon circulation as exhibited by the surface pressure field by examining the June anomaly patterns for each year produced by the hypothesized model of Equation 3.7..

The R^2 map (Fig 3.6) shows two major regions of interest - one in northeastern India and another in western India. The phase map for the nodal cycle (not shown) indicates that the pressure variation in northeastern India is close to 180° out of phase with the region in western India.

Looking at the two areas outlined in Figure 3.7, we see that the susceptibility threshold is greater than one for most of the stations of interest in the west while it is less than one in the northeast. No attempt has been made to analyze these data, since the values vary so much. In the northeast, then, as the hemisphere warms, the sign of the response anomaly reverses. Thus, for a time the west and northeast anomalies are in phase. The impact of this will be discussed below.

The oscillating nature of the anomaly pattern at the modulated nodal frequency can be seen by examining the years 1895, 1903, 1913, and 1922 shown in Fig 3.8. These years were chosen because they are the Junes that are at the extremes of the TMEDLF response at the nodal cycle. There was a maximum in the TMEDLF response in 1894; however, since the data set began in 1895, that year was used.

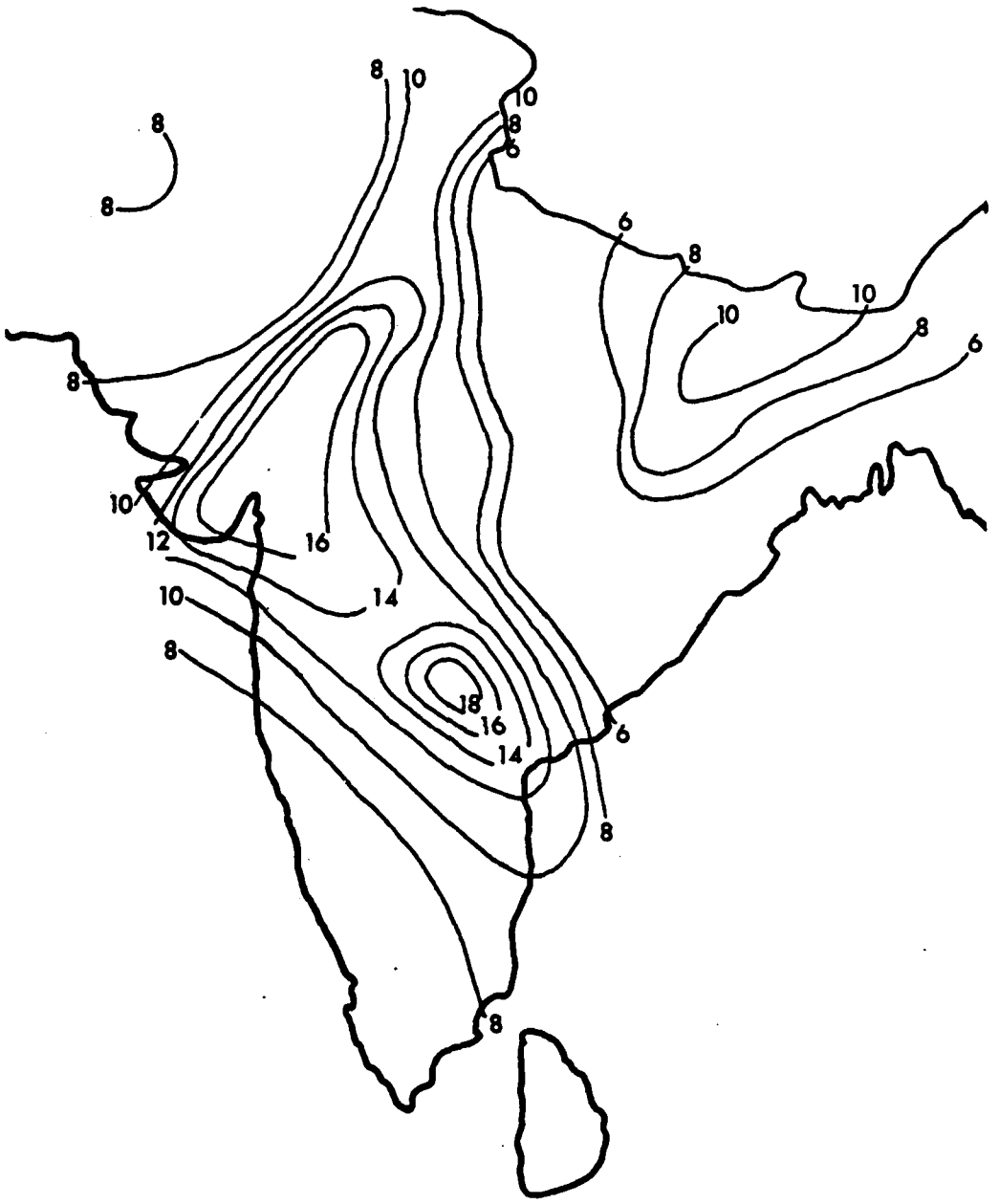

Figure 3.6. The percent of the station pressure variance explained by the kF_{05} model (units are percent).

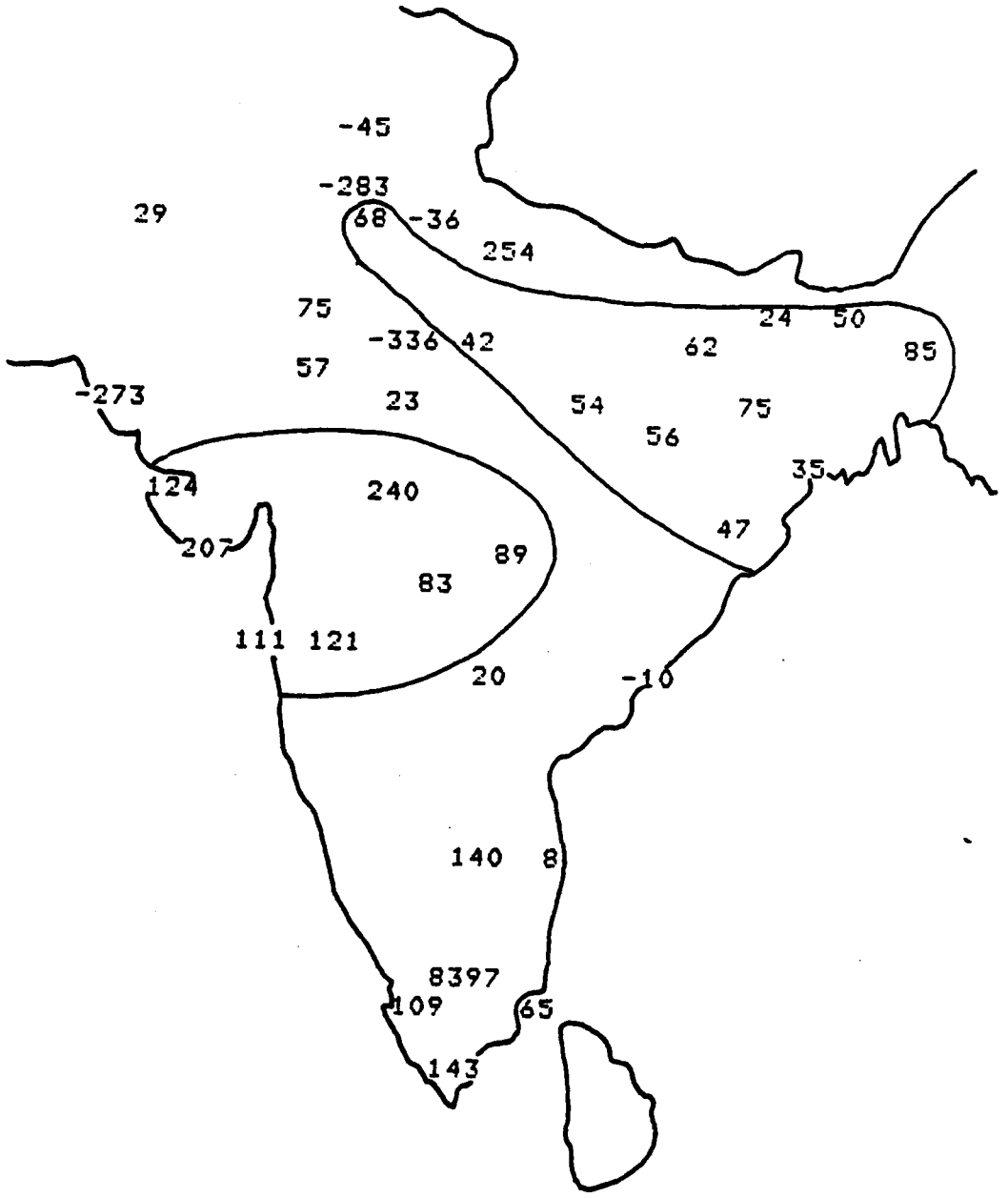

Figure 3.7. The value of the susceptibility threshold from the regression of the station pressure data against the kF_{05} model (units are value x 10^{-2}). The two areas outlined show that the threshold values are different in northeastern India from what they are in western India.

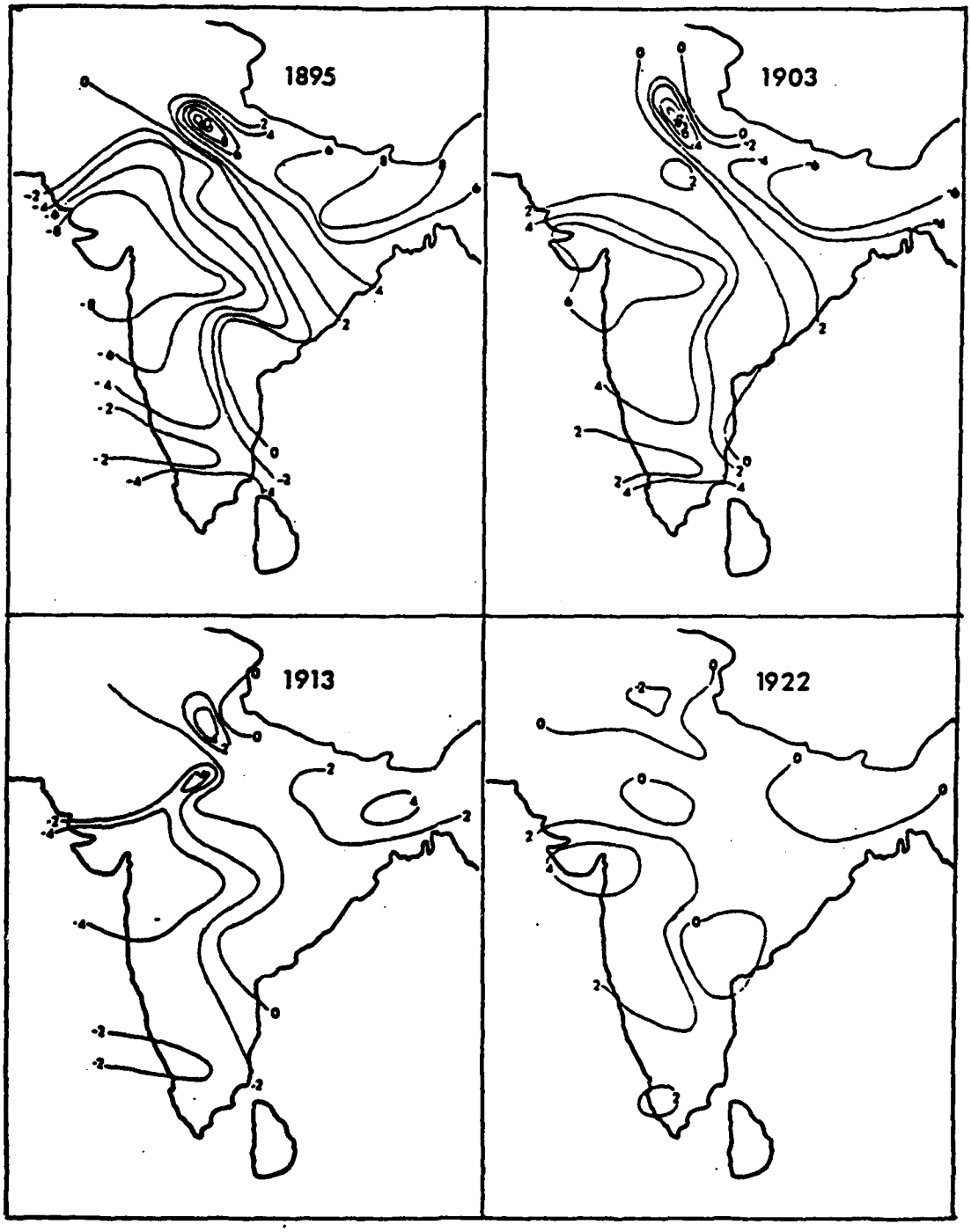

Figure 3.8. Anomaly maps of station pressure for the years indicated from the kF_{05} model (units are mb x 10^{-1}).

Also, the other years are not necessarily a maximum or minimum in the nodal cycle but may be a year off because of the effect of the amplitude modulation. For example, 1904 was an extreme in the nodal cycle while 1903 was the extreme in the TMEDLF response (see Table 3.1). In 1895 and again in 1913, a large positive anomaly dominated northeastern India, extending northwestard along the Himalayas, whereas a large negative anomaly occurred over western India. In the years 1903 and 1922 the reverse pattern occurred. We have postulated that the tidal effects are less important in warmer years and we see that the magnitude of the anomalies decreases from 1895 to 1922 - a period of warming in the cosine approximation to the Northern Hemisphere temperatures. The axis of the reversing pattern lies just about along the average position of the monsoon trough in June (see Figure 3.9) with the anomaly center to the north of this axis lying along the Himalayas. Research (e.g., Raghavan, 1973) has shown that when the pressure anomaly along the Himalayas is negative, breaks occur in the monsoon.

The effect of a large positive anomaly on the west coast would be to decrease the strength of the southwesterly monsoon current, thereby decreasing monsoon rainfall. An inference about the wind flow can also be made from these unnormalized pressure anomaly maps (Kutzbach, 1970). The high and low pressure anomalies, in the years depicted, create a strong NE/SW pressure gradient across the Gangetic Plain of India. Since we are dealing with monthly averages here, geostrophic equilibrium can be assumed (with some allowance

Figure 3.9. The average position of the monsoon trough (solid line) for the years 1899 through 1977 taken from the gridded Northern Hemisphere sea level pressure data tape which has been updated by Trenberth and Paolino (1980). The pivotal axis of the nodal cycle anomaly oscillation is shown with a dashed line.

for boundary layer friction). In the years when the high pressure anomaly is located along the west coast, the geostrophic wind is directed from the dry deserts of northwest India and Pakistan onto central India adding further to the dryness that has already been discussed in conjunction with this pattern.

We are dealing with the anomalies in the single month of June. However, it is interesting to note that Bhalme and Mooley (1980) in a study of the seasonal surface pressure anomalies during drought and flood years, found strikingly similar patterns as shown in Fig. 3.10. They were not dealing with any periodic component of the data in their analysis but with the total variability for the entire monsoon season. The magnitude of their west coast departures (-0.6 mb to +0.8 mb) are comparable to the magnitude of the anomalies from this periodic model (-1.0 mb to +0.8mb). This indicates that certainly some of the variance associated with drought and flood years is associated with this periodic component of the variability.

In order to establish the phasing of this periodic oscillation, let us examine the average pressure anomaly of the following seven western stations and eight northeastern stations:

WEST

WMO		Fig. 3.4 no.
42731	- Dwarka	20
42909	- Veraval	24
43057	- Bombay	27
43063	- Puna	28
42933	- Akola	25
42754	- Indore	21
42867	- Nagpur	23

NORTH

WMO		Fig. 3.4
42261	- Agra	8
42475	- Allahabad	15
42587	- Daltonganj	16
42970	- Cuttack	26
42807	- Calcutta	22
42599	- Dumka	17
42391	- Darbhanga	12
42099	- Ludhiana	5

AD-A135 441 POSSIBLE TIDAL MODULATION OF THE INDIAN MONSOON ONSET (U) AIR FORCE INST OF TECH WRIGHT-PATTERSON AFB OH W H CAMPBELL MAY 83 AFIT/CI/NR-83-60D 2/2

UNCLASSIFIED F/G 4/2 NL

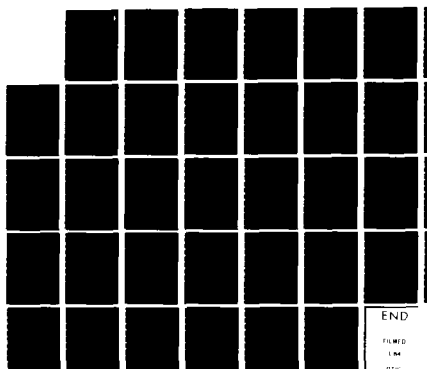

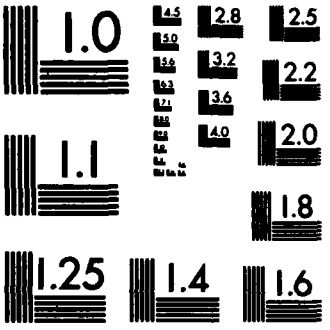

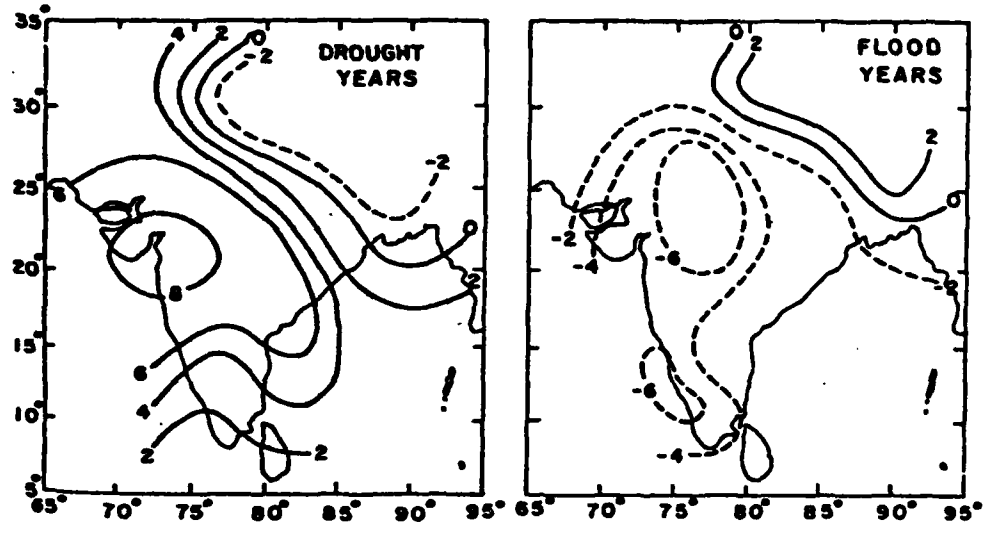

Figure 3.10. Composite surface pressure anomalies (units are 10^{-1} mb) for eight drought and eight flood years (from Bhalme and Mooley, 1980).

The difference between the two averages (North minus West) will provide a measure of the strength of the NE/SW pressure gradient discussed above. The difference was calculated so that it would be negative for dry years. Table 3.3 provides a comparison of this difference for the years surrounding the maximum effect of the TMEDLF response (i.e., the susceptibility factor times the forcing cosine). One thing to note is that the pressure anomaly difference is, in fact, strongest at the beginning of the data record which is well into the coldest period of the best fit Northern Hemsiphere cosine curve. Thus, the actual atmospheric response is much stronger when the hemisphere is coldest. Also, the year of the maximum pressure anomaly difference agrees with the year of the maximum TMEDLF response and the correlation of the 66 year time series of the pressure anomaly difference and the TMEDLF response is -.972 when using the average susceptibility threshold of .94. The minus sign of the correlation is a result of the way the difference in anomalies was calculated. Thus, the actual atmospheric response is very much in phase with the TMEDLF response. Note also that even though 1904 was the year that the lunar nodal cycle produced a minimum in the lunar tidal potential that when the susceptibility factor is applied to the forcing the minimum occurs in 1903 as it also does in the actual response.

The fact that the susceptibility term is less than one in northeastern India means that once the temperature cosine reaches

TABLE 3.3

Pressure Anomaly Difference Compared to the TMEDLF Response

Year	Pressure anomaly Difference (mb)	TMEDLF Response Threshold (B=0.94) (relative numbers)
1895	1.38	-128.9
1896	1.16	-109.8
1902	-0.96	90.1
1903	-1.07	100.7
1904	-1.04	99.4
1905	-0.91	87.1
1911	0.57	-58.2
1912	0.66	-67.0
1913	0.67	-67.5
1914	0.61	-60.4
1921	-0.29	37.1
1922	-0.31	37.7
1923	-0.30	34.0
1924	-0.27	27.0

Note: The pressure anomaly difference is calculated by taking the difference of the average anomaly for 8 northeastern stations and 7 western stations. The TMEDLF response uses the average susceptibility threshold for the 15 stations.

that value (on its way to a maximum of one at the warmest part of the cycle) the sign on the nodal forcing cosine reverses. Thus, where the signs of the pressure anomalies in the northeast and in the west were opposite in the early part of the record, they become the same as the hemisphere warms. This greatly decreases the NE/SW pressure gradient making the effect of the response at the nodal forcing frequency close to zero. This effect can be seen by looking at the anomaly map for 1941 (Fig. 3.11) where the northeastern pressure anomaly has a maximum of +.36 mb (and +.56 mb further to the northwest) and the western anomaly has a maximum of +.37 mb.

Calculation of the geostrophic wind for some of these anomaly patterns shows the magnitude of the interannual variability included in this nonlinear periodic model. For example, in 1895 the pressure difference between Jaipur and Agra (station numbers 11 and 8, respectively, in Fig. 3.4) was 0.86 mb. Between these two stations lies the pivotal line of the oscillating pressure anomalies. Using the geostrophic wind equation,

$$V_g = -(1/\rho f)\partial p/\partial n, \qquad 3.10$$

where f is the coriolis parameter,

ρ is the air density, and

$\partial p/\partial n$ is the pressure gradient,

we get V_g equal to 4.99 m/s from the south. In 1955 the pressure difference between Begampet and Vishakapatnam (numbers 29 and 30, respectively) was 0.98 mb which yields a geostrophic wind of 3.49 m/s from the south. Crutcher (1966) found that the average

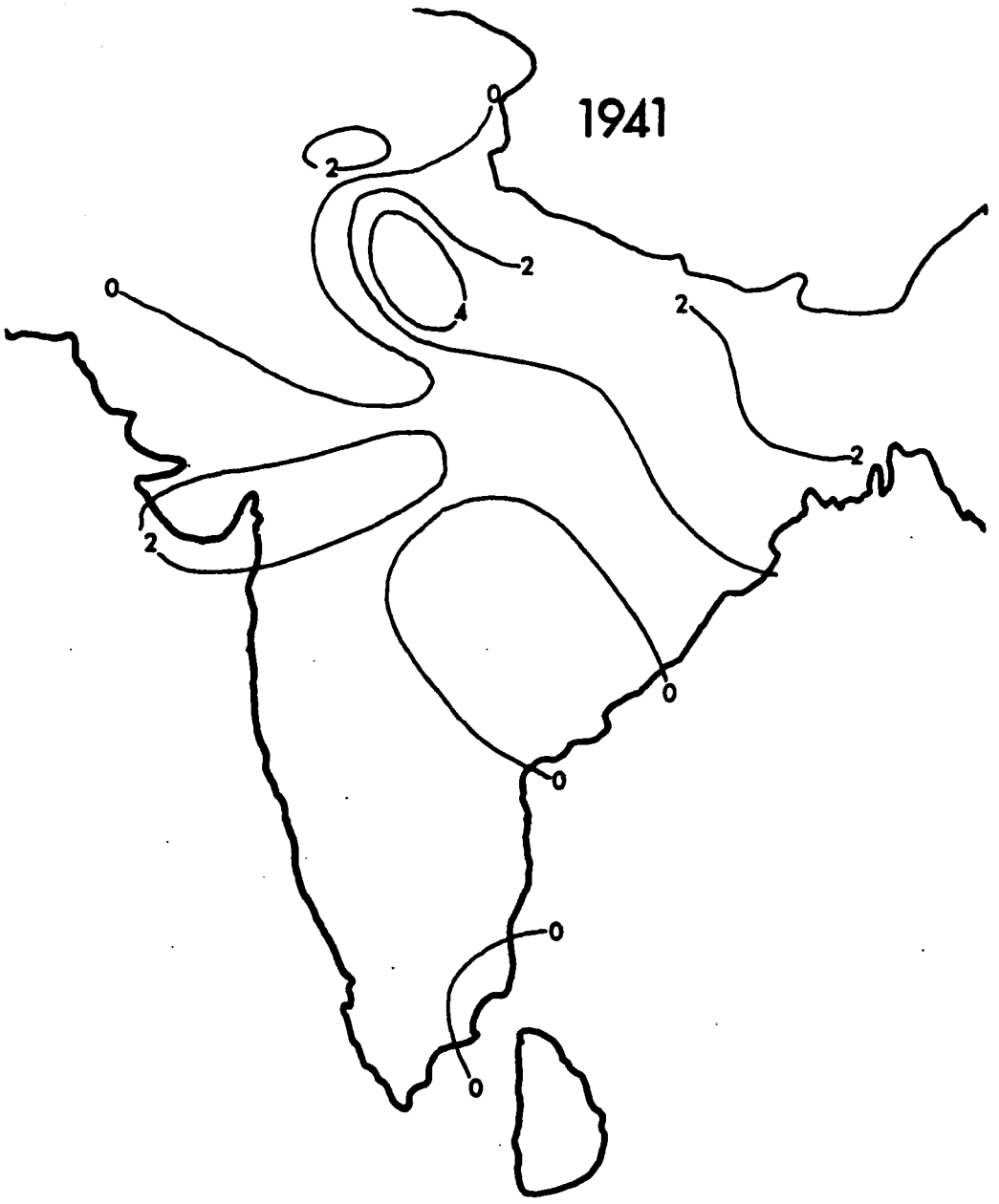

Figure 3.11. Station pressure anomaly map for 1941 from the regression against the kF_{05} model.

meridional component in this region is zero for June with a standard deviation of about 4 kts (or 2.1 m/s). This indicates that the meridional component is just as likely to be from the north as from the south and that a large part of that variation can be explained by the model under discussion.

3.3.2 Precipitation.

Having examined the response of station pressure using the hypothesized model (Eqn. 3.7) and having briefly discussed the pressure anomaly pattern's impact on the precipitation, let us look at the result of the nonlinear regression of precipitation for the same period (1895 - 1960) against the same model.

The percent variance map is given in Fig 3.12. The anomaly maps for the years 1895, 1903, 1913, and 1922 are shown in Fig 3.13. As the previous discussion indicated, years 1895 and 1913 should be wet in the northwestern half of India as they are. At the opposite extreme of the cycle the years 1903 and 1922 are dry. The decrease in the magnitude of the anomalies due to the amplitude modulation is definitely noticeable by 1922.

Rao (1976) has observed that, during breaks in the monsoon, rainfall still occurs in northeast India and in southern peninsular India. As noted in the last section, the deficient rainfall of 1903 and 1922 is associated with a pressure pattern observed during breaks in the monsoon and, consistent with this, the precipitation anomalies are positive in northeast and southern India.

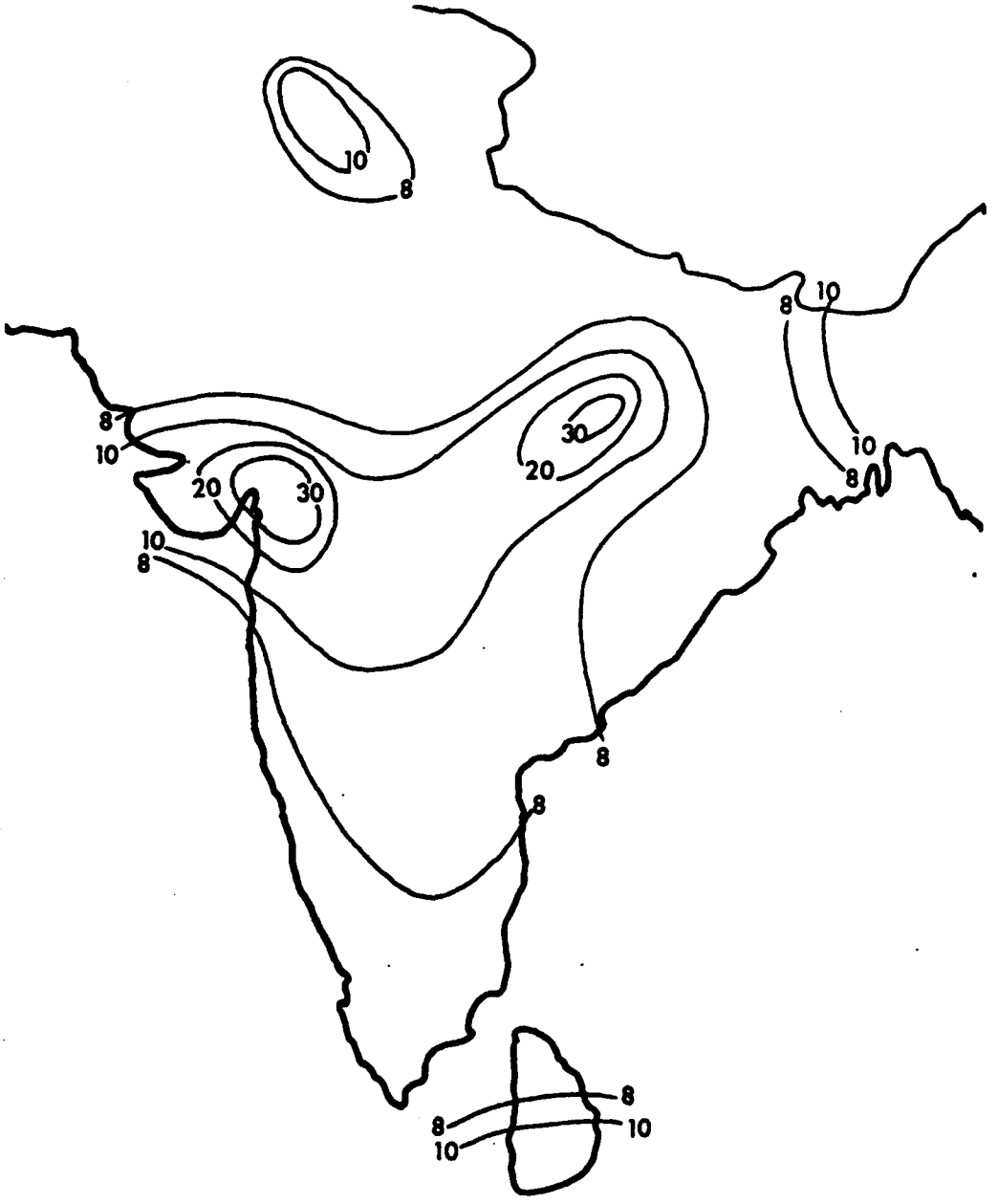

Figure 3.12. The percent of the precipitation variance explained by the kF_{05} model (units are percent).

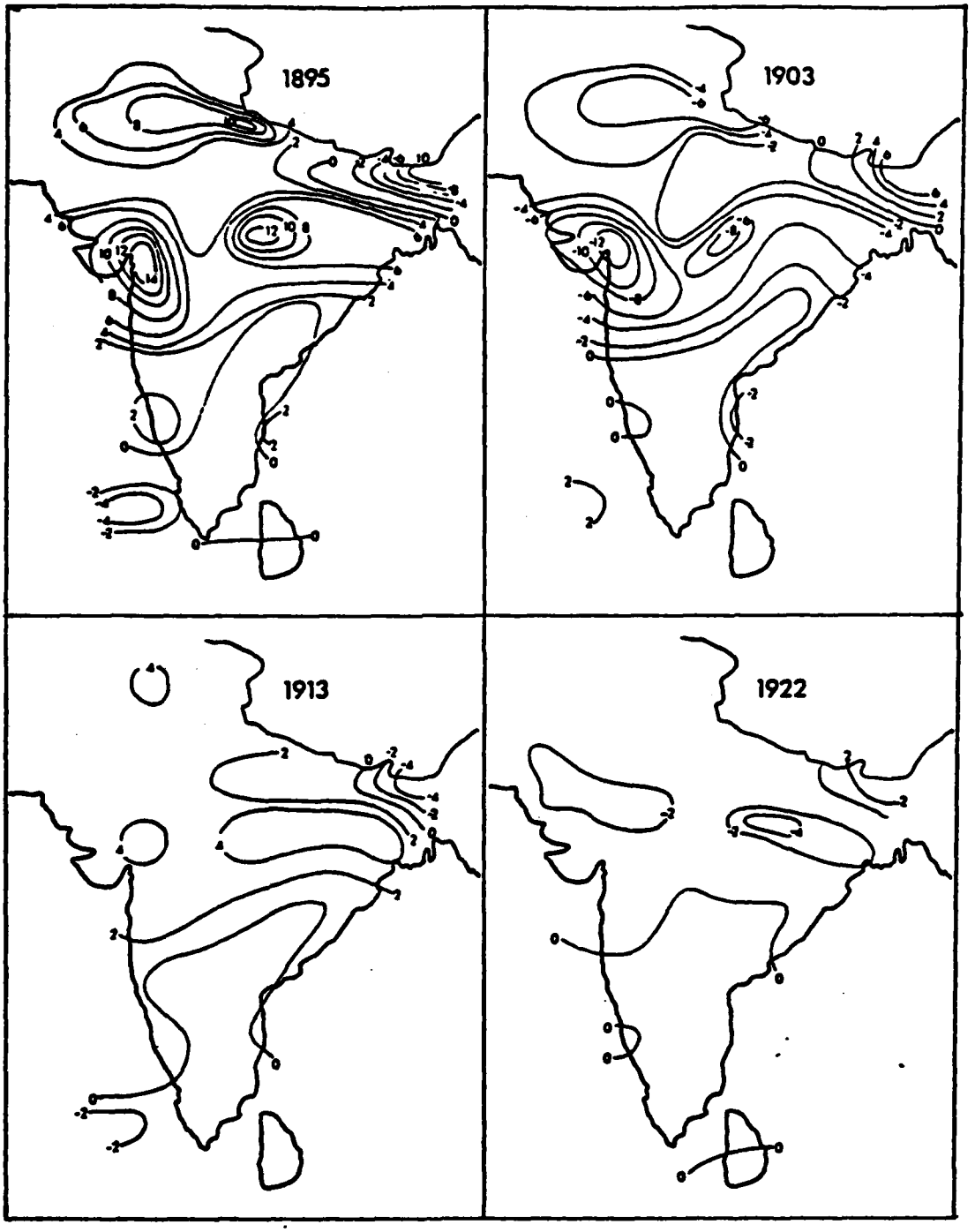

Figure 3.13. Normalized anomaly maps of precipitation for the years indicated from the kF_{05} model (units are standard deviations x 10^{-1}).

Looking again at Fig. 3.8 for the years 1895 and 1903, we see that Sagar (station 19 for pressure and 17 for precipitation) lies in the region where the effects of the reversing flow pattern should be felt the most; and we find that the correlation between Sagar's precipitation response and the TMEDLF response is -.998. This very high correlation is due to the fact that the phase of the forcing cosine in the TMEDLF response and the phase of the observed response at Sagar are almost identical. Thus, the lunar nodal cycle is exactly in phase (disregarding the sign of the correlation) with Sagar's response.

In order to gain a perspective on just how important the response is at this frequency in terms of the total variability of June rainfall let us turn for a moment to an eigenvector analysis. Campbell et. al. (1983), hereafter referred to as CBB, have shown that the spectrum of the coefficients of the first eigenvector of June cuberooted precipitation is dominated by a frequency at .0482 $year^{-1}$ and another at .262 $year^{-1}$ as shown in Figure 3.14 which is taken from CBB. This eigenvector explains 20.3 percent of the total interannual variance of Indian precipitation for June with the frequency .0482 $year^{-1}$ explaining 17.2 percent and the frequency .262 $year^{-1}$ explaining 15.1 percent of the variance of this eigenvector's coefficients. These are the two main frequencies that result when the susceptibility factor is applied to the lunar forcing as Figure 3.2.2 shows indicating that the lunar forcing frequencies have a significant role in explaining the interannual

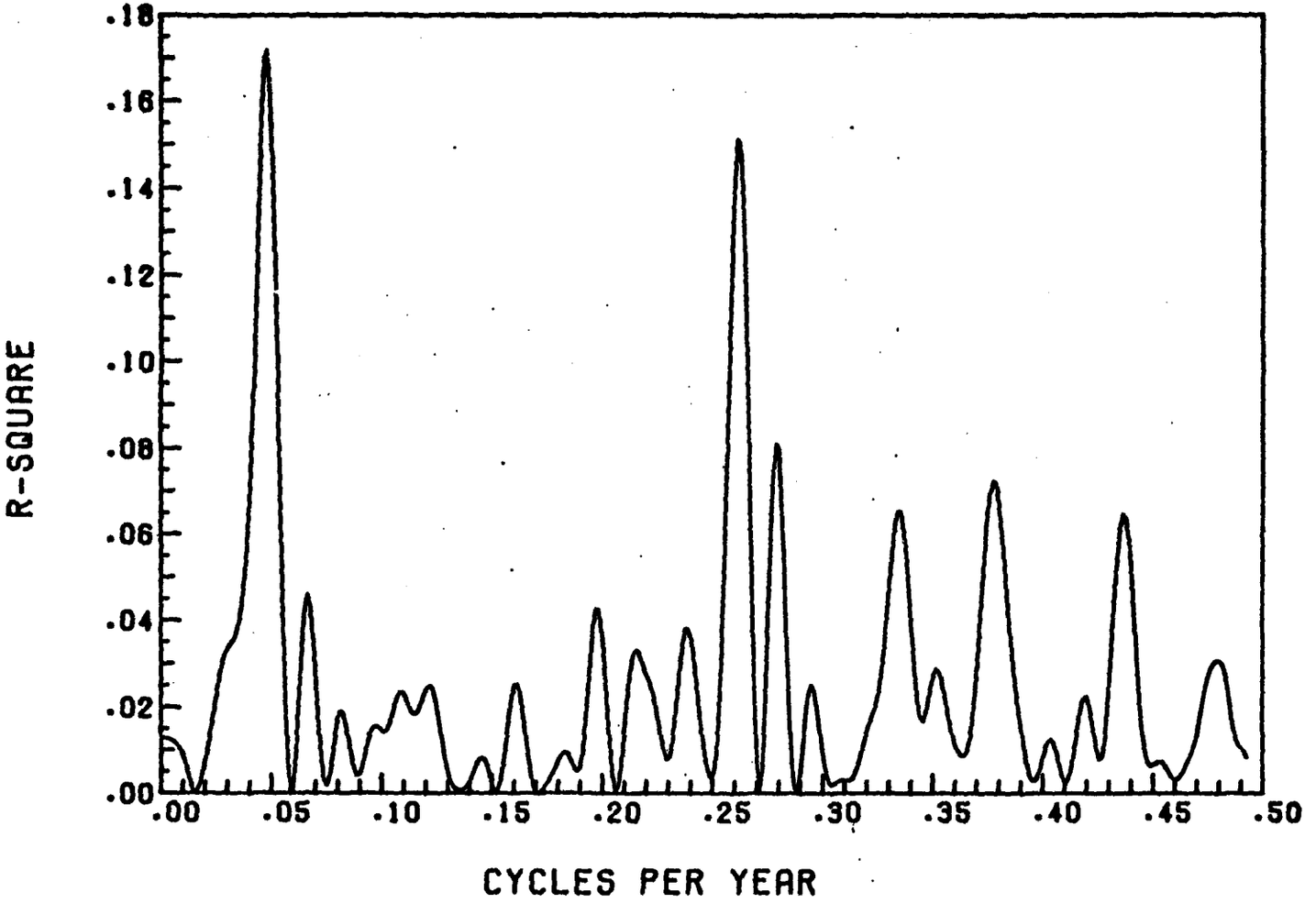

Figure 3.14. A periodogram of the coefficients of the first eigenvector of June cuberooted precipitation (1895-1975). The two dominant peaks are at .0482 yr^{-1} and .262 yr^{-1}.

variability of June precipitation, especially in northern India where this eigenvector has the largest component values.

The second eigenvector (non-normalized) of station pressure is also dominated by a frequency around .0482 year^{-1}, which explains 30.5 percent of the variance. This second eigenvector explains 17.4 percent of the total June station pressure variance. The eigenvector spatial patterns for both parameters are similar to the responses observed from the nonlinear model. The pressure eigenvector component values are opposite in sign in the northeast from those in the west and the precipitation component values are largest in the northwestern area of India with opposite signs in the northeast and in southern peninsular India. The frequencies and their phases (from a periodogram) for the two eigenvector analyses are:

	Frequency (year^{-1})	Phase (degrees)	Period
Precipitation	.04815	-157.0	1895-1975
Station pressure	.04848	-154.7	1895-1960

The correlation (over the period 1895-1960) between the two resulting time series is 0.993. Thus, at this frequency, which is predicted based on the concept of atmospheric susceptibility to the lunar forcing, the pressure and precipitation responses are almost perfectly correlated.

Note: All eigenvectors used above represent significant geophysical signals at the 95 percent level, using the same conservative significance test from Overland and Preisendorfer

(1982) that was used for the eigenvector analysis discussed in CBB.

As we did with pressure, to get a measure of the relationship between the forcing and the actual precipitation response, the correlation between the TMEDLF response and the average precipitation anomaly for 12 northwestern India stations was -.971 when using the average susceptibility threshold of .969. This is not surprising considering how closely related the precipitaion and pressure responses are.

Bryson (1975) published a graph showing the percent of stations in northwestern India having less than half of normal rainfall for the period 1900-1972 (Fig 3.15). The hypothesized forcing model (Eqn. 3.7) explains 25.1 percent of the variance of this graph. The susceptibility threshold from the regression is 0.89. The regression of the graph against just the Jones et. al. (1982) annual data explains 31.1 percent of the variance. Combining both of these predictors into a single model (the dashed line in Figure 3.15) explains 51.2 percent of the variance indicating some shared variance but not very much. Thus, northern Indian rainfall is highly dependent upon both the Northern Hemisphere temperature and the amplitude modulated nodal cycle.

As noted in Chapter 2, Bhalme and Mooley (1981) studied cyclic variations in the Flood Area Index (FAI) for India (see Fig. 3.16 for the FAI>1 and FAI>2 time series) and concluded that there is strong statistical evidence for the relationship between the double sunspot cycle and the areal extent of flooding over India for their

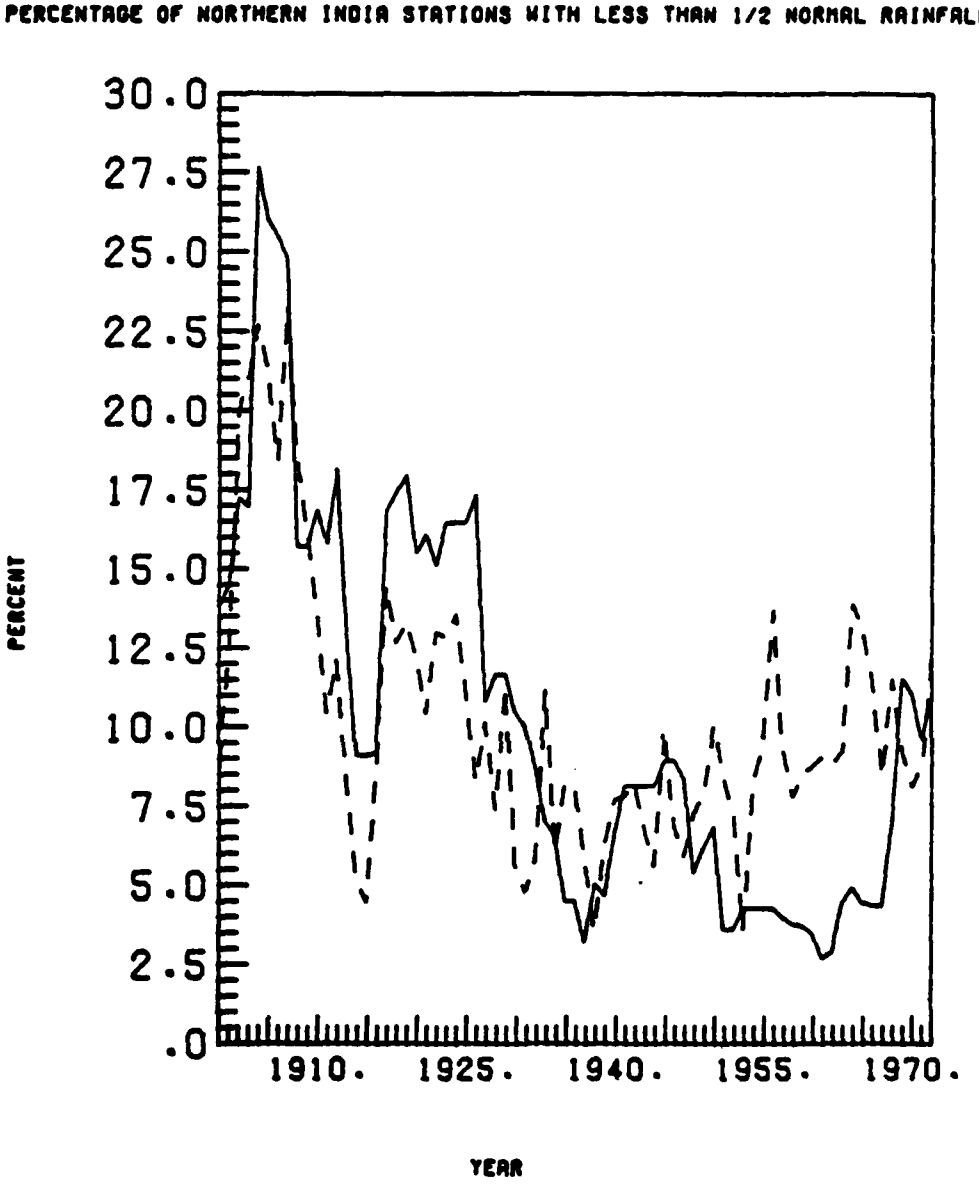

Figure 3.15. The solid line is the percent of the stations in northern India with less than half of the normal rainfall in a given year (running ten year averages). The dashed line represents the predicted values from a regression of the data against both the kF_{05} model and the Northern Hemisphere annual mean surface temperature. The dashed curve explains over 51 percent of the variance. The data for the solid curve were taken from Bryson, 1975.

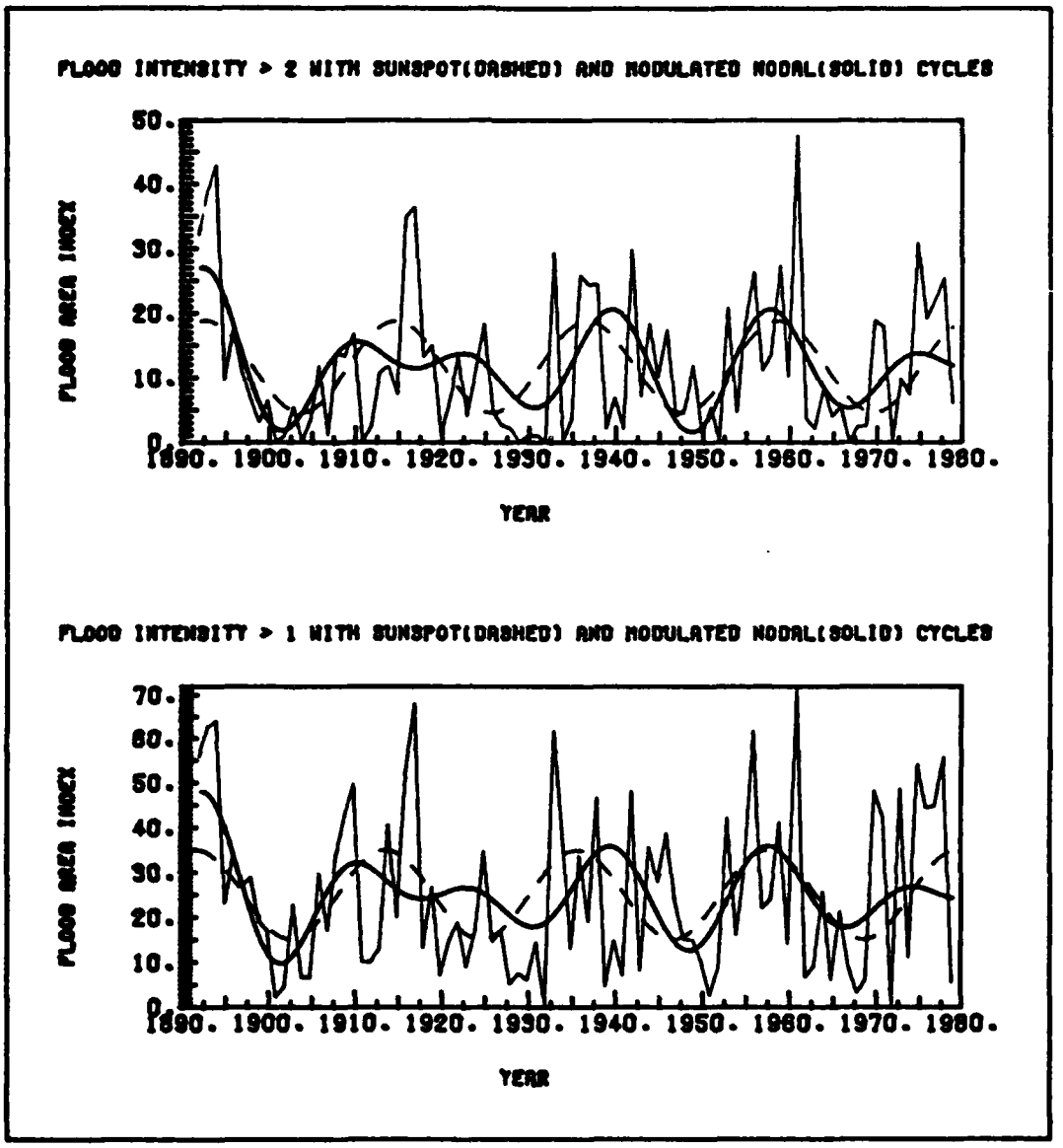

Figure 3.16. Flood Area Index time series for the indicated flood intensities (after Bhalme and Mooley, 1981). The dashed curves represent the predicted values of a regression of these data against the 22 year double sunspot cycle, while the solid curves represent the predicted values of a regression of these data against the kF_{05} model.

spectral analysis had a peak at band 4 (.0455 $year^{-1}$ which is a 22 year period). A periodogram analysis showed that the spectral peak was at a slightly higher frequency than their harmonic analysis could resolve. The periodogram frequency was about .048 $year^{-1}$ which is the same frequency found in the linear eigenvector analysis of June station pressure and precipitation.

When the two FAI indices were regressed against the kF_{05} model, the FAI>1 regression explained 17.8 percent of the variance compared to the 12 percent from their harmonic analysis. The respective percents for the FAI>2 regression were 26.9 and 16.0. One would expect the kF_{05} regression model to explain somewhat more of the variance since it has three parameters (which lead to four predictors in the linear equivalent) whereas the harmonic analysis only has two predictors. To be significant at the 99 percent level, a two parameter linear regression model must explain 10.3 percent of the variance and a four parameter linear regression model must explain 14.7 percent. Thus, both hypotheses produce statistically significant results showing that there is another way of explaining the periodicity observed in the FAI data.

A further comment on the significance of the pressure and precipitation analysis is needed. We have seen the oscillating nature of the pressure response at the amplitude modulated nodal frequency. Standard statistical tests for regression look at the percent explained variance to calculate an F-ratio and from there a significance level. Now, if a station is located on the pivotal

axis of the oscillating anomaly pattern, there will be a minimal response or amplitude at this location. Therefore, the explained variance will be low and the regression deemed statistically not significant. Nevertheless, the lack of response at this pivotal location is physically significant and explainable.

3.3.3 300 mb U_g component.

In order to enhance understanding of the synoptic climatology presented in the last two sections, the response of the 300 mb zonal geostrophic component of the wind (U_g) at the modulated nodal frequency will be examined. Unfortunately there were only 28 years of data available (1950-1977) for this analysis which allows only 1.5 cycles for an 18.6 year oscillation.

The U_g component was calculated using the following equation:

$$U_g = -(g/f)\partial h/\partial y \qquad 3.11$$

where f is the Coriolis parameter,

g is the acceleration due to gravity, and

$\partial h/\partial y$ is the north/south gradient of the 300 mb heights.

Since the heights were available at every 5° of latitude, this was the distance interval used for the height gradient. The value for f was calculated at the average latitude and the values were plotted at this latitude.

The percent variance map is shown in Fig 3.17. The nonlinear regression model for the U_g wind component located at 27.5°N, 75°E is:

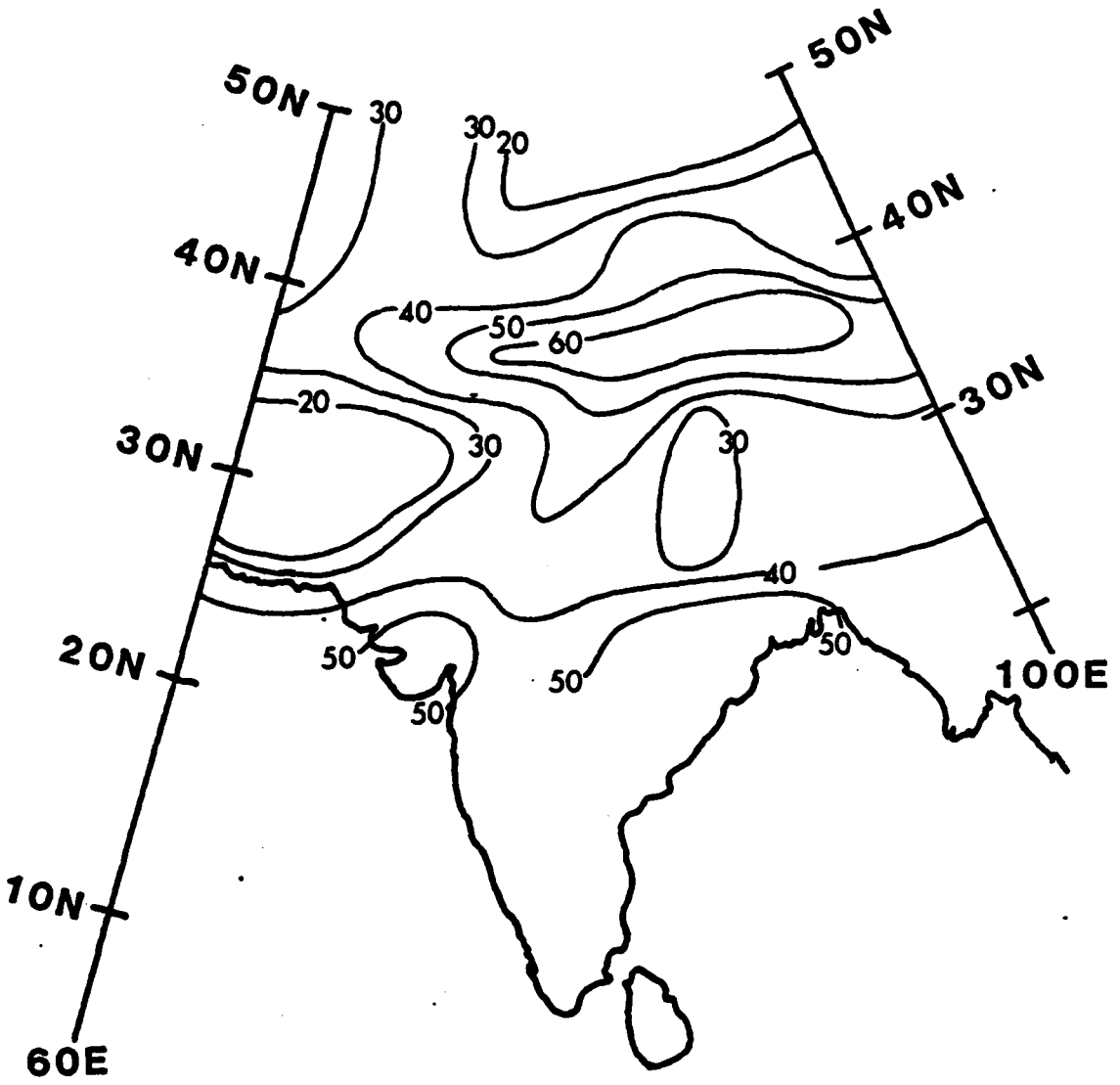

Figure 3.17. The percent of the geostrophic zonal wind (U_g) variance explained by the kF_{05} model (units are percent).
Level is 300 mb.

$$14.13[\cos(2\pi f_1 t + \phi) - 1.042]\cos(2\pi f_{No} t - 0.25^\circ). \quad 3.12$$

Thus the phase (with t=0 in June 1950) of the forcing cosine is almost exactly in phase with the lunar nodal cycle which had a maximum in August 1950. The correlation between this time series and the TMEDLF response with the susceptibility term equal to 1.04 is 0.997. At the same latitude the point directly to the east and west had a phase of 1.7° and -10.3°, respectively, making them nearly in phase with the lunar forcing also.

Since the early part of the 300 mb data record is at a time when the hemisphere was near its warmest, the amplitude of the response is quite low. Not until 1970 is the TMEDLF response again achieving a noticeable fraction of its maximum amplitude. Therefore, looking at the anomaly map for 1970 (Fig. 3.18) we see a 4 m/s easterly anomaly between 70°E and 75°E at 27.5°N over northwestern India and a 5 m/s westerly anomaly north of there between 65°E and 70°E. Both anomalies extend mainly eastward from the maximum. The last year of data is 1977 which is two years before the next peak in the TMEDLF response. Here we see (Fig. 3.18) the anomaly pattern is reversed in sign with larger magnitudes as is to be expected.

In order to get a clear relationship between the precipitation and 300 mb responses, it will be necessary to extrapolate the 300 mb U_g component back in time because the 11 years of overlap (1950-1960) are at a time when the response is minimal. Since the susceptibility threshold for northern India is greater than one, the 300 mb response does not change sign and, therefore, all one must do

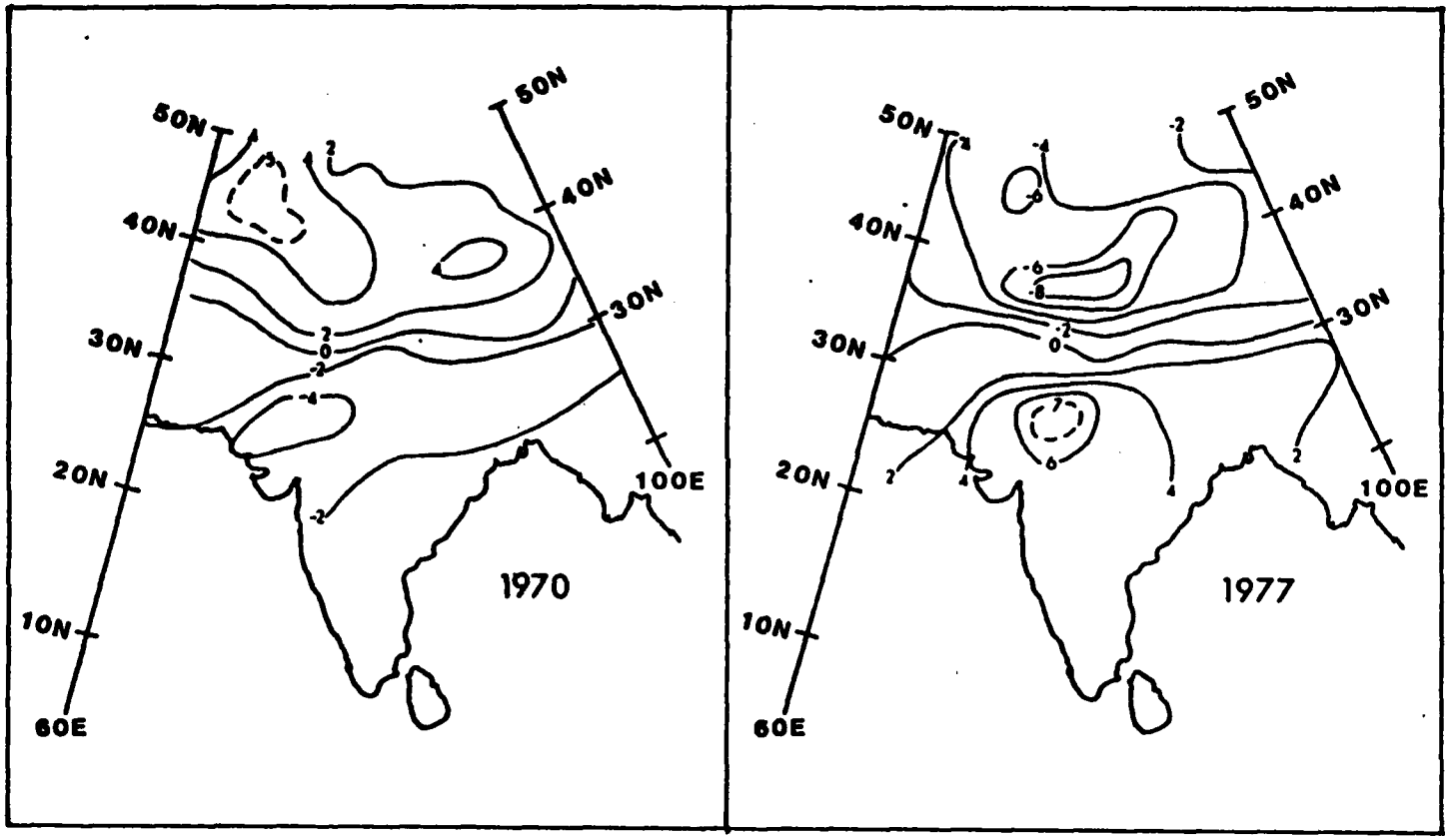

Figure 3.18. Anomaly maps of U_g for the year indicated from the kF_{05} model (units are ms^{-1}). Level is 300 mb.

is look at the phasing. The phasing is such that in 1903 a peak in the 300 mb response would have occurred (as it did in both the precipitation and pressure responses.) In this year there would have been a westerly anomaly. We have already seen that 1903 had a dry precipitation response in the nodal cycle. In 1913 the U_g anomaly would have been easterly, and as we have seen this was a wet year. Thus, there is a westerly wind anomaly in dry years and vice versa. Since we are dealing with a periodic forcing the validity of this extrapolation is acceptable; however, it would be more reassuring if a comparison could be made in a year covered by both data sets. Therefore, if we look at anomalies from a regression of precipitation that covers the years 1895-1978 we see that in 1978 when there was a westerly anomaly that the precipitation pattern was dry (Fig. 3.19) although the anomaly magnitudes are still relatively small.

3.3.4 Possible physical relationship between lunar forcing and the observed climatological data.

Up to this point, all that has been looked at is the correlation of the TMEDLF response (based on atmospheric susceptibility to lunar forcing) and the station pressure, precipitation and 300 mb U_g component. The station pressure anomaly patterns establish wind flow regimes that determine the character of the precipitation anomalies and all three of these climatological data sets are in phase with the hypothesized forcing in northern India. Why ?

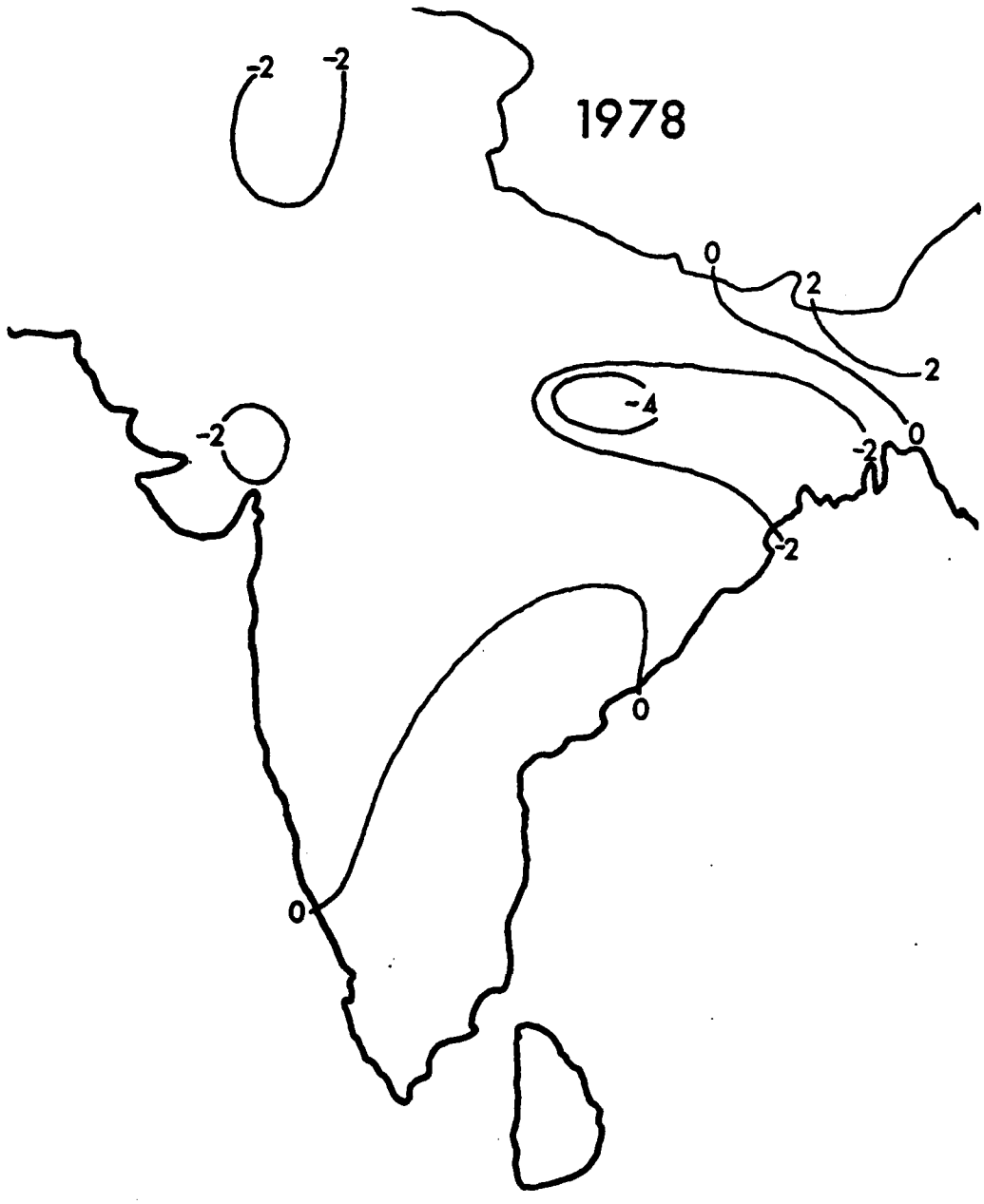

Figure 3.19. Normalized anomaly map of precipitation for 1978 (units are standard deviation x 10^{-1}).

To begin to answer this question let us apply the 300 mb susceptibility factor for northern India to the latitudinal distribution of the lunar potential nodal cycle anomaly as follows:

$$H_{05}(\phi) = 14.1[Q(t) - 1.04]F_{05}(\phi) \qquad 3.13$$

where ϕ indicates a latitude dependence. Then in years when the U_g component anomaly is negative at the latitude of northern India we get a latitudinal distribution for H_{05} which has the same gradient characteristics as seen in Figure 2.5.2.

If we were to calculate a geostrophic wind associated with this potential distribution we would see that an easterly component is produced. This was the case in 1970 when there were stronger than normal easterlies south of the Himalayas and, in fact, since the forcing and 300 mb U_g component are in phase, every year with this potential anomaly distribution has easterly anomalies south of the Himalayas. This is a physically consistent relationship.

However, to the north of the Himalayas there are westerlies in these years; and yet, as the distribution shows this region is also influenced by the same latitudinal gradient of potential as the region south of the Himalayas.

The following <u>possible</u> explanation is provided. In May and June the major synoptic event in the upper levels is the movement of the 200 mb ridge axis to the north from 10°N to 30°N. This movement decreases the westerlies in northern India, the subtropical jet moves north of the Himalayas and easterlies become established across northern India. In years when this synoptic feature is

subjected to an additional easterly component from lunar tidal forcing, the westerlies to the north of the ridge weaken faster than normal allowing the ridge axis to move northward, establishing easterlies across northern India earlier. This in turn allows the subtropical jet to move north of the Himalayas earlier than normal increasing the westerlies in that region. Thus, there is an easterly anomaly to the south of the Himalayas and a westerly anomaly to the north.

The lunar tidal forcing effect is being seen here because there is some singularity on which to act. The ridge axis moves north every year; however, in some years its northward movement is impeded and in other years helped by the small additional zonal component induced by the tidal potential distribution. And as discussed earlier, the lunar forcing effect is also contingent upon the strength of the monsoon circulation for a given year. If the circulation is particularly strong, as it is in warm years, then the effect is not very noticeable at all.

The lunar forcing mechanism acts on a hemispheric scale (e.g. see Fig. 2.5) and yet the observed response occurs on a regional scale (i.e., the northern half of India in June). As noted in Section 2.3 the nodal cycle (.0537 $year^{-1}$) has only a latitude dependence. An analogous situation occurs with the Sun's thermal forcing which also acts on a hemispheric scale with the amount of solar radiation received at the top of the atmosphere having only a latitude dependence. Then because of the difference in response of

the land and ocean to the thermal forcing, a strong temperature contrast develops producing the regional monsoon circulation over India. The lunar mechanical forcing which is acting over the entire Earth also produces a regional response through an interaction with the monsoon circulation and the regional topography, most notably the Himalayas.

Figure 2.5 shows the tidal potential anomaly values for the extremes of the nodal cycle. The value is $0.0400\ m^2s^{-2}$ at 25°N and $0.0216\ m^2s^{-2}$ at 30°N, giving a geostrophic zonal component of:

$$U_g = -(1/f)\partial\phi/\partial y = 3.14$$

$$-(0.0216-(0.0400))/(6.73X10^{-5})(5^\circ)(111000) = 0.00049\ ms^{-1}$$

The observed response in the 300 mb data is almost 10000 times this value in 1970.

Thus, we are not dealing with an equilibrium tide. This is not surprising, however, since the ocean tides do not respond as an equilibrium tide due to irregularities in the ocean basin (e.g., the enormous tidal amplitudes in the Bay of Fundy). In the region of northern India there is the largest and highest mountain barrier in the world which must have an impact on the magnitude of the atmospheric lunar tides. Nash (1982) has shown that the atmospheric pressure response to the Chandler pole tide is also nonequilibrium with magnitudes 100 to 1000 times what is predicted by equilibrium theory. Currie (1981) found evidence of the nodal cycle in temperature and drought conditions and noted that the atmospheric

tide is "strongly nonequilibrium". He also found that the nodal signal only appeared in regions which parallel the core of westerlies in winter. Similarly, as the analysis of the monsoon circulation seems to indicate the jet stream plays a major role in the interaction of the lunar forcing and the atmosphere. Others (Duperier, 1946 and Chapman and Lindzen, 1970) have provided evidence that the short period lunar tides produce highly nonequilibrium atmospheric tides at higher altitudes. Thus, it is not unreasonable to assume that the longer period tides behave in a similar manner, producing the observed response in the 300 mb zonal geostrophic wind component.

Since the nature of this tide is so highly nonequilibrium, the fairly straightforward explanation put forth in this section may very well be invalid. However, the characteristics of the dynamic long period atmospheric tides are not in the literature; and until research in this area is performed, there is no reference point from which to proceed with a more dynamically based explanation. Thus, for the present time, the empirically deduced physical link between forcing and response must suffice.

3.4 Response to lunar forcing at .263 year^{-1}.

3.4.1 Introduction.

After the nodal frequency is removed, the frequency that explains the most interannual variance in the lunar potential periodogram is .263 year^{-1}. The characteristics of the Moon's

orbit that produce this frequency have already been discussed. It now remains to look at the response in the station pressure, precipitation, and 300 mb U_g component at this frequency.

As with the nodal cycle response we will apply the same susceptibility factor to the forcing frequency. Further justification for doing this can be found by looking at the response in the coefficient time series of the first eigenvector of June precipitation (CBB, Fig. 6a) over a moving 19 year window. Each 19 year time series (e.g., 1895-1913, 1896-1914,..., 1957-1975) was regressed against $A\cos[2\pi(.263)t+\phi]$. The 19 year period allows for five cycles of the 3.8 year period. A plot of the normalized amplitudes versus the last year of the regression period (Fig. 3.20) shows that this frequency was much more important in the early and latter parts of the record than it was in the middle. The susceptibility factor applied to the forcing frequency captures this amplitude modulation. By regressing the time series against a single cosine with frequency .263 $year^{-1}$ one essentially gets an average amplitude over the data period (as suggested in Fig. 3.20); whereas, by regressing against the amplitude modulated model one can capture the larger amplitudes where they occur.

3.4.2 Station pressure.

The percent variance map (Fig 3.21) shows that the largest response to the nonlinear model is in northeastern India along and to the north of the mean position of the monsoon trough. The region

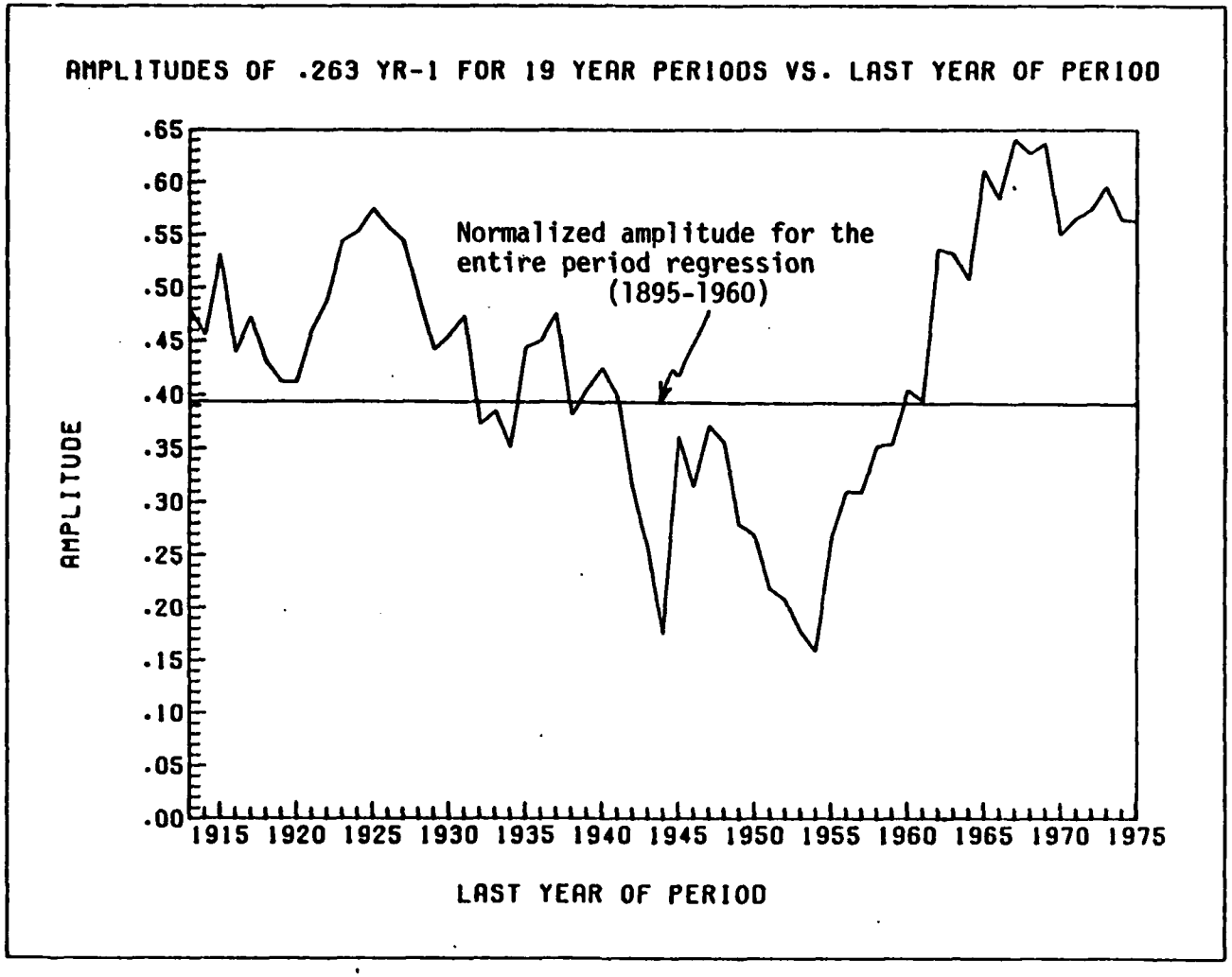

Figure 3.20. Normalized amplitudes of the regression of the first eigenvector coefficients (June precipitation) against the cosine with frequency .263 year^{-1} for overlapping 19 year periods plotted against the last year of the period.

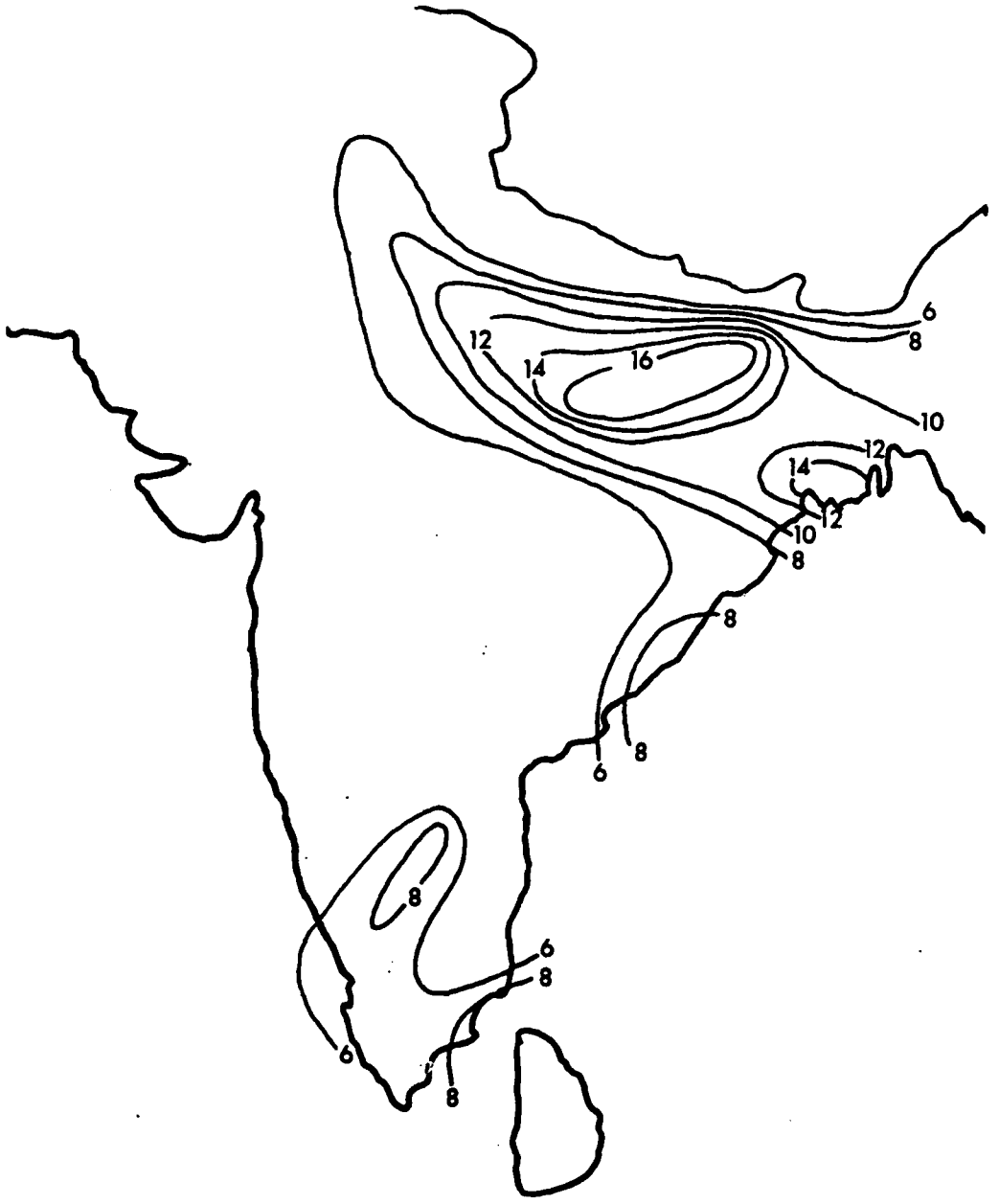

Figure 3.21. The percent of the station pressure variance explained by the kF_{26} model (units are percent).

in southern India also has an appreciable signal. The susceptibility threshold, B, (Fig. 3.22) in the northeast ranged from .95 to 2.03 indicating that the F_{26} forcing had some effect at all times and did not change sign except briefly at Calcutta which had the .95 value. Note that these values are considerably higher than the susceptibility thresholds for the nodal cycle response (Fig. 3.7). The B term in the southern peninsula range from .35 to .53.

The frequency, .263 $year^{-1}$, produces a 3.8 year period; thus, the anomalies for the first and third years of the data set (1895 and 1897) provide a good idea of the pressure response. In 1895 (Fig. 3.23) there is a strong positive anomaly extending all the way from the Bay of Bengal northwestward along the Himalayan foothills to Lahore City (31.6°N, 74.4°E). There is a negative pressure anomaly along the west coast, which creates a NE/SW pressure gradient. The geostrophically balanced wind would blow toward the northwest. Such a meridional pressure gradient would enhance the southwesterly monsoonal flow; and as we shall see in the next section, this year is wet through central and northwestern India. Two years later in 1897 the pattern has reversed, the geostrophic flow is from the northwest into central India, and one would expect a dry year.

This pressure anomaly pattern is similar to the one associated with the response to the lunar nodal cycle. In both cases the same NE/SW pressure gradient is established. Also, the maximum magnitude

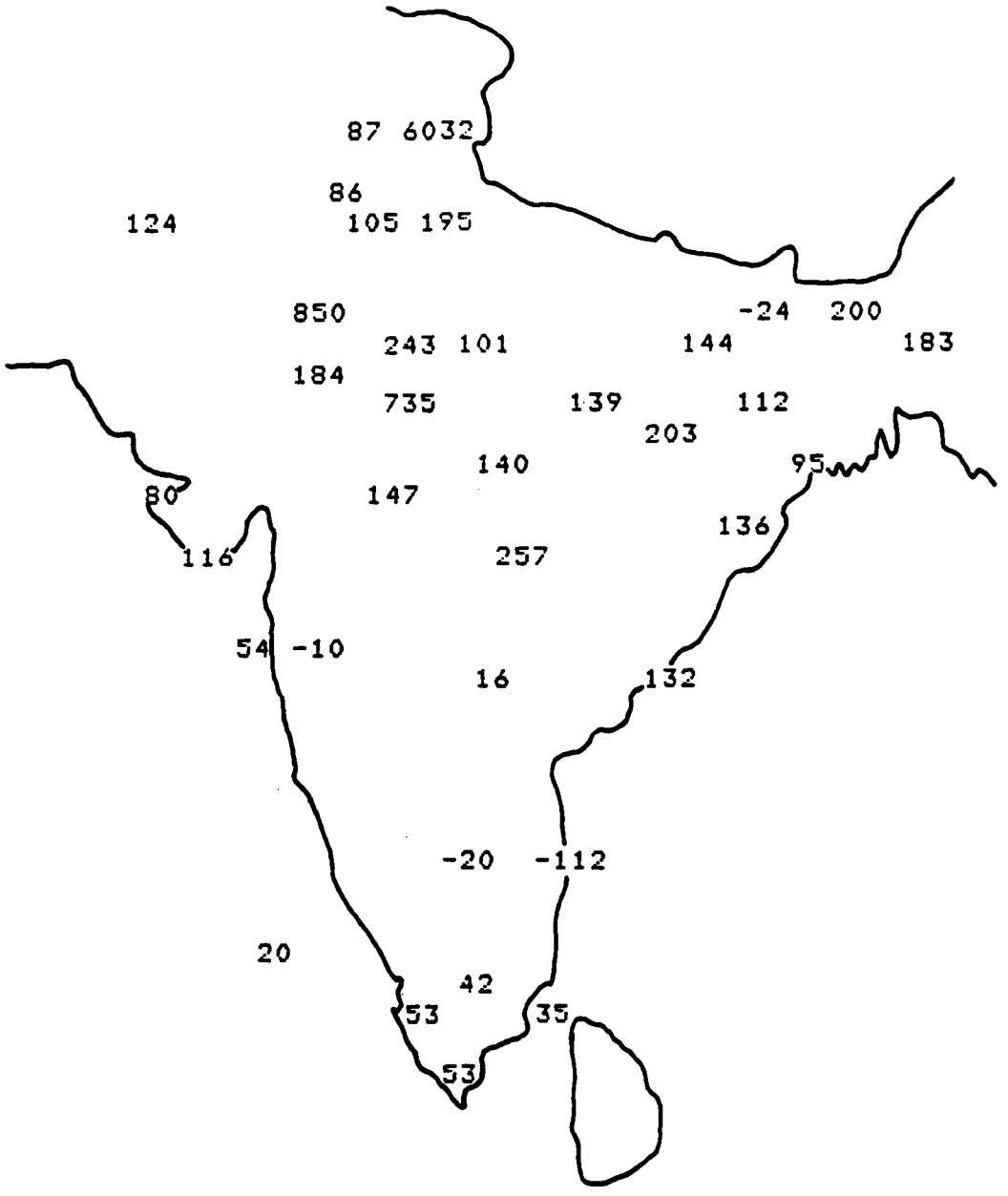

Figure 3.22. The value of the susceptibility threshold from the regression of the station pressure data against the kF_{26} model (units are value x 10^{-2}).

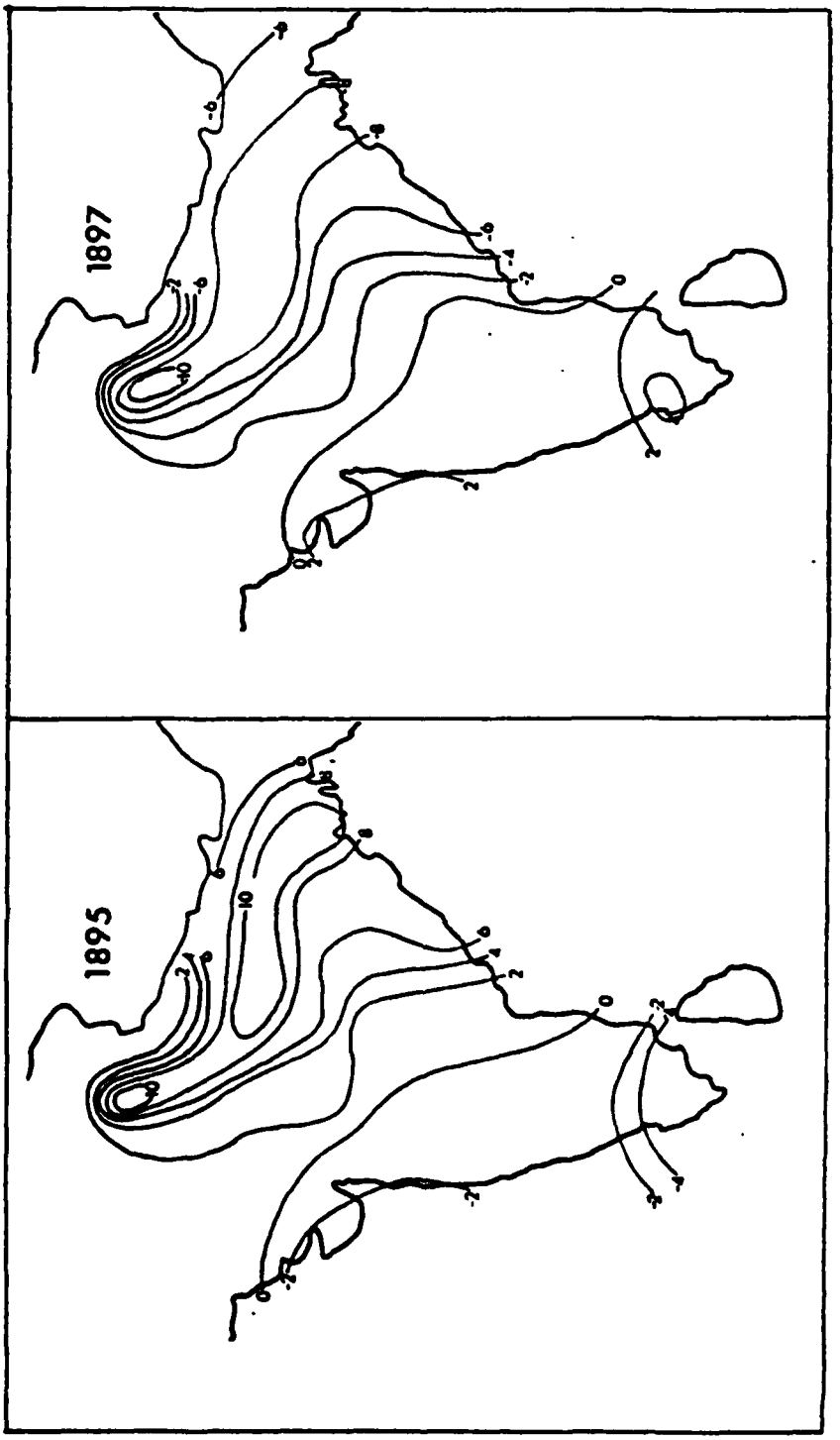

Figure 3.23. Anomaly maps of station pressure for the years indicated from the kF_{26} model (units are 10^{-1} mb).

of the anomalies in 1895 for both forcing frequencies are comparable (i.e., about 1 mb). One difference is that the western India anomaly is not as well developed in the F_{26} response as it is in the F_{05} response.

There is another anomaly center located in southern India. In 1895 the negative anomaly in this region produces easterly flow to its north inhibiting the southwesterly flow and creating dry conditions along the west coasts as is confirmed in the next section. In 1897 the southern India high pressure anomaly enhances the southwesterly flow to its north producing a positive precipitation anomaly.

In 1895 the geostrophic wind anomaly between Kota and Agra (station numbers 14 and 8, respectively in Fig. 3.4) is 2.7 ms^{-1}, and between Nagpur and Allahabad (numbers 23 and 15) it is 2.2 ms^{-1} from the southeast in a region where the mean meriodional wind is zero with standard deviation 2.1 ms^{-1} (Crutcher, 1966).

Because of the amplitude modulation, in 1950 (Fig. 3.24) the positive and negative anomaly centers are still discernible but their magnitude is greatly decreased and the low pressure anomaly is not as far to the north against the Himalayas.

To establish whether the pressure response is in phase with the lunar forcing of similar frequency, a pressure gradient time series was calculated by again taking the difference between the anomaly average of the eight northeastern stations and seven western stations. The average susceptibility threshold for these two groups

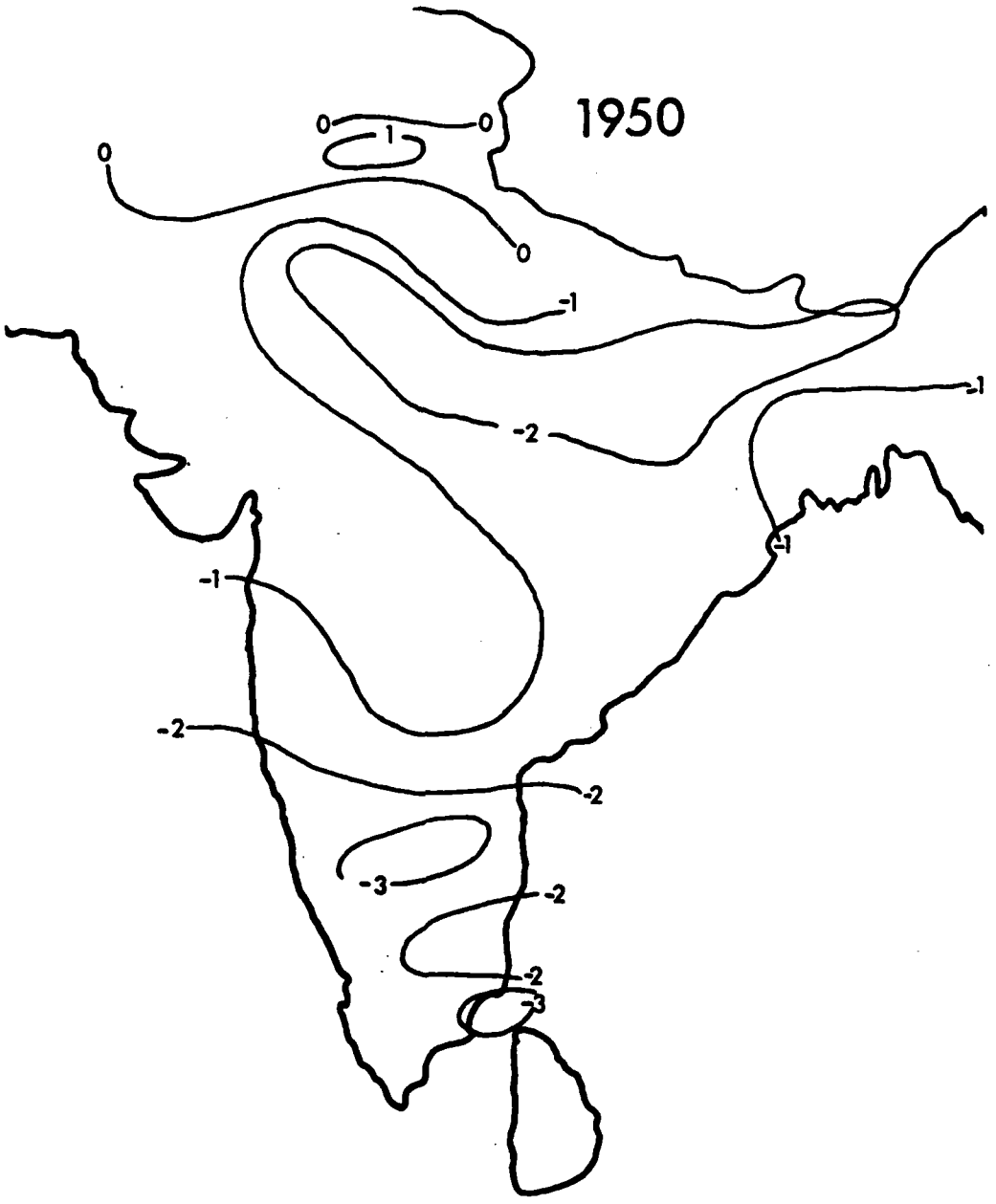

Figure 3.24. Anomaly map of station pressure for 1950 from the kF_{26} model (units are 10^{-1} mb).

of stations was 1.20 yielding a correlation between the TMEDLF response and observed response of -0.984.

Because the western anomaly is not as well developed in the kF_{26} response, the magnitude of the northeast minus west anomaly difference is not as great as that for the kF_{05} response. For example, in 1895 (a year of near maximum for both frequencies), the kF_{05} average anomaly difference is 1.38 mb and that for the kF_{26} model is 0.92 mb. Nevertheless, these values are comparable as one might expect from the TMEDLF response periodogram of Fig. 3.2.2. Because the surface pressure responds to the two lunar forcing frequencies with different susceptibility thresholds, the relative magnitude of the response at .263 $year^{-1}$ is much higher than the periodogram of the lunar tidal potential (Fig. 3.2.1) suggests, for the lunar tidal potential time series does not account for the susceptibility of the atmosphere to this lunar forcing.

3.4.3 Precipitation.

The percent variance map for precipitation (Fig. 3.25) shows a large response in central and northern India. This region lies between the 10 June and 1 July average positions of the monsoon front (see Fig. 1.1), suggesting that a large part of the variance might be due to the timing of the arrival of the monsoon.. There is also an area in southern India where a significant amount of variance is associated with the hypothesized model. The susceptibility thresholds are shown in Fig. 3.26.

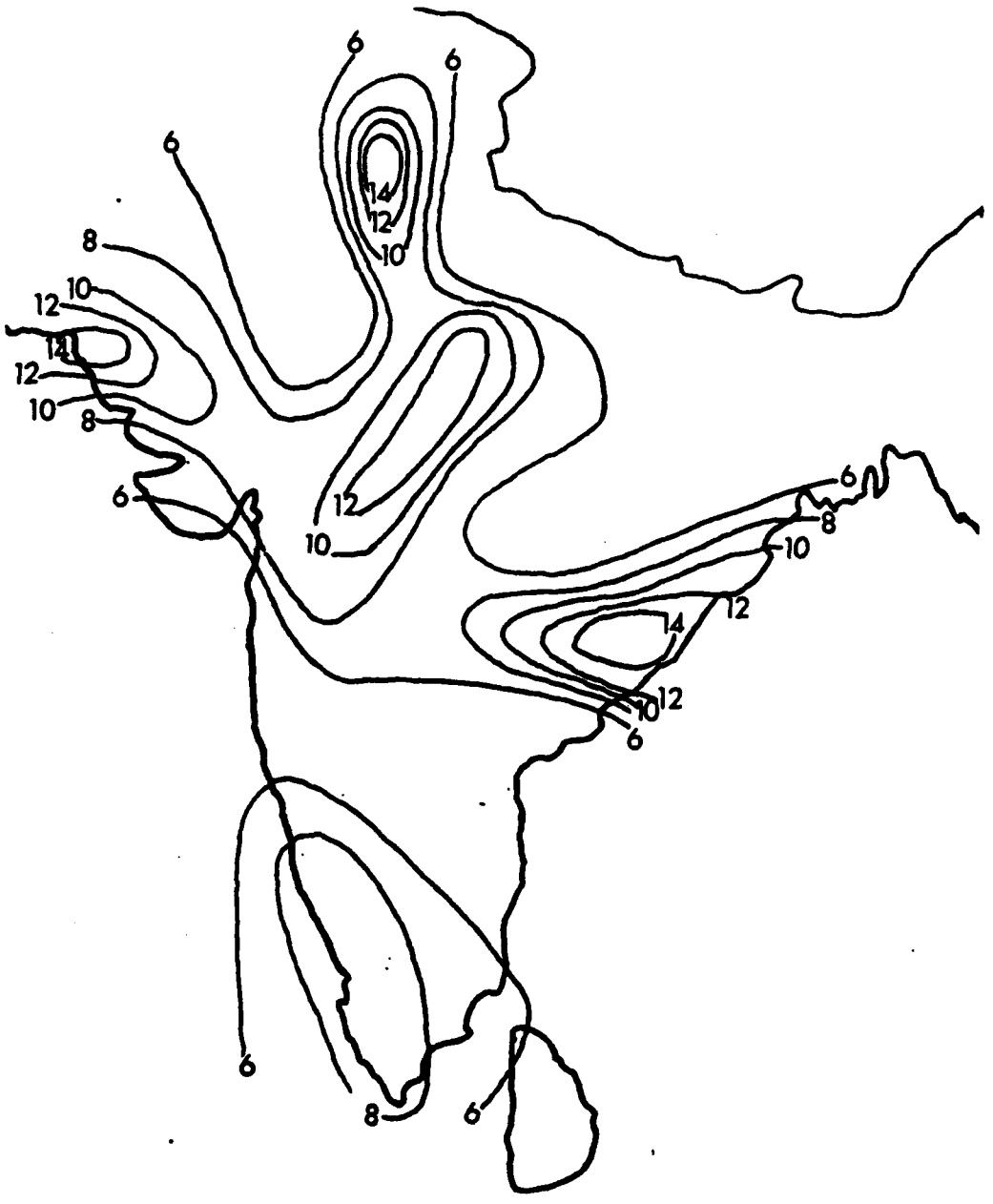

Figure 3.25. The percent of the precipitation variance explained by the kF_{26} model (units are percent).

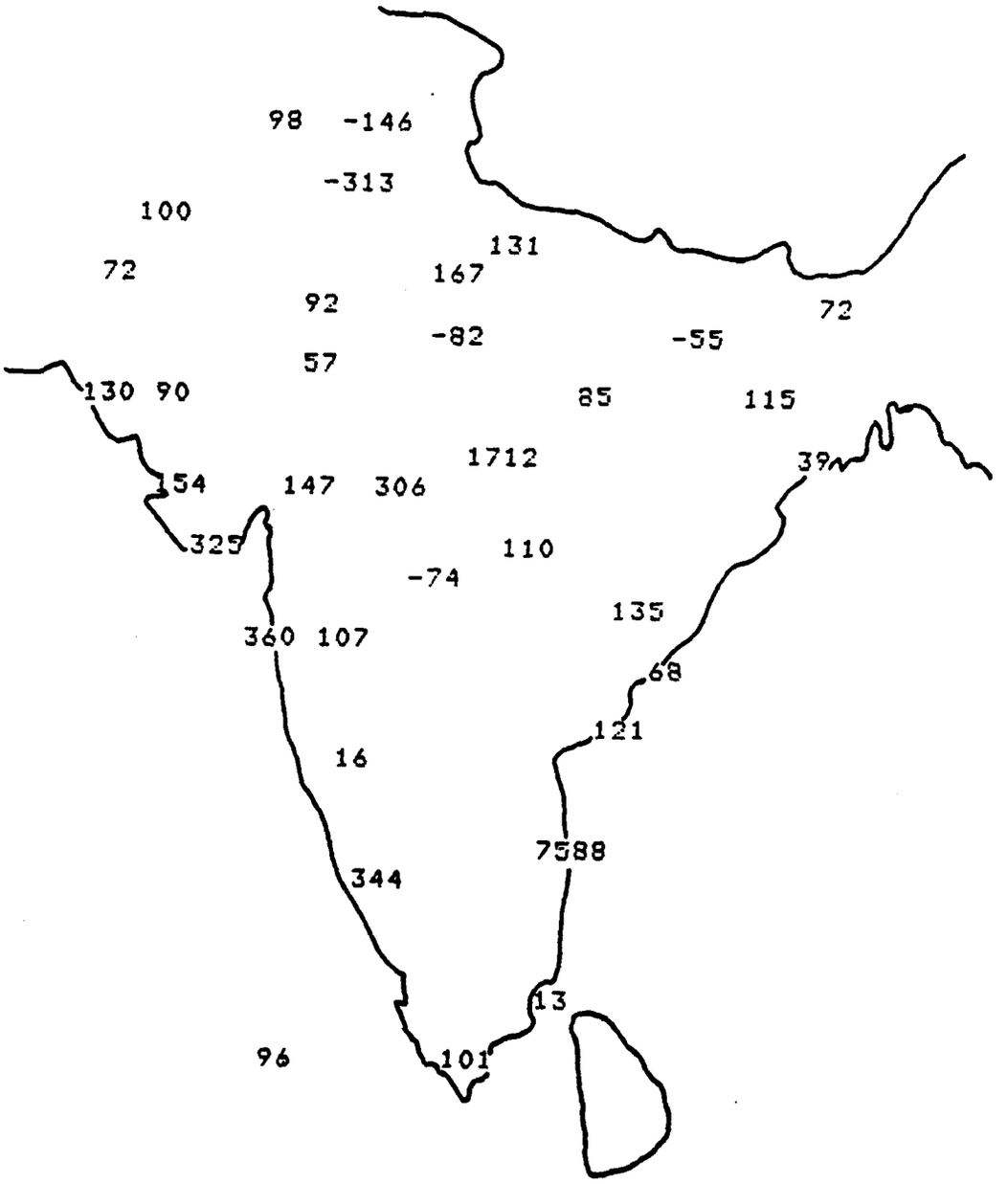

Figure 3.26. The value of the susceptibility threshold from the regression of the precipitation data against the kF_{26} model (units are value x 10^{-2}).

The anomalies for 1895, 1897, 1925, and 1927 are shown in Figure 3.27. In 1895 the moist southwesterly flow produced positive precipitation anomalies over the central and northern regions of India. In the region of the large positive pressure anomaly the precipitation anomalies are close to zero or negative. In the south the anomalous low pressure produced negative precipitation anomalies. In 1897 the precipitation anomalies are reversed as one would expect having already seen the associated pressure pattern. The years 1925 and 1927 again represent the two anomaly extremes of wet and dry, respectively. Now, however, the magnitude of the anomalies has been reduced due to the amplitude modulation.

The correlation between the average anomaly for the sixteen northern Indian stations with R^2 greater than or equal to six percent and the TMEDLF response time series is -0.983 with the average susceptibility threshold equal to 1.34 indicating that the observed precipitation response is again in phase with the TMEDLF response.

Even though the percent variance is low, the dissimilar behavior of Jodhpur (station number 11) is of interest. In 1895 when all stations around it have positive anomalies, Jodhpur has a negative anomaly and vice versa in 1897. Jodhpur is the "bullseye" in Figure 3.27 in northern India. Bryson and Swain (1981) reported that rainfall at Jodhpur was highly sensitive to whether the hemisphere was warming or cooling - that when the hemisphere was warming the rainfall for July and August was suppressed. The cosine curve used

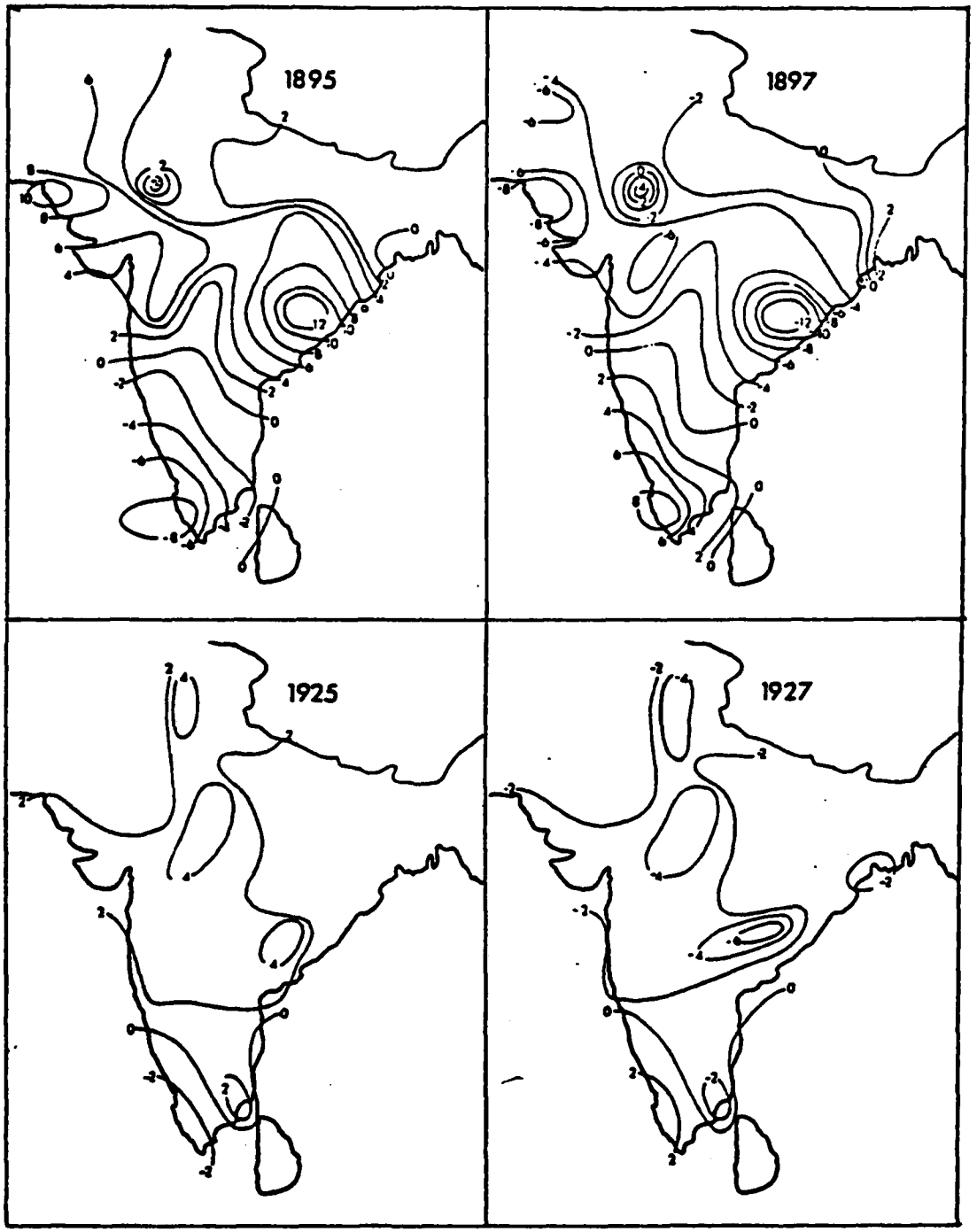

Figure 3.27. Normalized anomaly maps of precipitation for the years indicated from the kF_{26} model (units are standard deviations x 10^{-1}).

to approximate the hemispheric termperature curve is changing fast in 1895 (approximating warming) and rainfall at Jodhpur is below normal when all other stations have positive anomalies. When Jodhpur and Bikaner are regressed against a straight cosine with frequency of .263 year^{-1}, they are both in phase. It is not until the approximation of the hemispheric temperature trend is applied to the forcing cosine that this opposing effect appears. In 1925 and 1927 when the rate of warming has decreased these two stations are in phase. Jodhpur's response has changed sign because the susceptibility threshold is 0.57 whereas it is 0.92 for Bikaner. As Bryson and Swain (op. cit.) showed, once the rate of warming slowed, the two stations had similar responses.

When discussing the kF_{05} model for precipitation, studies by Bryson (1975) and Bhalme and Mooley (1981) were examined to see how well the hypothesized model fit the data and as reported significant variance was explained. Both studies involved precipitation over the total monsoon period. As a result the frequency 0.263 year^{-1} did not appear as an important factor in explaining the interannual variance in either of these studies, for this frequency is associated with a specific month and is out of phase with other months. This is because .263 year^{-1} is related to a 13.7 day period (1/2 the sidereal month) whose phasing changes from month to month because the length of the calendar month is not an integral number of 13.7 day periods (see Section 2.4 for a further explanation). On the other hand, the nodal period is 18.6 years

long so, for example, a minimum in the cycle for one month's average is followed by a minimum in the next month's average (i.e., this cycle is in phase from month to month).

3.4.4 300 mb data.

The U_g component is calculated from the 300 mb heights as in section 3.3.4 using Equation 3.11. Regression of the time series for Ug at locations along 75°E against a cosine with frequency .263 $year^{-1}$ yielded the following:

	Phase	Percent Variance	Amplitude(ms^{-1})
U_g at 37.5°N	174°	8.3	2.1
U_g at 32.5°N	-95°	0.3	0.5
U_g at 27.5°N	-3°	10.1	2.0

After applying the susceptibility factor and using nonlinear regression we have:

	Phase	Percent Variance	Susceptibility Threshold	1970 Value
U_g at 37.5°N	177	9.1	1.3	2.5
U_g at 32.5°N	-8	7.5	0.8	1.4
U_g at 27.5°N	4	10.3	1.8	-2.1

In both regressions the U_g component at locations north and south of the Himalayas are out of phase. The response of the middle location changes from what appears to be a node in the linear regression to a response that is closely in phase with either the location to the north or to the south of the Himalayas depending on the sign of the susceptibility factor which changes because the

susceptibility threshold is less than one. In either case, however, there is a definite oscillation north and south of the Himalayas.

Looking at the percent variance map (Fig 3.28) directly to the west of the Himalayas (e.g., along 60°E) the response is weaker than along the longitudes of the Himalayas, and downstream an even stronger response is observed. For example, along 100°E at 42.5°N and at 27.5°N the nonlinear model explains 24.0 percent and 26.8 percent of the variance, respectively. At latitude 32.5°N the explained variance is less than it is to the north and to the south all the way from 35°E to 120°E suggesting that a nodal line exists in this region. As we saw in Chapter 2 there is a node at 35.26°N in the lunar potential. Like the response along 75°E, the response downstream of the Himalayas is out of phase north and south of this nodal line as seen in the anomaly pattern for 1971 (Fig 3.29). These results, along with similar ones for the kF_{05} model, suggest that a dynamical interaction involving a forcing at these two frequencies, the Himalayas, and the subtropical jet creates a response in the vicinity of the Tibetan Plateau which then progagates downstream.

That the observed U_g response at 27.5°N, 75°E is, in fact, in phase with the kF_{26} TMEDLF response is seen from their -.978 correlation. Comparing the phasing of the precipitation and U_g response indicates that in dry years there is a westerly U_g anomaly over northern India and an easterly anomaly north of the Himalayas. This is consistent with the results for the kF_{05} model.

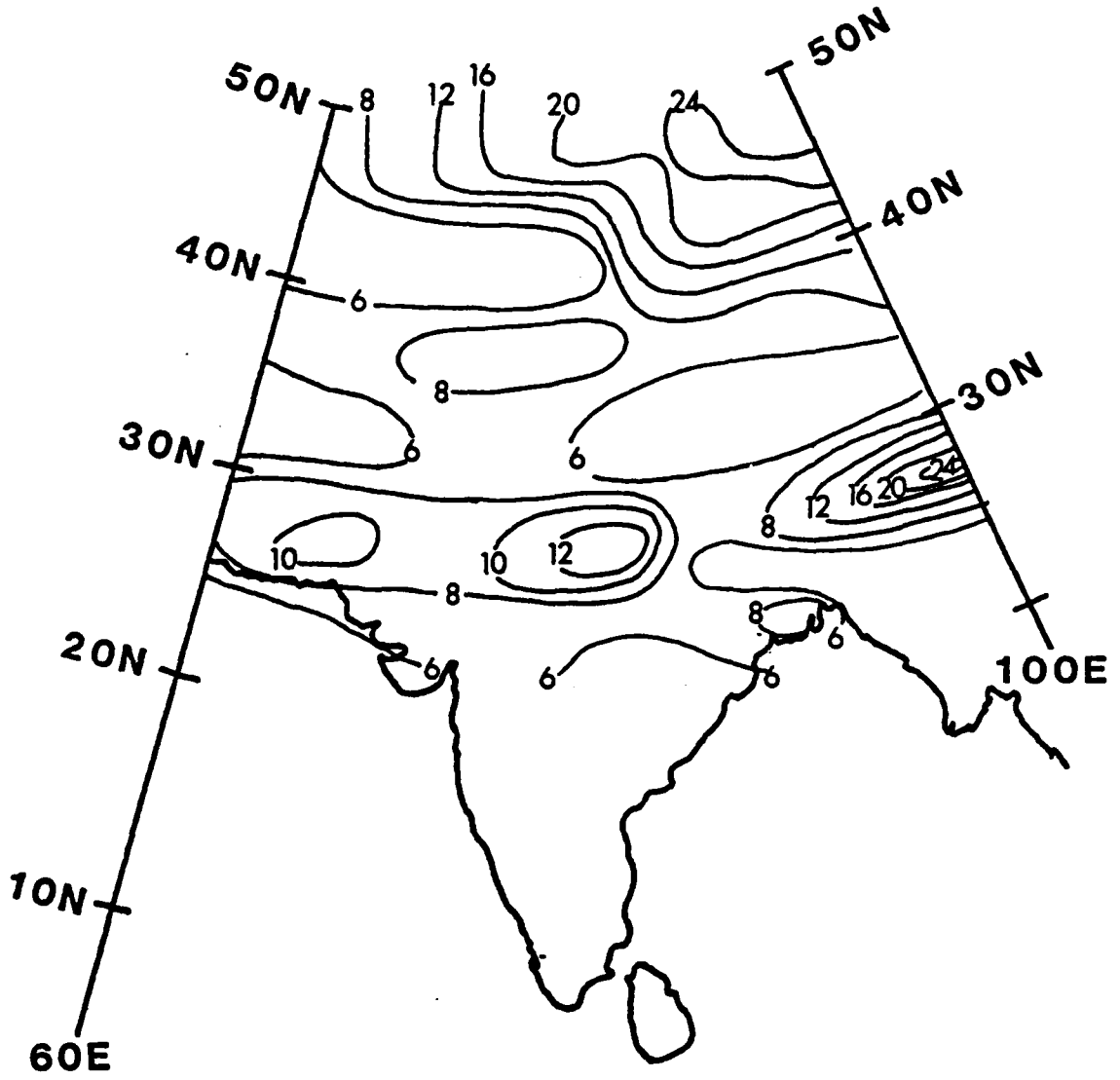

Figure 3.28. The percent of the geostrophic zonal wind (U_g) variance explained by the kF_{26} model (units are percent). Level is 300 millibars.

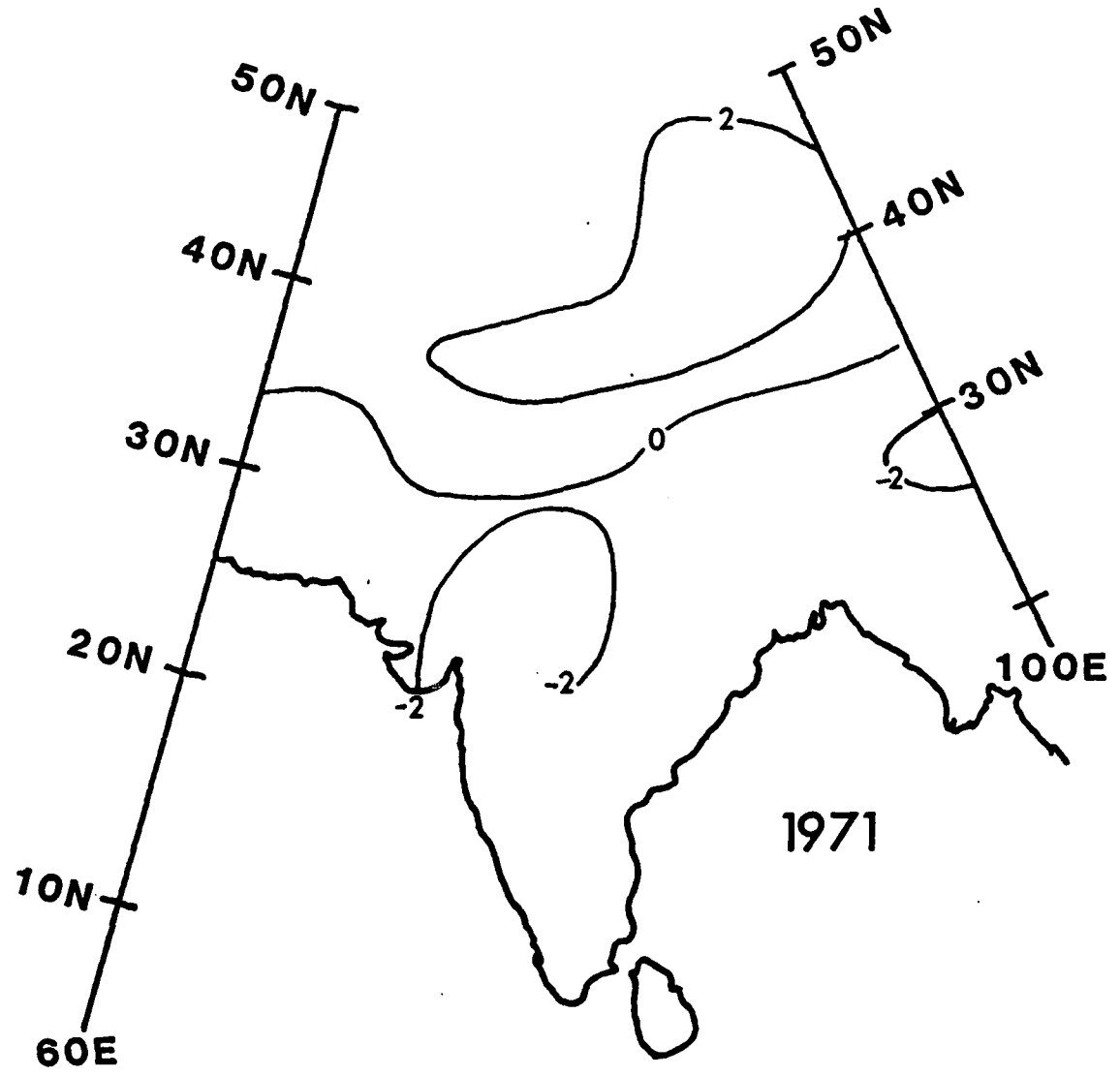

Figure 3.29. Anomaly map of U_g for 1971 from the kF_{26} model (units are ms^{-1}). Level is 300 mb.

3.4.5 Possible physical relationship between the hypothesized lunar forcing and the observed climatological data.

As with the kF_{05} model, if we apply the susceptibility factor from the 300 mb U_g component model in northern India at 27.5°N, 75°E to the lunar tidal potential as follows:

$$H_{26}(\phi) = -1.9[Q(t) - 1.81]F_{26}(\phi) \qquad 3.15$$

then in years when the U_g component anomaly is negative (as in 1971, Fig. 3.29) at this location, the latitudinal distribution of H_{26} is the same as it was for H_{05} in section 3.3.4. This distribution would then produce a negative or easterly U_g component if we consider geostrophic equilibrium. Thus, the synoptic relationships for the kF_{05} response discussed earlier apply equally well for the kF_{26} response, for both lunar forcing frequencies produce similar phasings in all three climatic variables.

3.5 Summary.

As we have seen, all three climatic variables (i.e., pressure, precipitation, and 300 mb U_g) are highly correlated with the lunar forcing response models, kF_{05} and kF_{26}, which means they are highly correlated with each other. Table 3.4 provides a summary of these statistics. The average susceptibility threshold values summarized in this table indicate that the values used to calculate the periodogram of Fig. 3.2.2 were quite reasonable.

As we have seen, a low pressure anomaly along the foot of the

Table 3.4

Summary of statistics for the kF_{05} and kF_{26} models for the three climatic variables

	kF_{05}		kF_{26}	
	R	Average Susceptibility threshold	R	Average Susceptibility threshold
Pressure gradient	-0.972	0.94	-0.984	1.20
Precipitation	-0.971	0.97	-0.983	1.34
U_g 300 mb	0.997	1.04	0.978	1.81

Himalayas plus a high pressure anomaly along the west coast leads to deficient rainfall over most of India. Ramaswamy (1958) examined the mean zonal wind component at New Delhi and Calcutta for both a weak and active monsoon period and found that at both stations the dry period was characterized not only by a northward shift of the low pressure trough to a position along the Himalayas but also by a westerly anomaly at these stations up to very high levels. More recently Raman and Rao (1981) have shown that establishment of an east Asia blocking ridge along 100°E, extending from 35°N to 70°N, anchors a westerly trough around 70°E to 75°E. With this trough extending into more southerly latitudes (30°N) than normal the lower tropospheric monsoon trough is then displaced northward into the Himalayas. This synoptic situation would produce a westerly anomaly at 300 mb in the region where we see it in Figure 3.18 for the year 1977

Between April and July along 75°E the subtropical jet moves from 25°N to 45°N while the 200 mb ridge axis moves from 10°N to 30°N. Yin (1949), Wright (1967) and many others have found that the timing of the onset of the monsoon is directly related to the movement of the subtropical jet from its winter postion south of the Tibetan Plateau to its summer position to the north of the plateau. Wright (op. cit.) derived several relationships between the 200 mb zonal wind and the onset of the monsoon. He found that the first main burst of the monsoon extended up to at least 13°N and occurred within "a fortnight of the date on which the 200 mb westerly wind

component at Bombay falls permanently below 5 kt ...". For the period 1891-1950 the average date for the monsoon to arrive at 13°N was 3 June with a standard deviation of 6.3 days. The second main burst of the monsoon extended up to 22°N and occurred "about a month after the start of the main decrease in the 200 mb westerly wind component at New Delhi ...". The arrival date at 22°N was 20 June with a range of 22 days. The observed climatic response to both hypothesized lunar forcing frequencies has shown that when a westerly anomaly at 300 mb lies across northern India, a low pressure anomaly lies along the Himalayas and rainfall is deficient. This is consistent with Wright's analysis since late arrival of the monsoon, and hence below normal rainfall, was associated with stronger than normal westerlies. It is important to note that the precipitation appears to be related more to the strength of the westerly anomaly over northern India than to the actual position of the subtropical jet. For the 27 years of 300 mb data, the jet was never located between 25°N and 30°N for the month of June and yet it is the zonal component of the geostrophic wind anomaly in this region that is so highly correlated to the precipitation at these two lunar frequencies.

From the analysis in this chapter, then, a consistent climatology emerges that is similar for both lunar forcing frequency models:

a. There is an external boundary condition, lunar tidal forcing, that is always acting upon the earth-atmosphere-ocean

system. This is an ultimate cause of the climatic state which establishes an array of weather patterns associated with the monsoon circulation.

b. South of the Himalayas, the 300 mb geostrophic zonal component of the wind responds to the latitudinal distribution of the lunar potential anomalies resulting from the two frequencies, .0537 $year^{-1}$ and .263 $year^{-1}$. These two frequencies account for almost 100 percent of the lunar tidal potential interannual variability in June. At one extreme of each cycle there is a westerly geostrophic wind anomaly and at the other extreme there is an easterly anomaly.

c. In years when there is a westerly anomaly at 27.5°N over northern India, the normal decrease in westerlies at this latitude is slowed. As other research has shown, the timing of the onset of the monsoon is directly related to the timing of the decrease in the westerlies over northern India. Thus, a westerly anomaly in this region results in a delay of the onset.

d. This delay in the monsoon onset is related to the surface pressure anomaly pattern that occurs at the same time as the 300 mb westerly anomaly. This surface pressure anomaly pattern is one of low pressure along the base of the Himalayas and high pressure in western India producing a NE/SW pressure gradient that supports anomalous northwesterly flow in direct opposition to the movement of the monsoon front toward the northwest. The high pressure anomaly along the west coast also decreases the southwesterly monsoonal flow

off of the Arabian Sea. With the normal low level monsoon circulation disrupted in this manner, the onset is delayed.

e. In northern India most of the June rainfall occurs after the monsoon has arrived. The normal onset date is late June. Therefore, any delay in this date will have a large impact on the percent of normal rainfall received in June.

f. As CBB showed, the precipitation response at the two lunar tidal frequencies, .263 $year^{-1}$ and .0482 $year^{-1}$ (the linear signature of the nodal cycle response), is observed to be most important in explaining the interannual variability of precipitation in northern India in June. Thus, it would appear that lunar tidal forcing plays a significant role in the interannual variability of June precipitation in northern India.

g. The Northern Hemisphere surface temperature is a proximal cause of the climate, for it is related to the amount of solar radiation reaching the Earth's surface which is controlled by such ultimate causes as volcanic activity and the Earth's orbital parameters. The Northern Hemisphere surface temperature determines to a large extent the intensity of the monsoon circulation. As a result, this proximal cause modulates the effects of the lunar tidal forcing described above. When the hemisphere is warm, the monsoon circulation is strong and the atmosphere is less susceptible to an external forcing, thus, diminishing the effect of the lunar tide. A nonlinear regression model was developed based on this idea of atmospheric susceptibility. As noted at the time the susceptibility

factor used was an approximation. Nevertheless, applying this factor to the hypothesized forcing frequencies virtually "unlocked" the nodal cycle in the data and made the amplitudes of the response at the beginning of the record for both lunar frequencies at least two to three times larger than those attained in a straight linear regression.

CHAPTER 4

Conclusions

1. This research has presented definitive evidence that there is an important periodic component in the interannual variability of pressure, precipitation, and upper air winds for the monsoon onset month of June and that the two dominant frequencies found in the precipitation records of northern India stations are the same two frequencies which explain almost 100 percent of the interannual variance of the hypothesized forcing mechanism - monthly mean lunar tidal potential. Not only are the response and forcing frequencies the same but they are also in phase which strongly suggests that lunar tides in the atmosphere do, in fact, produce an element of climatic variability.

2. Past research has typically examined monsoon variability using a stratified climatology approach, i.e., by studying certain variables during drought, flood, and/or normal years. However, by examining the periodic component of climatic variability we can include drought, flood and normal years into a single model based on a periodic forcing mechanism. Both lunar forcing frequencies, examined in this research, are associated with consistent climatic responses in surface pressure, precipitation and the 300 mb geostrophic zonal wind component. As a result, the work of many monsoon researchers could be synthesized into a coherent synoptic

climatology defined by a nonlinear periodic model of climatic variability.

3. A trend in the amplitude of the periodic response was found and related to the Northern Hemisphere surface temperature. Thus, in this case the trend and periodic components of climatic variability are inseparable. This dependence of the periodic component on the hemispheric temperature indicates that the period of time covered by a data set can determine whether or not an hypothesized periodic forcing will produce an observable signal in the data.

4. The synoptic climatology associated with the responses of surface pressure, precipitation and the 300 mb U_g component were similar for both lunar forcing frequencies. However, the characteristics of the susceptibility factors at a given location for each frequency can be quite different. For example, the susceptibility threshold is generally higher for the kF_{26} response than that for kF_{05}. As we saw, this resulted in the magnitude of the kF_{26} response being comparable to that for the kF_{05} response. A comparison of Eqns. 3.13 and 3.15 indicates another difference in that the signs on the susceptibility factor coefficients are opposite; and since in both cases the [Q(t)-B] factor is always less than zero, the sign on the

forcing factor is negative for the kF_{05} response and positive for the kF_{26} response. Thus, opposite latitudinal distributions of the lunar tidal potential produce similar 300 mb U_g anomalies. In a monthly average we can assume geostrophic equilibrium with the coriolis force (C) balancing the pressure gradient force (P). However, with the hypothesis of lunar tidal forcing, there is an additional force (L) to consider. With geostrophic equilibrium, we have,

$$C = P. \qquad 4.1$$

Considering the sign on the forcing for the kF_{05} response we have,

$$C = P - L \;\rightarrow\; P = C + L\ ; \qquad 4.2$$

and for the kF_{26} response we have,

$$C = P + L \;\rightarrow\; P + L = C\ . \qquad 4.3$$

The reason for this difference in sign is not known at the present time but it may be due to the different time scales associated with each frequency. F_{26} arises from a 13.7 day period which goes through two complete cycles during a calendar month with a 2.7 day residual in the month of June. On the other hand, F_{05} arises from the nearly 6800 day nodal cycle and, therefore, acts in the same sense throughout the entire calendar month. Such a difference in time scale certainly has implications, for example, in the interaction between the atmosphere and the oceans.

5. The impetus for this research was to improve long range climate forecasting capabilities. This research has provided an

analysis of one segment of the past climatic variability during the monsoon onset month of June and found that there is an important periodic component to this variability that is in phase with lunar tidal forcing. Therefore, there is an inherent predictive capability in the nonlinear model used, for the Moon's position can be very accurately predicted. The other factor in the model, Northern Hemisphere surface temperature, must also be forecast. These forecasts are currently available using an atmospheric optical depth model. The susceptibility factor must then be modified to use the temperature forecast instead of the cosine approximation used in this research.

6. The nature of the nonlinear kF_{05} response shifts the spectral peak in the forcing at .054 $year^{-1}$ to a lower frequency around .048 $year^{-1}$. As we have seen, this is very close to the sunspot frequency and both hypothesized forcings happen to be closely in phase during the period of time covered by the data sets used in this research. The lunar tidal forcing hypothesis, therefore, sheds some doubt on the sunspot hypothesis at least to the extent that this research provides another explanation for the periodicity; and certainly, at this point in time, there is a stronger physical relationship between atmospheric tides and the observed climatic variability than there is for the sunspot hypothesis. This finding also points out the limitations of a linear analysis like the Fast Fourier Transform or periodogram, for

the true forcing frequency will not necessarily show up if it is being modulated by some susceptibility factor.

7. The averaging period of the data used in one's research will determine what lunar signals are observable. For example, data averaged over a 27.3 day period would not show a signal at .263 $year^{-1}$. Thus, the meteorologist's standard method of averaging over a 30 or 31 day period allowed this frequency to show up in the data. Similarly, an average of June, July, August, and September data would wash out the .263 $year^{-1}$ signal since this frequency has a different phase in each month. On the other hand because the nodal cycle is such a long period phenomenon any averaging period at least up to a year would allow it to appear.

8. External forcing on the atmosphere seems to be observable on the interannual time scale only in regions where a synoptic singularity exists (e.g., the arctic front in December in the upper midwest or the onset of the monsoon in June in northern India) and then only if the atmosphere is susceptible to that forcing. Therefore, these sensitive regions need to be identified so that the predictive capability of periodic external forcing can be explored further.

REFERENCES

Adderley, E.E. and E.G. Bowen, 1962: Lunar component in precipitation data. Science, Vol 137, 749-750.

American Ephemeris and Nautical Almanac (1895-1960), United States Government Printing Office, Washington, D.C., 1980

Bhalme, H.N., 1972: Trends and quasi-biennial oscillation in the series of cyclonic disturbances over the Indian region. IJMG, Vol 23, 355-358.

_____ and D.A. Mooley, 1980: Large-scale droughts/floods and monsoon circulation. MWR, Vol 108, 1197-1211.

_____ and _____, 1981: Cyclic fluctuations in the flood area and relationship with the double (Hale) sunspot cycle. JAM, Vol 20, 1041-1048.

_____, _____, and S.K. Jadhav, 1983: Fluctuations in the drought/flood area over India and relationships with the Southern Oscillation. MWR, Vol 111, 86-94.

Bhargava, B.N. and R.K. Bansal, 1969: A quasi-biennial oscillation in precipitation at some Indian stations. IJMG, Vol 20, 127-128.

Bradley, D.A., 1964: Tidal components in hurricane development. Nature, Vol 204, 136-138.

Brier, G.W., 1968: Long-range predictions of the zonal westerlies and some problems in data analysis. Rev. Geophys., Vol 6, 525-551.

_____ and D.A. Bradley, 1964: The lunar synodical period and precipitation in the United States. JAS, Vol 21, 386-395.

Brinkmann, W.A.R., 1979: Associations between temperature trends. Annals of the Association of American Geographers, Vol 69, 250-261.

Brouwer, D. and G.M. Clemence, 1961: Methods of Celestial Mechanics. Academic Press, New York, 598 pp.

Brownlee, K. A., 1965: Statistical Theory and Methodology. John Wiley a Sons, Inc., New York, 590 pp.

Bryson, R.A., 1948: On a lunar bi-fortnightly tide in the atmosphere. Trans. Am. Geophys. Union, Vol 29, 473-475.

Bryson, R.A., 1975: The lessons of climatic history. Environmental Conservation, Vol 2, 163-170.

_____ and T.B. Starr, 1977: Chandler tides in the atmosphere. JAS, Vol 34, 1975-1986.

_____ and B.M. Goodman, 1980: Volcanic activity and climatic change, Science, Vol 207, 1041-1044.

_____ and A.M. Swain, 1981: Holocene variations of monsoon rainfall in Rajasthan. Quaternary Research, Vol 16, 135-145.

Campbell, W. H., J.B. Blechman, and R.A. Bryson, 1983: Long-period tidal forcing of Indian monsoon rainfall: An hypothesis. JCAM, Vol 22, 287-296.

Chapman, S. and R.L. Lindzen, 1970: Atmospheric Tides. Gordon and Breach, New York, 200 pp.

Crutcher, H. L., 1966: Components of the 1000 mb. winds (or surface winds) of the Northern Hemisphere. NAVAIR 50-1c-51, Office of Chief of Naval Operations, 77 pp.

Currie, R.C., 1981: Evidence for 18.6 year M_N signal in temperature and drought conditions in North America since AD 1800. J. Geophys. Res., 86, 11055-11064.

Das, P.K., 1968: The Monsoon. National Book Trust, New Delhi, 162 pp.

Doodson, A.T., 1921: The harmonic development of the tide generating potential. Proc. Roy. Soc., Ser. A, Vol 100, 305-329.

Duperier, A., 1946: A lunar effect on cosmic rays. Nature, Vol 157, 296-299.

Gill, A. E., 1980: Some simple solutions for heat-induced tropical circulation. QJRMS, Vol 106, 447-462.

Godbole, R.V., 1973: Numerical simulation of the Indian summer monsoon. IJMG, Vol 24, 1-14.

Goldstine, H. H., 1973: New and Full Moons 1001 B.C. to A.D. 1651. American Philosophical Society, Philadelphia, 221 pp.

Groveman, B.S. and H.E. Landsberg, 1979: Reconstruction of Northern Hemisphere temperature: 1579-1880. Publ. No. 79-181, June, 1979, Meteorology Program, Univ. of Maryland, College Park, MD 20742, 46 pp.

Hahn, D.G. and S. Manabe, 1975: The role of mountains in the south Asian monsoon circulation. JAS, Vol 32, 1515-1541.

_____ and J. Shukla, 1976: An apparent relationship between Eurasian snow cover and Indian monsoon rainfall. JAS, Vol 33, 2461-2462.

Jagannathan, P. and B. Parthasarathy, 1973: Trends and periodicities of rainfall over India. MWR, Vol 101, 371-375.

Jones, P. D., T.M.L. Wigley, and P.M. Kelley, 1982: Variations in surface air temperatures: Part 1. Northern Hemisphere, 1881-1980. MWR, Vol 110, 59-70.

Koteswaram, P. and S.M.A. Alvi, 1969: Secular trends and periodicities in rainfall at west coast stations in India. Current Science, Vol 38, 229-231.

Kutzbach, J.E., 1970: Large-scale features of monthly mean Northern Hemisphere anomaly maps of sea level pressure. MWR, Vol 98, 708-716.

_____ and B. L. Otto-Bliesner, 1982: The sensitivity of the African-Asian monsoonal climate to orbital parameter changes for 9000 Years B.P. in a low-resolution general circulation model. JAS, Vol 39, 1177-1188.

Krishnamurti, T.N., 1971: Observational study of the tropical upper tropospheric motion field during the Northern Hemisphere summer. JAM, Vol 10, 1066-1096.

_____, S.M. Daggupaty, J. Fein, M. Kanamitsu, and J.D. Lee, 1973: Tibetan high and upper tropospheric tropical circulations during northern summer. BAMS, Vol 54, 1234-1249.

_____ and H.N. Bhalme, 1976: Oscillations of a monsoon system. Part I. Observational aspects. JAS, Vol 33, 1937-1954.

Maksimov, I.V., 1958: Nutational phenomena in the high latitude atmosphere andtheir role in the formation of climate. Ottawa, Problems of the North, No 1 (1960), Nat. Res. Council Canada, 103-123.

_____, V.P. Karklin, E.I. Sarukhanian, and N.P. Smirnov, 1967: Nutational migration of the Icelandic low. Dokl. Akad. Nauk. SSSR, Vol 177, 88-91. (English trans. Dokl. Acad. Sci. USSR, Earth Sci. Section)

Matsuno, T., 1966: Quasi-geostrophic motions in the equatorial area. JMSJ, Vol 44, 25-43.

Nash, E. R., 1982: A critical comparison of two theories of the atmospheric Chandler "pole tide". Masters thesis, University of Wisconsin, 28 pp.

Overland, J.E., and R.W. Preisendorfer, 1982: A significance test for principal components applied to a cyclone climatology. Mon. Wea. Rev., 110, 1-4.

Parthasarathy, B. and D.A. Mooley, 1978: Some features of a long homogeneous series of Indian summer rainfall. MWR, Vol 106, 771-781.

Pearson, D. C., 1982: Periodic interannual variations of midwestern United States temperatures in December. Masters Thesis, University of Wisconsin, 76 pp.

Raghavan, K., 1973: Break-monsoon over India. MWR, Vol 101, 33-43.

Raman, C. R. V. and Y. P. Rao, 1981: Blocking highs over Asia and monsoon droughts over India. Nature, Vol 289, 271-273.

Ramaswamy, C., 1958: A preliminary study of the behaviour of the Indian southwest monsoon in relation to the westerly jet-stream. Geophysica, Vol 6, 455-477.

Rao, Y.P., 1976: Southwest Monsoon. India Met. Dept., Poona, 367 pp.

Shukla, J., 1975: Effect of Arabian sea-surface temperature anomaly on Indian summer monsoon: A numerical experiment with the GFDL model. JAS, Vol 32, 503-511.

_____ and B.M. Misra, 1977: Relationships between sea surface temperature and wind speed over the central Arabian sea, and monsoon rainfall over India. MWR, Vol 105, 998-1002.

Trenberth, K.E. and D.A. Paolino, Jr., 1980: The Northern Hemsiphere sea-level pressure data set: Trends, errors and discontinuities. MWR, Vol 108, 855-872.

van Loon, H. and J. Williams, 1976: The connection between trends of mean temperature and circulation at the surface: Part I. Winter. MWR, Vol 104, 365-380.

Visvanathan, T.R., 1966a: Formation of depressions in the Indian seas and lunar phase. Nature, Vol 210, 406-407.

_____, 1966b: Heavy rainfall distribution in relation to the phase of the moon. IJMG, Vol 17, 369-372.

Voigt, H. H., 1974: Outline of Astronomy, Vol I., Noordhoff International Publ., Leydon, The Netherlands, 272 pp.

Walker, G.T., 1924: Correlation in seasonal variation of weather IX. Mem. India Meteor. Dept., Vol 24, 275-332.

Weare, B.C., 1979: A statistical study of the relationships between ocean surface temperatures and the Indian monsoon. JAS, Vol 36, 2279-2291.

Webster, P.J. and L.C. Chou, 1980: Seasonal structures of a simple monsoon system. JAS, Vol 37, 354-367.

Wood, Fergus J., 1976: The Strategic Role of Perigean Spring Tides. U.S. Department of Commerce, National Oceanic and Atmospheric Administration, Washington, D.C., 538 pp.

Wright, P.B., 1967: Changes in 200 mb circulation patterns related to the development of the Indian south-west monsoon. Met. Mag., 96, 302-315.

Yin, M.T., 1949: A synoptic-aerologic study of the onset of the summer monsoon over India and Burma. Journal of Meteorology, Vol 6, 393-400.

END

FILMED

1-84

DTIC